Master's thesis

Max-Planck-Institute for Meteorology in Hamburg

Meteorological Institute, University of Hamburg

The impact of snow on sea-ice salinity

March 21, 2017

Niels Fuchs

MSc Meteorology studies

University of Hamburg

Matriculation number: 6202547

Supervisors:

Dr. Dirk Notz,

Max-Planck-Institute for Meteorology

Prof. Dr. Felix Ament,

University of Hamburg

Master's thesis

„The impact of snow on sea-ice salinity“ - *Niels Fuchs*

Abstract

Sea ice contains salt, which is dissolved in liquid brine and stored in the interstitial of the solid ice skeleton. The salt content strongly affects the intrinsic physical properties of the ice and is reduced in the seasonal cycle by different desalination processes. A decrease in salt content for instance reduces melt rates of the ice. Vertical profiles of sea-ice salinity derived from ice cores show that melting snow on top of sea ice can desalinate the ice by melt-water flushing. Sea-ice model parametrizations of snow melt and its impact on the ice beneath are based on such conventional ice core measurements. The temporal evolution of melt-water flushing is poorly represented and differently parametrized in models, due to certain limitations of ice core measurements. The destructive method of taking ice cores inhibits successive measurements of exactly the same ice bulk. Furthermore, ice core data has a low spatial and temporal resolution and is inaccurate in the lower parts. Thus, no exact conclusions could be drawn about the impacts of snow on sea-ice salinity so far.

The deployment of a well-developed sea-ice salinity sensor array allows me to measure internal processes in an unprecedented temporal as well as spatial resolution. Of particular interest in this work is therefore melt water flushing and its temporal evolution, as well as impacts that are not captured by the low resolved ice core data. First, I evaluate the so-called salinity harp measurement system and perform subsequently five sea ice freezing and thawing cycles in lab experiments with increasing snow thickness. Comparisons of the results with the one-dimensional thermodynamic sea-ice model SAMSIM show that the overall impact of flushing during a whole thaw cycle is indeed captured by the model but not the temporal evolution during the snow melt phase. I find that in contrast to the former parametrization only one quarter of the snow melt water remains on top of the ice and forms a slush layer together with the lowest snow layers. The remaining three quarters flow off directly into the interstitial sea-ice brine system. I investigate further impacts of the snow on the sea-ice salinity below and quantify the influence of the amount of snow that melts on the ice.

Contents

Variables

Variable	Symbol	Unit
air temperature	T_{air}	[°C]
brine density	ρ_l	[kg m^{-3}]
brine salinity, NaCl	$S_{br,NaCl}$	[g kg^{-1}]
brine salinity, sea salt	S_{br}	[g kg^{-1}]
bulk salinity	S_{bu}	[g kg^{-1}]
freezing temperature	T_f	[°C]
freshwater ice density	ρ_s	[kg m^{-3}]
gas fraction	ϕ_g	[1]
heat capacity of sea ice	c_{ice}	[J kg^{-1} K^{-1}]
heat conductivity of sea ice	k_{ice}	[W m^{-1} K^{-1}]
ice thickness	h_{ice}	[cm]
impedance	Z	[Ω]
liquid mass fraction	ϕ_l	[1]
liquid volume fraction	$\phi_{l,v}$	[1]
liquid water density	ρ_w	[kg m^{-3}]
mass freshwater	m_w	[kg]
mass salt	m_s	[kg]
mass salt per area	$m_{s,A}$	[kg m^{-2}]
melt water column height	h_{mw}	[cm]
oceanic heat flux	F_{oc}	[W m^{-2}]
salinity	S	[g kg^{-1}]
sea ice density	ρ_{ice}	[kg m^{-3}]
sea ice permeability	Π	[m^2]
snow thickness	h_{snow}	[cm]
solid mass fraction	ϕ_s	[1]
solid volume fraction	$\phi_{s,v}$	[1]
surface temperature	$T_{surface}$	[°C]
temperature	T	[°C]

Abbreviations

H1cm	Salinity harp with 1 cm vertical spacing
H2cm	Salinity harp with 2 cm vertical spacing
MPI-M	Max-Planck-Institut für Meteorologie in Hamburg
SAMSIM	one-dimensional semi-adaptive grid thermodynamic sea ice model
SAMSIM_original	original SAMSIM model with snow cover
SAMSIM_styrofoam	original SAMSIM model with styrofoam cover
SAMSIM_2017	modified SAMSIM model with snow cover
SAMSIM-HARP	SAMSIM post processing tool
SHEBA	Surface heat balance in the Arctic campaign

empty page

1 Snow on ice - Salt in ice

Sea ice is a powerful boundary between the polar atmosphere and the polar oceans. Beside strongly affecting radiative and heat fluxes (Untersteiner, 1961; Hibler, 1979), the floating sea ice covers the ocean below mechanically. Instead of melting into the open ocean, atmospheric precipitation - in polar latitudes mostly snow - accumulates on the ice surface. This snow cover differs strongly in its physical properties from sea ice due to the different structure of snow, its lower density and the lack of salt. The impact of a snow cover on the subjacent sea ice relating to heat and radiative fluxes is well studied. The most famous examples are the alternation of the albedo due to a snow cover (Grenfell and Maykut, 1977), the insulating properties of snow (Sturm et al., 2002) and the impact of snow on satellite measurements of sea ice. The latter are also strongly influenced by the weight load of a snow cover that changes the freeboard of ice floes (Ongoing research: F. Bunzel and D. Notz).

But how does a snow cover influence the salt content in the sea ice below? - This is the central question I examine in this thesis.

All important processes, which are mentioned in the following, are further described in section 1.2. Sea ice always contains salt. However, the salinity of the ice varies with time. Desalination processes decrease the bulk salt content in sea ice by replacing salty brine with low-salt ocean or surface melt water (Untersteiner, 1968; Notz and Worster, 2009). Snow introduces pure freshwater ice on the surface of the polar sea ice system. Melting snow can either percolate into the ice (Vancoppenolle, Bitz et al., 2007), run off directly into the ocean through cracks in the ice as proved by tracer studies (Eicken, Krouse et al., 2002) or gather first of all on the ice and form meltponds. Meltponds can temporarily be above sea level as long as the ice below is strongly impermeable. However, meltponds absorb much more shortwave radiation than the surrounding snow, which leads to an increasing liquid fraction at the ice–meltpond interface. This results in an increase in permeability below the pond. As soon as the hydraulic head is large enough, the meltpond drains and remains at sea level. The fraction of freshwater that percolates into the ice matrix replaces saline brine and thereby desalinates the ice (Untersteiner, 1968).

These impacts of snow on sea-ice salinity are described in various scientific works which are quoted above to name but a few. All these works share that they either present numerical solutions of the processes based on theories and compare the data to ice cores or executed tracer studies in the ice cover together with ice coring. However, ice core measurements are sensitive to errors in the lower ice layers due to brine drainage (Notz, Wettlaufer et al., 2005) and suffer from a low temporal and spatial resolution. Due to the required manpower ice core data can never reach the temporal and horizontal resolution of several deployed automatic measurement systems. Furthermore, the vertical resolution is limited by the precision in which

the core is cut into slices. And finally, since ice core drilling is destructive, no time series of exactly the same ice bulk can be recorded. Nevertheless, ice core data describes sufficiently the bulk salinity in the upper ice layers before and after snow melt and was therefore used to parametrize the impact of melting snow in sea-ice models without taking into account the exact temporal evolution. One can divide the preliminary ways of modeling snow melt processes on sea ice into two groups. The first group was used among others by Notz and Worster (2009) and by Vancoppenolle, Fichefet et al. (2006). Central idea is that as soon as snow melts, melt water drains off directly into the ice below and either refreezes or flushes the brine system. The second group is formed by SAMSIM, in which Griewank and Notz (2015) describe the snow melt process as snow-to-slush conversion. The conversion means that all snow meltwater together with the lowest snow forms a slush-ice layer on top of the ice. Only when all snow has turned to slush, meltwater starts to flush the brine system in the ice. Griewank and Notz (2015) argue to average over the heterogeneous ice surface during melting by this parametrization.

A relatively new alternative to ice coring is the in situ measurement of vertical profiles in the ice to detect temperature and electric conductivity by so-called salinity harps. The bulk salinity of the ice can be obtained from these two quantities. The measuring method was firstly introduced by Shirtcliffe et al. (1991), established by Notz, Wettlaufer et al. (2005) and continuously further developed by Leif Riemenschneider (LR) within the *Sea Ice in the Earth System* research group at the Max-Planck-Institute for Meteorology in Hamburg (MPI-M). The salinity harps allow for a very high measurement frequency, a much higher vertical resolution as well as an improved horizontal resolution limited by the number of deployed instruments and do not share the uncertainties of ice cores in the deeper ice (section 1.3).

To the best of my knowledge, there is no data set so far that covers the impact of the introduction of a snow cover as well as its melting on the sea ice below in a comparable high temporal and spatial resolution. To fill this gap, I deployed five salinity harps in an ice tank of the MPI-M ice lab and measured the impact of snow on sea ice in five experiments that simulated a whole freezing, thawing and re-freezing cycle. On the basis of this unique time series, I investigate the impacts of snow on the ice below resulting in a more comprehensive understanding of processes other than melt water flushing and the direct dependency of the amount of snow that melts. Furthermore, the temporal highly resolved data improves the understanding of the temporal evolution of melt water flushing and allows for an evaluation of the different model parametrizations. This is done by the help of the 1-d sea-ice model SAMSIM.

1.1 Outline of this work

Due to the further development of the harps and their temperature sensors, a calibration and standardized error estimation was necessary within this work. Methods, results and conclusions are presented in section 3 and 7. Additional surveillance of the measurement credibility was performed during the main experiments. Having this unique set of instruments, I performed five snow experiments that simulates a whole freezing, thawing and refreezing cycle (section 4). These experiments were conducted with different amounts of snow deployed on the ice surface. With this, I measured the impact of the snow amount on sea ice salinity and was able to determine horizontal differences as well as the temporal evolution of the snow impact (section 8). In the same section, these results are compared to the numerical model approach of snow melt and flushing in the one-dimensional thermodynamical sea ice model SAMSIM. It turned out that the previous model approaches of melting snow assumed another temporal evolution of flushing. A change in the parametrization was implemented in SAMSIM and the improved results are presented and discussed in section 10. Further evaluation is made in terms of the overall performance of SAMSIM in comparison to the measured data set. Additionally, I investigate the impact of the amount of snow melt on the absolute salt content change of the subjacent sea ice as well as examine if a snow cover has impacts on the sea-ice salinity in addition to flushing.

1.2 Sea ice is salty

The main physical properties of sea ice that are used and discussed in this work are the temperature T, the liquid fraction ϕ_l and the bulk salinity S_{bu}. In the following, these properties are outlined together with further important characteristics of sea ice and processes therein.

Sea water is a solution consisting of freshwater and sea salt, which is a mix of different salts, dominated by sodium chloride (NaCl). The small percentage of biomass dispersed in sea water shall be neglected here. The mass relation of salt m_s dissolved in fresh water m_w is called salinity S and is defined by:

$$S = \frac{m_s}{m_s + m_w}. \tag{1}$$

In the literature, a broad band of possible units for salinity can be found. The most frequently used are the now outdated practical salinity scale (psu), defined by the conductivity of sea water in Fofonoff and Millard Jr (1983), and the mass relation from equation (1) given in g kg^{-1} or ppt. The difference in values between both of them is marginal, hence no conversions will be made in this work and all values are given in g kg^{-1}, which complies

the newest standard (Pawlowicz, 2013). Psu is still mostly outputted by commercial salinity sensors. The salinity of sea water directly influences its freezing temperature T_f: the higher the salinity S [g kg^{-1}] and the higher the pressure p [db], the lower the freezing temperature T_f [°C]:

$$T_f = -0.0575S + 1.710523 \cdot 10^{-3} S^{3/2} - 2.154996 \cdot 10^{-4} S^2 - 7.53 \cdot 10^{-4} p. \quad (2)$$

The formula is defined for the salinity range of 4-40 psu at atmospheric pressure and given in Fofonoff and Millard Jr (1983). The freezing temperature of salt water is more precisely called liquidus temperature, which is by definition the temperature of a medium when solidification of ice crystals starts. Both notations are used in the same context in this work.

Sea ice is a mixture of solid ice, salty brine and gas inclusion. When it forms out of sea water, pure water solidifies into solid freshwater ice. Sea salt starts to accumulate in liquid brine inclusions in the ice. The colder the ice is, the higher the salinity of the brine S_{br} gets. This effect is covered by equation (2) and in its continuation for higher salinity values, which is here given as inverse function to calculate the brine salinity S_{br} for sea ice directly from its temperature T:

$$S_{br} = -1.20 - 21.8T - 0.919T^2 - 0.0178T^3. \quad (3)$$

The equation is valid for sea water brine in a temperature range between -22.9 °C to -2 °C. For practical reasons and due to an existing jump discontinuity between equation (2) and equation (3) at -2 °C, the latter was used in this work for brine salinity determinations up to 0 °C. For NaCl salt water ice, the brine salinity $S_{br,NaCl}$ can be obtained from:

$$S_{br,NaCl} = -17.6T - 0.389T^2 - 0.00362T^3. \quad (4)$$

Both formulas for brine salinity are taken from Notz (2005) and are based on empirical data.

The inner composition of sea ice can be characterized by fractions of the components. The common way is to give mass fractions for the solid ice ϕ_s, the liquid brine ϕ_l and the gas content ϕ_g. Sometimes it is necessary, to use volume fractions: $\phi_{s,v}$, $\phi_{l,v}$ and $\phi_{g,v}$. The relationship $\phi_s + \phi_l + \phi_g = 1$ must always apply while biomass is neglected.

With having the brine salinity S_{br} and the mass liquid fraction ϕ_l, we can determine the bulk salinity S_{bu} by:

$$S_{bu} = S_{br} \cdot \phi_l. \quad (5)$$

The small amount of gas in sea ice is neglected in this equation. The bulk salinity is equivalent to the salinity of the melted sea ice sample and therefore considers the freshwater in the liquid and in the solid fraction in the ice. One is able to calculate the area specific salt content

$m_{s,A}$ in kg m^{-2} of an ice sample in the depth range z_i to z_{i+1} with:

$$m_{s,A} = \int_{z_i}^{z_{i+1}} \frac{S_{bu}(x) \cdot (\phi_{l,v}(x)\rho_w + \phi_{s,v}(x)\rho_s)}{1 - S_{bu}(x)} \, \mathrm{d}x. \tag{6}$$

In this equation, the density of the brine ρ_w is assumed to be constant. ρ_s is the density of the solid ice.

Ice formation is the result of a phase change in the water from liquid to solid. Hence, latent heat L gets released by the ice during freezing and is needed for melting. The amount of latent heat L which needs to be transported away for freshwater ice formation is L = 333500 J kg^{-1} (value used in the SAMSIM model code, further described in section 5). The same amount is needed to melt the ice. Since sea ice includes liquid parts, the amount of phase change during melting is smaller and thus less energy is needed to melt sea ice in comparison to pure freshwater ice. Furthermore, sea ice has a lower heat conductivity k_{ice} and a higher heat capacity c_{ice} due to its liquid fraction. It is therefore a good thermal insulator with a temperature gradient in the ice that is thus also influenced by the bulk salinity. At the bottom of the ice, the ice temperature T is always at freezing temperature T_f dependent on the local salinity S of the underlying ocean water. Following an upward direction, the temperature T of the ice then is determined by local heat fluxes which are mainly dependent on heat exchange with the atmosphere above the ice. A snow cover on the ice can strongly influence that heat exchange. Snow has a much lower heat conductivity than solid ice due to its high gas content and forms a freshwater source on the ice.

Temporal temperature changes $\partial T/\partial t$ in sea ice due to a vertical temperature gradient $\partial T/\partial z$ can be estimated by the heat conduction equation, which is dependent on the heat conductivity k_{ice}, the density ρ_{ice} and the heat capacity c_{ice} of sea ice:

$$\frac{\partial T}{\partial t} = -\frac{\frac{\partial}{\partial z}(k_{ice}\frac{\partial T}{\partial z}) + q}{\rho_{ice} c_{ice}}. \tag{7}$$

Other fluxes in sea ice are considered through the source and sink q.

Floating sea ice grows at the bottom if enough heat is transported away by heat fluxes to allow a phase change from liquid to solid. Interstitial solid ice formation also comes along with cooling of sea ice. In order to preserve the physical equilibrium state of the brine salinity relative to the temperature, liquid fraction needs to change when temperature changes. Sea ice melting mostly happens on top of the ice, when temperatures rise above local freezing temperature as well as in the ice when it warms. However a heat flux from the water below towards the ice, referred to as oceanic heat flux F_{oc}, is also able to contribute energy for ice melting at the bottom of the ice.

The salt content in sea ice can decrease, caused by so-called desalination processes. So far, five different processes are mentioned in literature: brine segregation, brine expulsion, brine diffusion, gravity drainage and flushing. All this process are well described and characterized in Notz and Worster (2009). The authors suggest that only three of them matter, hence only these are outlined in the following. Brine segregation is disproved by the authors and brine diffusion leads to vertical brine migration with a velocity of about 4 cm a^{-1} and is thus neglectable.

Brine expulsion is an important process for brine redistribution within the ice. Solid ice is less dense than liquid brine. That imbalance causes a pressure increase in brine pockets during freezing and internal phase changes. Brine expulsion leads mostly to brine migration away from the colder towards the warmer parts of the ice. The reason for that is the weaker structure of warmer and saltier ice in comparison to colder and less saline ice. That means in nature during freezing, downwards migration of brine and thus salt transport from the upper to the lower layers of the ice cover. However Notz and Worster (2009) demonstrate that the migration velocity of brine pockets due to brine expulsion can never exceed the growth rate of the ice and thus, no salt can be expelled at the sea–ice interface.

The density of water increases with salinity. The salty brine in sea ice is thus denser than the surrounding sea water. It remains in the ice as long as the ice matrix is impermeable. When the ice gets permeable due to a high liquid fraction, which can be caused by warming or high bulk salinities, gravitational overturning occurs and the salty brine gets washed out of the ice. Less saltier sea water replaces the brine and therefore reduces the bulk salinity of the ice. In literature persisted for a long time the „rule of 5“:sea ice changes its fluid transport properties towards good permeability for a temperature rise above -5 °C, for bulk salinities larger than 5 g kg^{-1} and liquid fractions above 5% (Golden et al., 1998). Modern approaches uses an empirical approximation of the permeability Π of sea ice by the liquid fraction ϕ_l:

$$\Pi(\phi_l) = 10^{-17}(10^3\phi_l)^{3.1} \tag{8}$$

and the theory of a critical Rayleigh number to determine when gravitational overturning happens (Griewank and Notz (2013), Griewank and Notz (2015) and references therein). Gravity drainage is strongest during ice growth due to the high salt content of the ice and during warming due to the increase of liquid fraction. It is the main process of sea ice desalination. Since a strong temperature gradient must have evolved within the ice during growth before gravitational overturning can occur, the upper and thus oldest ice layers mostly remain saltier then areas further down in the ice. Density differences in the brine relative to the underlying ocean water are dependent on the temperature as described by formula (3). With having the bulk salinity of the ice at the bottom always at the salinity of the ocean

water as proved by Notz and Worster (2009), a typical bulk salinity profile in sea ice after freezing has a c-shape.

Snow is a freshwater source on the ice that showed in model studies (Vancoppenolle, Fichefet et al., 2006) and in tracer studies (Eicken, Krouse et al., 2002) the possibility to desalinate the sea ice underneath during melting. The concerning effect is referred to as flushing. With the onset of snow melt the temperature profile of the ice below is likely close to melting too. That causes permeability of the ice if there is still salty brine in the ice matrix. Meltwater from the snow percolates into the brine system and replaces saltier brine which gets either transported further down in the sea ice or escapes the ice completely through cracks or at the bottom. These cracks can be also direct pathways of the snow meltwater. A small field study on Svalbard in 2016 showed that colored freshwater can easily penetrate 10 cm deep into even colder sea ice (sketch figure 1). For the measurement, I placed a cylindrical tube with a diameter of about 22 cm on blank ice and filled it with 3 kg colored freshwater. A lot of colored water flowed off to the side into the snow since the tube was not sealed to the ice surface. However, an ice core that I took below the tube showed that the colored freshwater penetrated 10 cm deep into the ice even though the temperature of the ice was well below melting.

Meltwater that flushes the ice comes not necessarily only from snow, it can also have its origin in a melting ice surface. Blank sea ice can thus desalinate during melting too. However, more likely during snow melt, the downwards transport of replaced brine can lead to an increase of bulk salinity in the lower ice layers if there is an increase of temperature in the downwards profile, which would not be the case if blank ice is melting.

Since flushing occurs at the end of a winter cycle, the grade of desalination is smaller than that of gravity drainage, but flushing strongly influences the salinity of multi-year ice. As soon as the ice reaches a bulk salinity where the brine salinity is smaller than the salinity of the surrounding ocean water at a point when the permeability of the ice is high enough for circulation, gravity drainage cannot further desalinate the ice. Up from this point, only flushing can desalinate the ice further. One approach to investigate flushing is Darcy-law of liquid flows through porous material, which determines the characteristic speed of a liquid flow v through a medium with permeability Π:

$$v = \frac{g\Delta\rho\Pi}{\mu}. \tag{9}$$

$\Delta\rho$ is here the difference in density between the liquid brine and the ocean water below (Griewank and Notz, 2013). The real structure of sea ice is more heterogeneous than approached by Darcy, hence more complex parametrizations are needed to model flushing in sea ice. One possible way is described in Griewank and Notz (2015) and outlined in section 5.

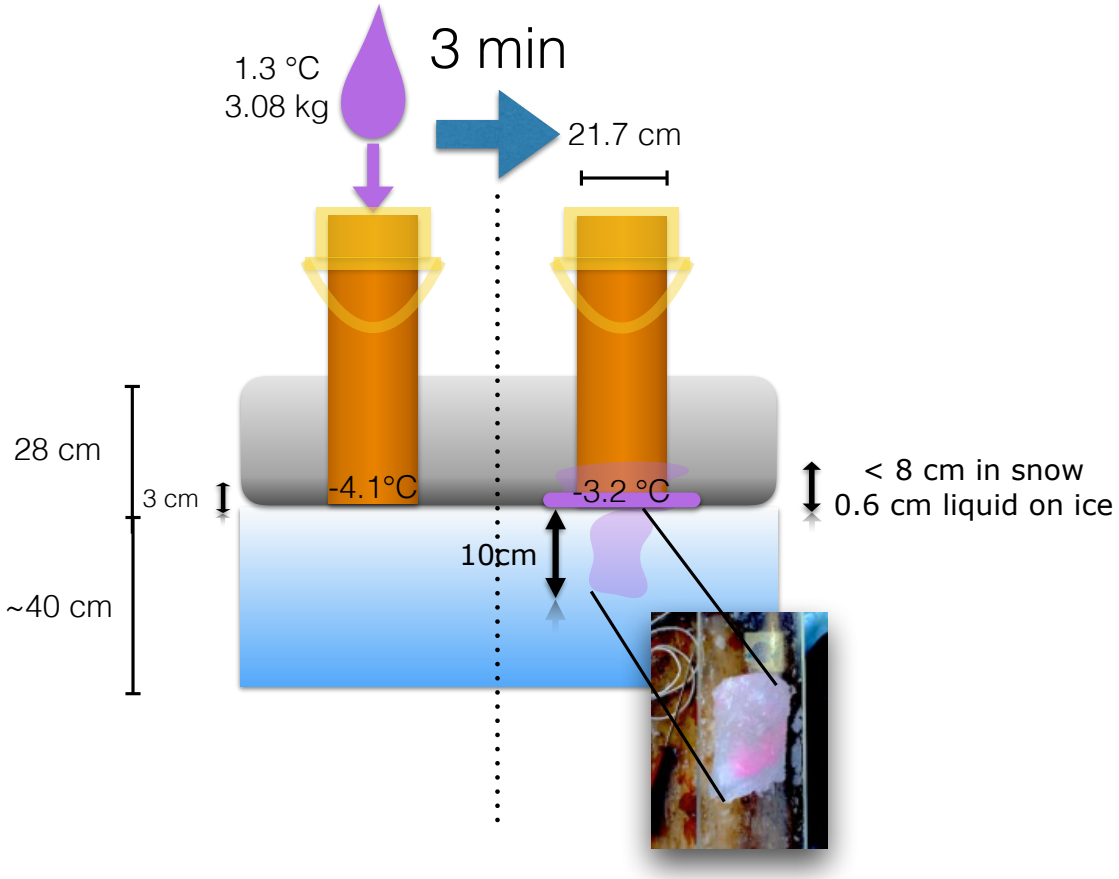

Figure 1: Flushing experiment in Woodfjorden, Svalbard during a field campaign in April 2016. A cylindrical tube of 21.7 cm diameter was placed on the ice and filled with 3.08 kg purple colored freshwater with a temperature of 1.3 °C. The snow cover around the tube was 28 cm thick including a 3 cm thick snow ice layer. The ice underneath was about 40 cm thick and -4.1 °C cold at the surface. A 0.6 cm thick liquid layer remained on the ice after 3 minutes. The snow around the tube was colored up to a height of 8 cm. An ice core that was taken just beneath the tube showed purple dyeing down to 10 cm depth. The tube was covered with a bucket for insulation.

Snow is furthermore a good thermal insulator between the ice and the atmosphere. Sturm et al. (2002) measured the heat conductivity of snow on sea ice in the Beaufort Sea during the SHEBA campaign. The heat conductivity increases with the density of the snow but is also strongly dependent on the snow metamorphism. The snow used in this work is very dense and equals most likely their snow category D: „depth hoar“ and A: „snow ice“. The heat conductivity of the lab snow is thus expected to be in a range between 0.164 W m^{-1} K^{-1} and 0.574 W m^{-1} K^{-1}. They further explain that the heat conductivity of the snow cover on sea ice can be even more complex due to lateral heat flow and convection. However, this heterogeneity is not further investigated here and the heat conductivity seen as constant in the lab as it is in SAMSIM (Griewank and Notz, 2013).

1.3 How salty is sea ice

Beside temperature, sea ice salinity is the most dominating physical property of the ice. Nevertheless, measuring the salinity is a quite demanding task. The most used method is taking ice cores, which determines directly the bulk salinity and the temperature from which the brine salinity can be obtained. Taking ice cores has the great advantage that it can be done everywhere and at any time without treating the ice before. That means, completely undisturbed ice is getting measured. On the other hand, taking ice cores is an invasive method that needs a lot of manpower to get time series. And finally, an immediate brine loss is happening while pulling the core out of the ice. This causes large and uncertain errors in the salinity profile. The error emerges especially at the ice–ocean interface, where smaller bulk salinities are measured in the cores than in the surrounding water while theories and other measurement methods confirm a steady salinity profile at the interface.

Another measurement method, the so-called „salinity harp“, was first introduced by Shirtcliffe et al. (1991) and further developed by Notz (2005). Vertical temperature and conductivity profiles are measured in the ice. From these two quantities, salinity profiles can be obtained. Since all measurements are happening in situ, the instruments have to be frozen into the ice. But with having deployed the instruments once, the method is non-destructive, there is no limitation of measurement frequencies and as Notz (2005) found out, a more accurate salinity profile is measured.

With the great effort of higher vertical and temporal resolution as well as a likely higher accuracy, I decided to use the salinity harp to log salinities in my master thesis.

To better understand the measurement principle of the harp, I recapitulate the idea of two different salinity variables in the ice:

Brine salinity depends on a micro scale physical equilibrium between the liquid brine and its

surrounding solid ice. Only the chemical properties of the salt and the temperature T define the steady state. Temperature measurements and empirical functions for NaCl and Seawater (equations: 3, 4) are used to calculate the brine salinity S_{br}. The lower the temperature, the higher the brine salinity.

With the assumption that there is no gas included in sea ice, respectively salt included in the solid part of sea ice, the bulk salinity is then simply the product of the brine salinity S_{br} and the liquid mass fraction ϕ_l of the ice. And furthermore, the solid volume fraction of the ice is so defined to be $\phi_{s,v} = 1 - \phi_{l,v}$.

The volume liquid fraction $\phi_{l,v}$ is finally the outcome of the conductivity measurements:

$$\phi_{l,v}(t) = \frac{Z_0}{Z(t)} \cdot \frac{\gamma_0}{\gamma(T,S)}. \tag{10}$$

The lower the liquid fraction, the lower the conductivity Z^{-1} in the ice, which can be scaled by the impedance Z_0 in liquid water before ice starts to freeze. Benefiting from this relation, the harp consists of 8 horizontal and parallel titan wire pairs and a control unit that measures the ohmic resistance R between this wire pairs successively (scetch 2). For that, we have to assume that the measured impedance Z is ohmic which is technically not the case. Solid ice forms an electric insulator between the wires, while the liquid brine sets up an inductive cell. Both effects affect the conductivity in different degrees, depending on the AC frequency used for the conductivity measurement. Notz, Wettlaufer et al. (2005) used 2 kHz for their measurements. With the aim to reduce the inductive effect and leading the impedance Z to ohmic resistance R, higher frequencies have been tried out for this work too.

The second term γ_0/γ in equation (10) is called brine sensitivity. It takes the change of conductivity due to temperature and salinity changes into account. While falling temperatures lead to a decrease in conductivity in the brine channels, they do also increase brine salinity, which in contrast increases the conductivity. The latter effect predominates in temperature ranges that I investigate.

Similar to the first term in equation (10), the brine sensitivity forms out of the relation between the conductivity during the onset of freezing γ_0 and the conductivity $\gamma(T(t), S_{br}(t))$ at time t. The theoretical equations (11 and 12) to be used to derive γ are given in Notz, Wettlaufer et al. (2005). The authors refer to deviations between theory and their measurements, so they use slightly different coefficients than the theory proposes.

$$\gamma_{20}(S) = 0.05 S^{0.33} \tag{11}$$

$$\gamma = \gamma_{20} - 0.0015 \Delta T \tag{12}$$

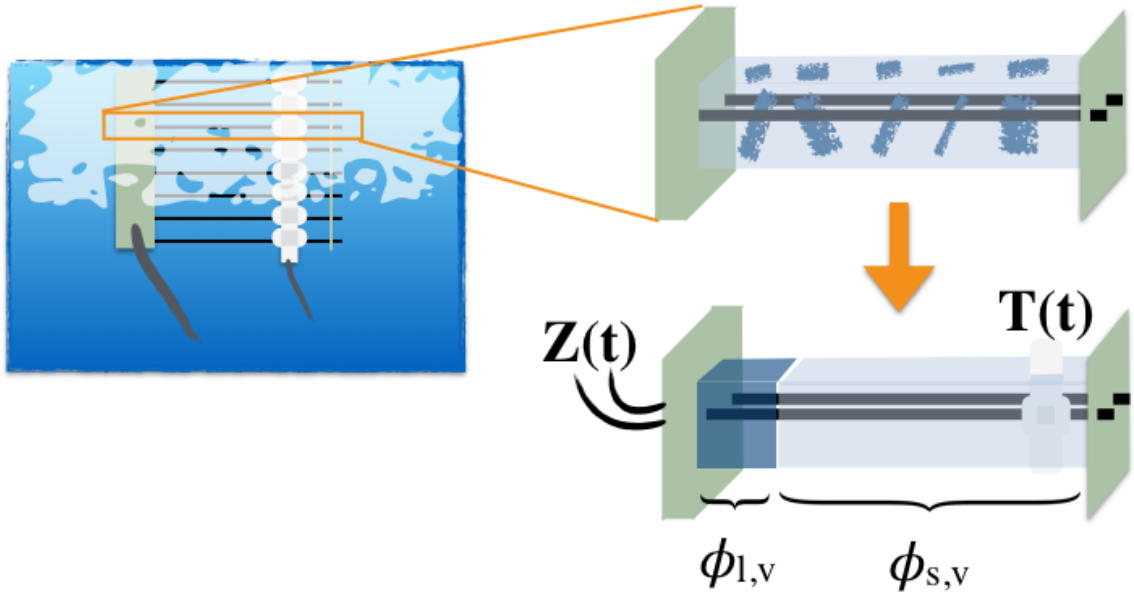

Figure 2: Sketch of the harp measurement principle. The harp is mounted close to the water surface. Sea ice starts to form around the harp, it consists out of solid ice with a volume fraction $\phi_{s,v}$ (lightblue) and scattered liquid brine channels with a volume fraction of $\phi_{l,v}$ (darkblue). The fractions can be theoretically splitted. Temperature $T(t)$ and resistance $Z(t)$ is measured by the harp. The white modules display the corresponding temperature sensors.

Both parameter setups did not fit to the harps I use. Hence, I calculated new coefficients as described in section 3.3, which are then given in section 7.2.

To be able to calculate brine salinity, the obtained volume solid fraction $\phi_{s,v}$ needs to be transferred into mass solid fraction ϕ_s by:

$$\phi_s = \frac{1}{1 + (\frac{1}{\phi_{s,v}} - 1)\frac{\rho_l}{\rho_s}}, \tag{13}$$

in which ρ_s represents the density of solid ice with $\rho_s = 920$ kg m^{-3} and ρ_l the density of the liquid part with $\rho_l = 1028$ kg/m^{-3}, (Values are taken from Matlab script mentioned in section 3.1.1 for comparison reasons).

2 Methods - Commercial reference sensors

Several commercial sensors were used in the work progress to obtain either reference data or to complete the experimental setups. The used sensors are:

Table 1: Reference sensors

Sensor	**operating range**	**measurand**	**Serial number**	**calibration**
SeaBird Electronics SBE37SM MicroCat	water	Temperature ($\pm$ 0.002 K), Salinity (via conductivity ($\pm$ 0.0003 S m^{-1}))	37SM55750-7247	July 2015
RBR XR-620 CTD	water	Temperature, Salinity, Depth (via pressure)	18573	missing, see section 4.5
Greisinger GTH 3700 Series Pt-100 (handhold)	air, water	Temperature ($\pm$ 0.02 K)	32503104	July 2016
Hach HQ40d multi (handhold)	water	Temperature, Salinity ($\pm$ 1 g kg^{-1})	081100026390	missing, see text
Young platinum temperature probe model 41342	ventilated air	Temperature ($\pm$ 0.3 K)	missing	missing, see text

The salinity of the salt water in the reference experiments is measured with the *Hach HQ40d multi*, which I calibrated last time in autumn 2015. The calibration is quite demanding, since the temperature of the standard has to be very precise and temporal constant, which is hard to accomplish. Hence I assume a very vague accuracy of $\pm$ 1 g kg^{-1}. The *Young platinum temperature probe* is also not professional calibrated at the moment, but was checked relative to the handhold reference thermometer *GTH 3700* and to mercury reference thermometers. The accuracy of 0.3 K given in the product data sheet covers the measured deviations by far.

3 Methods - The harp: from evaluation to workhorse

Since the harps I use in my master thesis are a further development of the harps used in Notz, Wettlaufer et al. (2005), I additionally need to evaluate the new models and confirm the credibility of my measurements. To do so, an error estimation method was used similar to the work in Notz (2005) and values were compared to a set of commercial reference sensors, which are described in section 2.

3.1 Reference experiment

The reference experiment was introduced by Notz (2005) and is based on the idea of water being cooled by a cooling plate beneath. This has the great advantage that no salt can be released from the so growing ice neither gravitational to the bottom nor at the ice–water interface on top of the ice. A steady salt profile prohibits salt release through segregation at the ice–water interface (Notz and Worster, 2009). Salt within the ice only gets redistributed vertically in a small range by brine expulsion. The measurement results help us to classify the behavior of the harps regarding different AC measurement frequencies, initial resistance Z_0 determination and measurement accuracy.

3.1.1 Analytical solution

As a reference, I use an analytical solution for mushy layers, the so-called mushy layer equations. Based on heat and salt conservation, they allow for calculations of the temperature and salinity field in a gravitational overturning free condition. This is the case for upward growing ice. Mushy layer equations were used by Worster (1992) and revised later by Chiareli et al. (1994) and again by Notz (2005). My evaluations are based on an implementation of the equations into a Matlab script developed by D. Notz. The code is initialized with the salinity of the water, the bottom temperature which is simultaneously the temperature of the cooling plate, the temperature of the liquid water and the type of salt: NaCl or sea salt. I'm assuming a measurement error of 1 g kg^{-1} for the salinity meter (liquid water salinity measurement), of 0.3 K for the Greisinger GTH 175/Pt handhold thermometer (liquid water temperature measurement) and very broadly of 1 K for the cooling plate (bottom temperature). To take into account all these uncertainties, I'm running the analytical solution for each of the expected value and the largest assumed errors. As a result, the analytical solutions thereby become an ensemble of the different initializations and their corresponding standard deviations. I focus on the ensemble mean in my evaluations. The output solid fraction from the model is actually volume solid fraction, and is therefore directly comparable with the measured solid fraction $\phi_{s,v}$. For bulk salinity calculations it must be transformed

into mass solid fraction as mentioned in section 1.3.

Since I evaluate measured values relative to an analytical solution, some words about the credibility of the computed values should be given here. As mentioned in section 1.2, there are only two dominating desalination processes in sea ice - gravity drainage and flushing - and two further salt redistribution processes - brine expulsion and brine diffusion. Since gravity drainage is dependent on open lower boundaries that allow mass exchange and flushing only occurs in melt situations, both effects cannot occur in the described reference experiments. This means that the mean bulk salinity of the ice can neither decrease nor increase and thus never varies from the salinity of the start solution. Even though the vertical profile of bulk salinity could be modeled imprecisely, the mean bulk salinity gives me a powerful value to evaluate the harp salinity measurement. Furthermore do high solid fractions lead to a linear temperature profile in the ice. Thus temperature is also a powerful variable for evaluation purposes. Since bulk salinity is the product of liquid fraction and the temperature only-dependent variable brine salinity, liquid fraction can be thus also used to evaluate the harp data.

3.1.2 Setup

The reference experiments were carried out in a quadratic acrylic glass tank of the size 34.6 cm x 34.6 cm (picture 3c). The tank is located in a cooling chamber, whose air temperature was always set to freezing temperature of the used NaCl solution (further descriptions to the chamber are given in section 4). Two harps were placed close to the center of the footprint. One harp with a vertical resolution of 2 cm (referred to as H2cm) (picture 3a) and one with 1 cm (referred to as H1cm) (picture 3b). The tank was filled up to 25 cm height with a well steered NaCl in water solution at a temperature slightly higher than its liquidus temperature. The liquidus temperature is the temperature of salt water when ice crystals start to form. Both harps were connected to a control unit that was supplied with power by a lead battery and which logs the raw data on a SD-card. In order to test different AC frequencies for the impedance measurements, six different frequencies were logged: 0.5 kHz, 1 kHz, 2 kHz, 4 kHz, 8 kHz and 16 kHz. That led to a relatively long timespan for one measurement of about 25 seconds per wire pair. And hence, of about 6 minutes to go successively through all 2 x 8 sensors. The tank was cooled from below by an aluminum cooling plate that is drained by an antifreeze mixture. The antifreeze mixture gets cooled by a Julabo FP50-HL Refrigerated/Heating Circulator with a setting resolution of 0.01 °C that is located outside the cooling chamber. Setpoint and actual values of the Julabo were logged and evaluated for unexpected malfunction during night time. None has been observed.

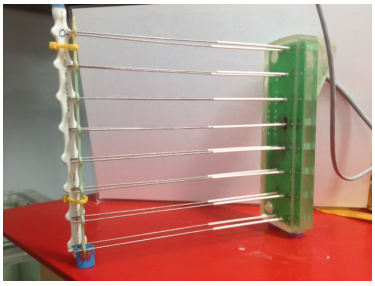

(a) Harp2cm, 2cm vertical spacing

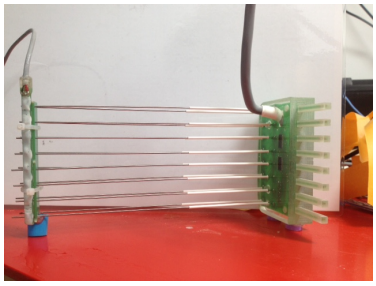

(b) Harp1cm, 1cm vertical spacing

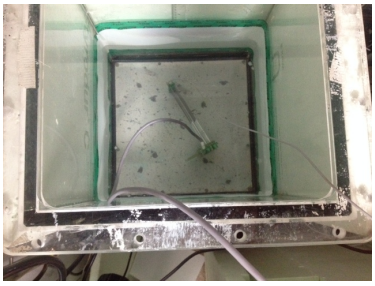

(c) Harp1cm in the cooling tank seen from above

Figure 3

3.1.3 Initialization

I have carried out four reference experiments for the measurement accuracy evaluation (table 2). Three experiments with different salinities and a bottom temperature of 10 K below liquidus temperature of the solution, and one with a somewhat higher bottom temperature of 5 K below liquidus temperature. A fifth experiment was made with sea salt instead of NaCl to transfer the results to the salt combination I used for the later presented snow experiments.

Table 2: Reference experiments

Experiment	Temperature cooling plate [°C]	Salinity [g/kg]	Room temperature [°C]	Ice thickness at the end [cm]
1	-12	34.6	-2	>25
2	-10.6	10.18	-1	17
3	-10.3	5.02	0	22.6
4	-5.3	5.02	0	20.5
5	-5.8	14.78	0	missing

There are no DS temperature values in the first experiments for H1cm and no conversions have been made for salinity values between psu and g kg^{-1}.

3.1.4 Non-dimensional height conversion

The ice thickness is irrelevant in the reference experiments due to constant boundary conditions, only the relative height in the ice defines its physical properties (Notz and Worster, 2009). I can therefore connect each measurement from a sensor with its current relative location in the ice. To do so, I'm dividing the distance between cooling plate and sensor h_{Sensor} through the current over-all ice thickness $h_{ice}(t)$ for each time step to get its non-dimensional height h:

$$h(t, Sensor) = \frac{h_{Sensor}}{h_{ice}(t)}. \tag{14}$$

Since I can only assume the ice thickness for each time step by fitting observational data or using analytical ice growth solutions, a small error must be expected in the non-dimensional height calculation. The error is largest in the beginning of the ice growth due to the ice thickness h_{ice} in the denominator of equation (14). This can be physically explained by the square-root shape growth of the ice and thus, a larger uncertainty in the beginning.

To do statistic evaluation of the data, it is necessary to have values at the same non-dimensional height. Hence, all data is linear interpolated on height-vectors with a vertical resolution of 0.01. Where no data is available from a sensor, the value is set to missing value.

3.1.5 Statistic

The following assumptions have been made for statistic evaluations of the reference experiments:

- standard deviations for all variables are calculated from the set of obtained data instead of using error propagation
- means do not include missing values
- standard deviations are not divided by the square root of the number of measurements as it could be made for a set of several experiments
- calculated BIAS are absolute values

3.2 Temperature sensor calibration

Sea ice is a good thermal insulator as described in section 1.2. Heat conductivity values are in the range of 0.5 - 2.5 W m^{-1} K^{-1} with higher values the colder and fresher the ice is. The water at the ice–ocean interface is always at freezing temperature while the temperature at the air–ice interface varies strongly dependent on the local heat flux balance and thus, in the lab on the air temperature. Hence, strong vertical temperature gradients can develop in the ice, which makes a single point temperature measurement in the ice useless. It is rather expedient to measure the in-ice temperature in several levels in the ice, preferably at the same depths as conductivity and to implement temperature sensor recordings into the controller unit. For this purpose, the so-called T-Sticks were developed by L. Riemenschneider. T-Sticks consist out of eight digital temperature sensors mounted in 1 cm, respectively 2 cm, spacing on a board that has in great measure air inclusions between the sensors to decrease thermal conductivity which would falsify the measurements. The whole T-Stick is coated by a white shrinking hose, for protection reasons as well as to hinder absorption of radiative

fluxes (picture 4a and 4b). The sensor modules have a vertical expansion of 4 mm and it is unclear where exactly on the chip they measure the temperature which introduces a small uncertainty into the measurements. The integrated sensors have a measurement resolution of 0.06 - 0.07 K. The T-Stick measurements showed deviations to the reference sensor I used. Hence a calibration measurement was necessary. To do so, all T-Sticks were mounted together with the reference sensor in a small tank. The tank was filled up with a well steered water solution with calcium chloride ($CaCl_2$) that slowly warmed up from -25 °C to 5°C. The analog reference sensor values were recorded by a Campbell CR2000 data recorder. Since the recorded analog values showed small deviations from the display values of the reference sensor, both values were regularly noted and a linear correction was applied. Two calibration measurements were made: One to obtain calibration values for the T-Sticks and one as a test sample, which I used to obtain an error estimation. Beside the T-Stick calibration values and error values, the reference sensor value correction is given in section 6. Since I used additional T-Sticks beside the temperature sensors of the harps and thus calibrated them too, I distinguish in the following between the two by calling the sensors which are mounted at the harps „DS-Sensors“ and the additional ones „T-Sticks“. The additional T-Sticks have a much higher sampling frequency of about 0.5 Hz.

During the reference experiments, the here used DS-Sensors were tested against Pt-1000 temperature sensors which have a better defined vertical expansion. Finally I decided to use the digital sensors since the Pt-1000 sensors showed a tendency to be temporal unstable.

The sensor alignment of the DS-Sensors was inverse to the conductivity wires for practical reasons in the reference experiments. Hence, they get mirrored in the evaluation, which affects the timestamp marginally.

3.3 Brine sensitivity

The conductivity of the interstitial brine in sea-ice is only dependent on temperature. Temperature influences the agility of electrons as well as the amount of electrical conductive salt ions. While the first dependency showed to be linear for the here approached temperature range, the latter is non-linear. The concerning equations are given in section 1.3. A linear regression for the temperature dependency is made based on measurements with slightly different harp models relative to a temperature value of 0.5 °C, in contrast to Notz, Wettlaufer et al. (2005) who used 20 °C as reference temperature.

Since the impact of the non-linear equation is much higher in the temperature ranges I use than the impact of the linear part, it is determined especially for the new harp models. I obtain the equation from the initial conductivities of the reference experiments extrapolated with equation (12) to 0.5 °C. In doing so, I was able to get specific values for exactly the

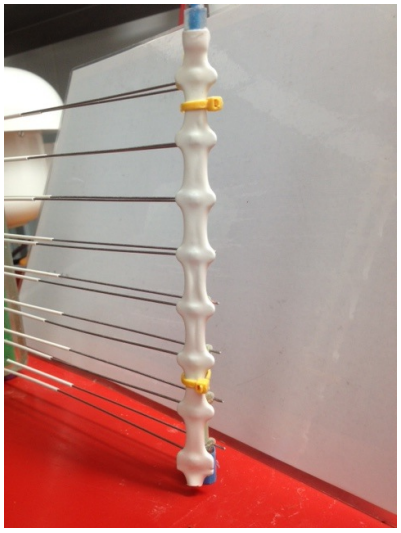

(a) DS-Sensors of H2cm

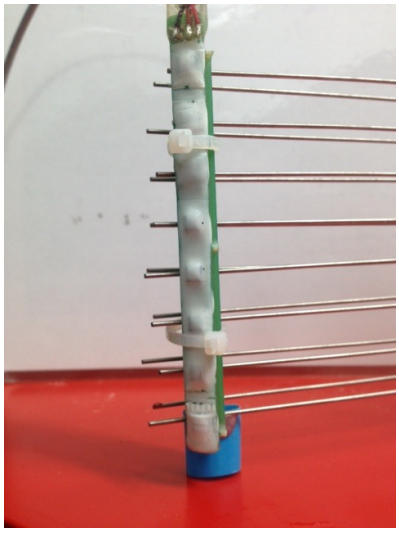

(b) DS-Sensors of H1cm

Figure 4

harp models I use. The non-linear fit is calculated relative to the brine salinity rather than the temperature, to make it independent of the different brine salinity equations which differ dependent on the salt combination. Results are given in 7.2.

3.4 Ongoing evaluation and ice cores

Reference salinity sensors were deployed during all snow experiments in order to keep the credibility of the harp measurements. The way to do so, is described in section 4.5 since further assumptions must be explained before.

Furthermore, ice cores were taken during experiment 4 and 5: two cores in experiment 4 and four in experiment 5. As described in section 1.3, taking ice cores is another method to measure salinity and temperature profiles in the ice. For this work, only salinity was measured with the help of ice cores. Even though these values show large uncertainties in lower levels due to immediate brine outflow, as mentioned in section 1.3, taking ice cores is the most-used method to measure bulk salinity and so, a comparison with the harp appeared reasonable. Moreover ice core data is quite trustable for the upper levels of the ice. The method should be sketched here only, a more exact description is given e.g. in Eicken and Salganek (2010). First of all a reference location similar to the harps is needed that is not too close to the harps, in order to minimize the impact on the harp measurements. Then I use an ice core drill with an inner-diameter of 5 cm to get the core. A picture from the drilling is given in figure 5. Right away after taking the core out of the ice, the drill gets turned into a horizontal position to minimize the brine discharge. Afterwards I measure the length of the core, cut it

into slices of 2-3 cm and melt this samples in hermetic plastic cups. Finally I measure the salinity of the liquid water, by definition this salinity equals the bulk salinity in the core before. The small amount of cores is due to an expected high impact on the other measurements. The following disadvantages occur potentially due to drilling:

- leaves behind a hole of 7.5 cm diameter in the ice that gets filled with slush again, but still affects heat fluxes
- drilling needs downwards pressure that reduces the freeboard, up to a negative freeboard that floods the ice
- saltwater can splash on the ice while taking the core out of the ice
- only a small amount of reference locations is given in the ice tank

All cores that were taken had a very small impact on the other measurements, since the pressure was as low as possible, the few optimal locations were used and no saltwater flooded the ice above the harps.

The cores were taken at the following times and locations (further term definitions are given in section 4):

Table 3: Ice cores

Core	**Time**	**Location**	**Core length [cm]**
	Experiment 4		
Core 4.ref1	during refreezing	between ref and snow	8.5
Core 4.ref2	during refreezing	close to ref	10
	Experiment 5		
Core 5.before	before snow deployment	between ref and snow	12.5
Core 5.snow1	after melting	close to snow harps	10
Core 5.snow2	after melting	close to snow harps	14.5
Core 5.ref	after melting	close to ref harps	6.5

Figure 5: View on the ice core drill from the side during drilling close to reference harp 1.

4 Methods - Snow experiments

No lab measurements focusing on the impact of snow on sea-ice salinity have been made so far to the best of my knowledge. Hence, being provided with this unique measurement instrument setup, I recorded five freezing and melting cycles in the ice lab of the MPI-M which I refer to as „snow experiments 1 - 5“. In the following I outline the technical data of the lab and the tank, the arrangement of instruments and the specifications of the five snow experiments I conducted.

4.1 The tank

All experiments were carried out in the MPI-M ice lab. The ice lab consists of a cooling chamber that contains a large glass tank in which I mixed sea water out of freshwater and *Tunze Reef Excel Lab Marine Salt*. The salt ionic combination is very close to that of Atlantic seawater. The water level in the tank was 94 cm for all experiments, while the salinity changed a bit in the range of 25.3 - 31.4 g kg^{-1} (table 5). The water in the tank gets cooled by the air above while the walls and the bottom are well insulated with styrofoam. This setup equals natural circumstances, since horizontal fluxes are almost non-existent in ice. The floor area of the tank is 196 cm x 66 cm, thus it contained about 1216 l seawater.

4.2 Free floating ice

Due to it's buoyancy in water and the strong local heat fluxes, ice forms initially at the air–water interface. While growing downwards, ice occupies more space than the water it grows from, due to it's lower density. Thus, the pressure in the underlying water rises rapidly if the ice sticks to the wall. Since sea ice is a permeable medium, salt water from below would get pressed through the ice, or the tank could even burst. At least the salinity measurements would get disturbed by the water percolating through the ice. Hence, I needed free floating ice, which I realized by a heating wire, being attached in a helix pattern around the tank from 0 cm to 20 cm water depth. Furthermore a non-sticking Teflon foil covers this heating wires, reaching from 3 cm above the water to 30 cm water depth. The combination of heating, non-stick Teflon and convection in the water allows the ice to float freely (sketch 6a). Even though the convection cell was enclosed between the Teflon and the glass wall, the ice got melted stronger at the lower outsides and became a lens shape at the bottom side.

Free floating ice requires free floating ice-sensors too. Epoxy resin has the largest volume fraction of the instruments, it's density is only slightly higher (about 20%) than the density of water. Hence, I neglect the instruments weight force in water. But they must not be fixed against upward movement, since the thicker the ice gets, the more freeboard it develops.

Fixed instruments would hinder the freeboard to develop, or even the instruments would get damaged. To avoid this, I developed mountings that keep the instruments horizontally fixed and prevent them from moving deeper than the start depth with the help of thick rubber bands (sketch 6b). The upward motion is unhindered. The technique has the positive side effect that from elongated mountings one can always see if the ice floats freely and measure the freeboard. I used plastic as material for the mounts to avoid extra weight and artificial heat fluxes. The latter are also reduced since the mounts are completely immersed.

4.3 The cooling

The ice in the tank should experience a complete freezing and melting cycle, initiated by different air temperatures. The air temperatures in the cooling chamber can be set from outside with a resolution of 1 K. Since it's a common cooling chamber there are several limitations in doing so:

- every six hours the refrigeration element is de-freezing, which introduces strong spikes in air temperature up to 0 °C
- the cooling chamber has no heating, hence temperature rises can only be initiated by heat fluxes from outside into the chamber and by the heating wires in the tank
- the refrigeration element is mounted above the left side of the tank (picture 7), making the ice thickness horizontally heterogeneous
- there is a threshold up to which the air temperature in the chamber can rise until the cooling switches on again. This behavior introduces fluctuations in the air temperature of about 3 K.

Measurements in different distances to the water surface have shown that at least the temperature fluctuations reduce by 1 K to 2 K close to the water surface, respectively ice surface. The thickness heterogeneity was damped by a fan above the tank and additionally by a shield between the tank and the refrigeration fan, being established after experiment 1.

4.4 Heat fluxes

To be able to reconstruct measurement results later on and as model input, heat fluxes to the ice, respectively water, needed to be recorded. I outline these fluxes in the following from the ice bottom up, starting with the so-called oceanic heat flux, which includes all heat fluxes that reach the ice from below. In the tank that means: heat fluxes through the insulation and heat fluxes introduced by the pumps as well as by the heating wires. The total

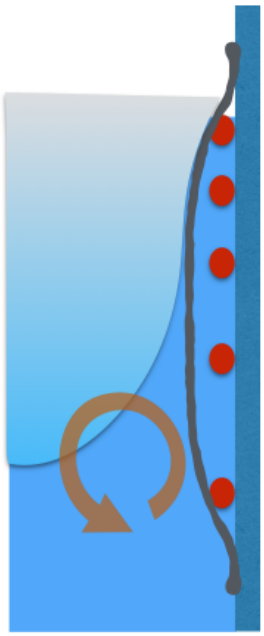

(a) Side view sketch of the tank wall. Heating wires (red) are fixed horizontally at the glass wall (darkblue) and covered with a Teflon foil (grey). The ice gets a lens shape due to a convection cell at the wires (orange).

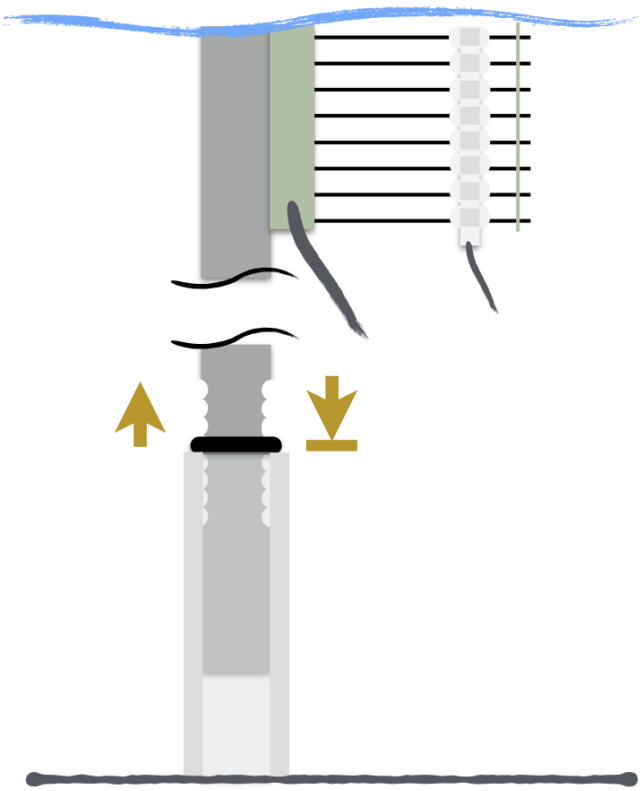

(b) Sketch of the harp mounts. A cylinder is fixed on the tank bottom, a rod with notches and a thick rubber ring for height adjustment sticks therein. Two instruments can be fixed easily at one rod.

Figure 6

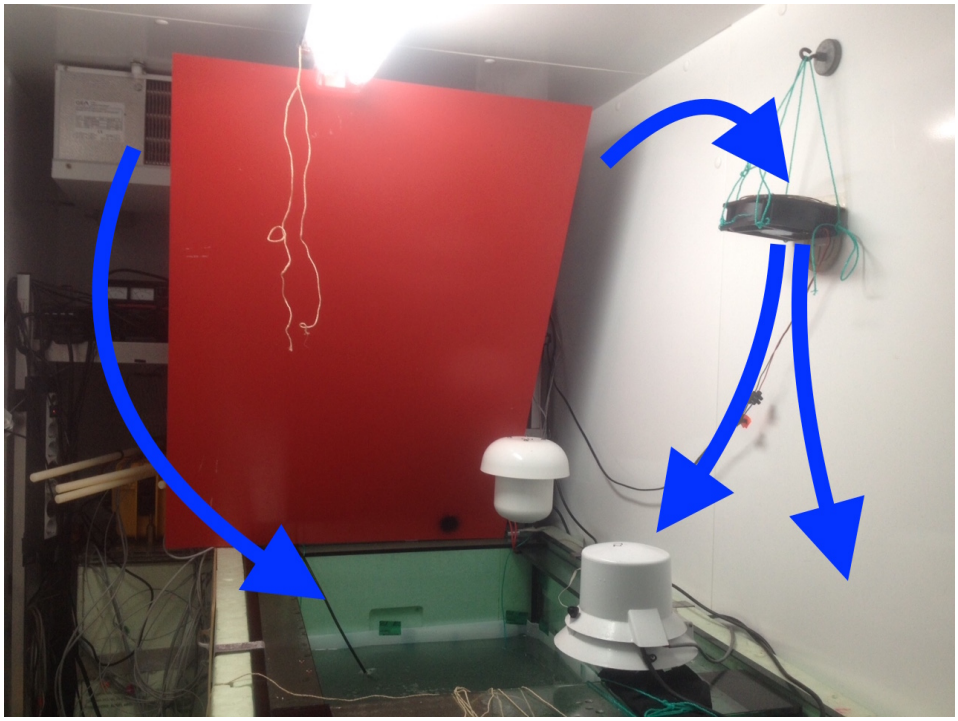

Figure 7: View from the right side of the large tank into the cooling chamber. The refrigeration element is mounted at the ceiling in the back. The red shield in front of the cooling as well as the ventilation on the right side in the picture ensure an uniform distribution of the cold air in the chamber. The blue arrows indicate cold air flows in the chamber and the insulation of the large tank is visible through the green styrofoam plates around the tank.

amount of heat $P_{heating}$ initiated by the heating wires is simple to measure, because I set it on the power supply myself. In contrast the heat flux initiated by the wires Q_{heat} is hard to distinguish, since one cannot perceive the amount of heat that affects the ice bottom. I have to assume that the heat is partly also diffusing into the wall and into the air, between ice and wall. A simple parametrization should be used for this work: $Q_{heat} = k_{heat} \cdot P_{heating}$, where k_{heat} is a constant for all experiments. The heat flux by the pumps Q_{pumps} and through the walls Q_{wall} are not measured, they are assumed to $Q_{pumps} = 5$ W and $Q_{wall} = 0$ W. Horizontal heat fluxes in the ice are small and thus neglected. Eventually I reach the ice surface, respectively water surface, in my description. Only sensible heat fluxes and longwave radiation should be considered here. The reason is that latent heat fluxes were small during the measurements in comparison to sensible heat fluxes (about 6.5 l water evaporated during three weeks), the same counts for shortwave radiation. Two 18 W lamps are installed in the chamber, but they have been switched off most of the time during the experiments, especially during the freezing times in experiment 3-5. Furthermore, ice has a high albedo and most of the shortwave radiation would be still reflected. Longwave radiation is proportional to T^4, I assume that temperature differences in the ice chamber are small enough that it can be linear approximated as part of the subsequently presented sensible heat flux approach. Sensible heat fluxes Q_{sens} at the interface are formed by temperature gradients between the water or ice surface $T_{surface}$ and the air T_{air}. Standard parametrizations from meteorological standard work to calculate sensible heat fluxes cannot be used, since the properties of the lab differs strongly from natural conditions. The higher walls of the tank form a basin above the ice and ventilation in the chamber disturbs every type of typical meteorological stratification. Hence, a linear approach is used for this work, which was already implemented in the numerical model SAMSIM:

$$Q_{sens} = \alpha_{st,unst} \cdot (T_{surface} - T_{air}). \tag{15}$$

The effectivity parameter α has two values, one for stable α_{st} and one for unstable stratification α_{unst}. The stratification is unstable if the air above the ice is colder than the ice and vice versa.

In order to derive all heat flux parameters (k_{heat}, α_{unst} and α_{st}), I combine them into one equation for heat fluxes at liquid water surface conditions:

$$c_l \cdot m_{water} \cdot dT_{surface} = Q_{sens} \cdot dt + Q_{heat} \cdot dt + Q_{pumps} \cdot dt \tag{16}$$

which leads to

$$\frac{dT_{surface}}{dt} = \frac{\alpha}{c_l \cdot m_{water}} \cdot T_{surface} - \frac{\alpha}{c_l \cdot m_{water}} \cdot T_{air} + \frac{k_{heat} \cdot P_{heating} + Q_{pumps}}{c_l \cdot m_{water}}. \tag{17}$$

Since $c_l, m_{water}, T_{surface}, t, T_{air} and P_{heating}$ are measurable or literature values, I can obtain all parameters from a measurement which I explain in the following.

1216 l of seawater with a density of 1023 kg m^{-3} gets warmed and cooled in the large tank by varying the ocean heat flux, the air temperature and the pumping. I simultaneously record all necessary values to determine the heat flux parameters afterwards. The pumping is varied too, because I wanted to double check my assumption of 5 W. The SBE 37SM temperature sensor is used to get the reference temperature value. It is, due to practical reasons - mounted on the bottom of the tank, while the RBR temperature sensor is mounted right bellow water level. I used the RBR values to check for stratification in the tank, regarding temperature and salinity. Considering also the impact of pumps, I need at least four different combinations of heat forcings. To get a more precise result, I eventually decided on seven cases which are given in table 4. T_{Room} is in that respect the temperature that I set for the whole cooling chamber.

Table 4: Heat flux forcings

Case	α	T_{Room}	$P_{heating}$	**Pumps**
1	stable	11	0	On
2		11	32	On
3		11	72	On
4	unstable	-3	72	On
5		-3	0	On
6		-1	0	On
7		-1	0	Off

The air temperature gets measured by the Young ventilated air temperature sensor (section 2). It was mounted close to the center of the tank with the air intake 5 cm above water level. The sensor was mounted in the same way for all snow experiments in the large tank.

Some further assumptions I have to make, to be able to measure and use the results afterwards are: First of all, I avoid an ice surface, since latent heat fluxes through ice formation are hard to distinguish. Hence, measurements take place at water temperatures above freezing point and in this way the differential equation (17) can be used to obtain the parameters. Furthermore I assume that sensible heat and longwave radiation fluxes are the same at water–air and ice–air interfaces, so that I can use the results later on also for ice surfaces.

I approach the temporal evolution of the air temperature by a quadratic fit function:

$$T_{air} = a_1 \cdot t^2 + a_2 \cdot t + a_3. \tag{18}$$

With different a_1, a_2, a_3 for each heat flux forcing.
Furthermore it should be

$$a = \frac{\alpha}{c_l \cdot m_{water}}; d = \frac{k_{heat} \cdot P_{heating} + Q_{pumps}}{c_l \cdot m_{water}} \tag{19}$$

and so, a possible solution for the differential equation (17) is:

$$T_{surface}(t) = \frac{2a_1}{a^2} + \frac{2a_1 t}{a} + \frac{a_2}{a} - \frac{d}{a} + k \cdot e^{at} + a_1 t^2 + ct + a_3 \tag{20}$$

with k being defined by the start conditions:

$$k = T_{surface}(t_{start}) - 2 \cdot \frac{{a_1}^2}{a} - \frac{2bt_{start}}{a} - \frac{a_2}{a} + \frac{d}{a} - a_1 \cdot t_{start}^2 - \frac{a_2 \cdot t_{start} - a_3}{e^{at_{start}}}. \tag{21}$$

Results and an interpretation is given in section 5.2.

4.5 Salt balance

This section describes an ongoing harp evaluation method that is mentioned in section 3.4. Since the tank is a closed system for salt, I deployed two reference temperature and salinity sensors in the tank, as well as pumps at the short ends of the tank. Thereby, I could measure the salt discharge from the ice into the liquid water and monitor the credibility of the harp salinity measurements. The SBE 37SM temperature and salinity sensor measured at the bottom of the tank, while the RBR sensor measured between a water depth of 17 cm to 33 cm, varying between different experiments. I trust the SBE 37SM data very much, since it had been calibrated professionally short time before my measurements. The RBR sensor had no up to date calibration, but in tests in which both sensors (RBR and SBE) were mounted close to each other, its values equal the one measured with the SBE 37SM. In conclusion, I used the RBR to monitor stratification in the tank, to be sure that the SBE 37SM values can be used for mass balance calculations which neglect stratification. Due to extreme small values, it is furthermore valid to neglect water evaporation, which would also lead to an increase in salinity int the tank.

4.6 Five different experiments with increasing snow cover

The here introduced measuring sensors give us a unique possibility not only to investigate flushing in sea ice, but they also create a reference data package for future model evaluations as well as an error estimation for future lab experiments. To do so, I performed five different measurements with increasing snow covers but same over-all procedures. I first want to outline the procedure I used for all experiments:

The sensor setup is showed in figure 8. Snow harps 1 - 3 were covered with snow, while reference harps 1 - 2 served as reference harps that were not covered with snow. All harps except for harp snow 3 have 2 cm vertical spacing and measure temperature and impedances in 8 vertical levels. Harp snow 3 consists out of two harps with 1 cm vertical spacing, each having 8 vertical levels too. That means, harp snow 3 has 1 cm spacing and 16 vertical levels. All commercial reference sensors were mounted as described in section 4.4 and 4.5.

The common temporal course of the snow experiments was then:

1. very low air temperatures and freezing up to an ice thickness of about 14 cm, P_{heat} high to avoid sticking
2. temperature at about -5 °C to reach equilibrium state, ice thickness constant, P_{heat} lower to avoid high heat influx
3. freeze plastic frame to ice with freshwater
4. bring a specific amount of snow on the ice. cover no snow areas with styrofoam.
5. wait until snow is in thermal equilibrium
6. air temperatures up to 5 °C, $P_{heat} = 0W$ until melt rates of the snow cover decrease again
7. temperatures below freezing point in order to simulate autumn time. low P_{heat}
8. melt the ice

The styrofoam cover was used to compensate the insulation properties of snow (picture 9). Since I want to investigate the impact of snow on sea-ice salinity rather than on temperature, it is important that sensible heat fluxes on the ice surface are the same for the snow and the reference harps. I used 2 cm thick styrofoam plates which have a heat conductivity of about 0.17 W m^{-1} K^{-1}. That is almost the same as the heat conductivity of powder snow. Since the snow I produced was much denser than powder snow and coarser in shape, it had a higher heat conductivity as described in section 1.2. The thicker snow cover in comparison

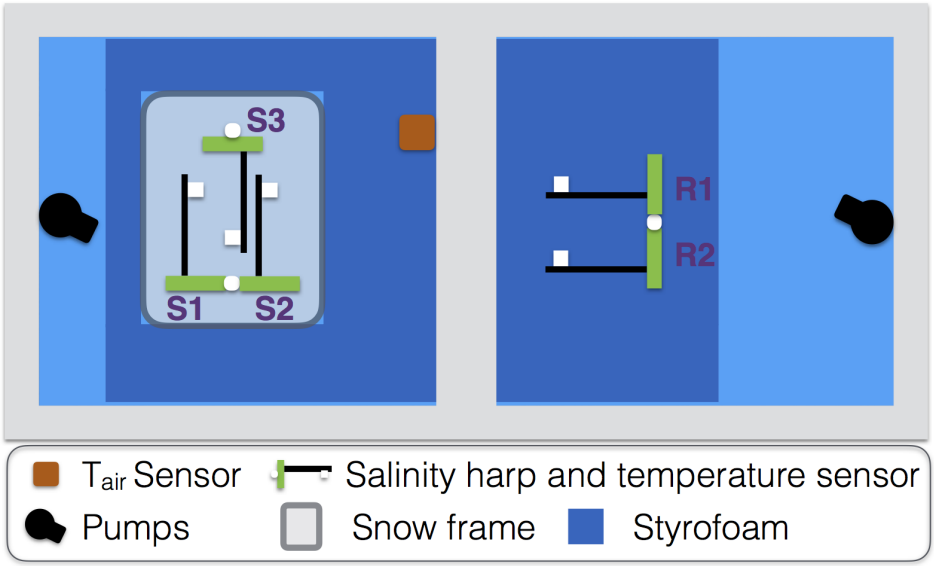

Figure 8: Top view sketch of the large tank. On the left side of the tank are snow harps 1-3 (S1 - S3) and on the right side reference harps 1-2 (R1 and R2). The bar in the center is a glass bridge above water level, it serves as mounting point of the air temperature sensor T_{air}. The snow frame and styrofoam areas show where both are deployed on the ice during melting.

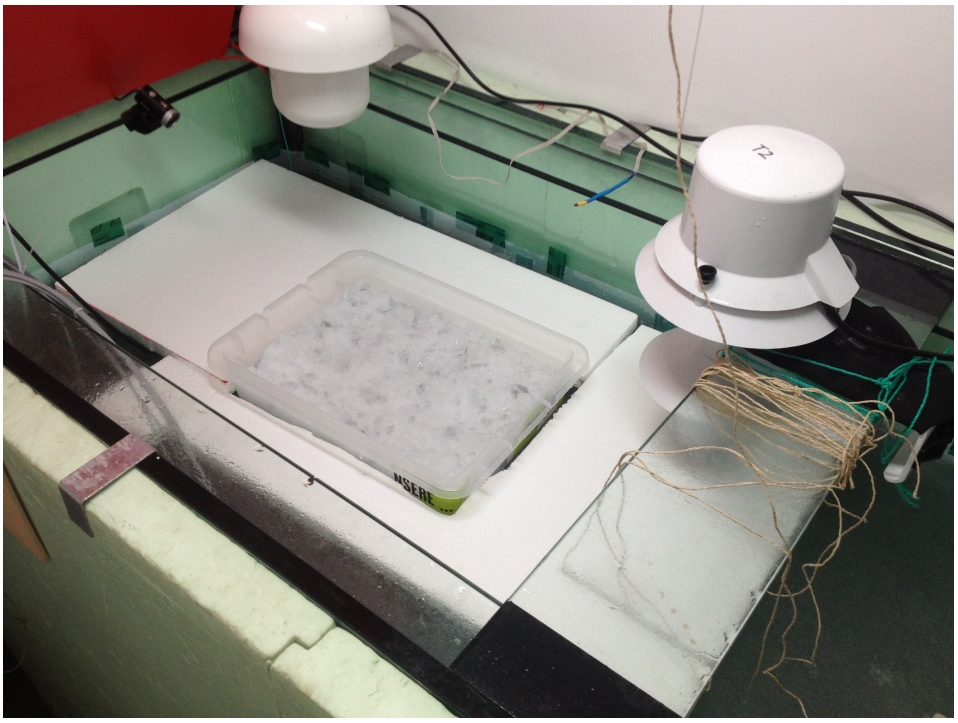

Figure 9: Styrofoam plates deployed on the ice during melting.

to the thin styrofoam should be thus comparable in heat conductivity. Temperature profiles given in section 8 approve this assumption.

One whole experiment took between 2 to 3 weeks. Thus, the relationship from length- to timescales in the heat diffusivity equation (7) is almost similar between the lab and natural circumstances. For that, I assume to simulate one year of about 1 m thick sea ice in nature with 15 cm thick sea ice in the lab. However, the Rayleigh number as main non-dimensional parameter in the setup is even constant, since all parameters included in the definition stay the same in the lab as in nature and the change in length scales reduces in the fraction. The Rayleigh number strongly governs the desalination due to gravity drainage (Griewank and Notz (2015), equation: 1).

Since the circumstances in the tank are similar for the snow and the reference harps until snow is introduced into the system, I can easily investigate horizontal homogeneity in the tank up to this moment and calculate error values for harp lab measurements. Results are given in section 8.2.

Artificial snow that is equivalent to natural grown snow in density and grain size is impossible to produce in the lab. Since my aim was to have a less dense frozen freshwater source on the ice that melts slowly into the ice, I decided to use shredded crushed ice as snow equivalent. Grain sizes, liquid water fraction and thus densities are higher in comparison to natural snow, but the mentioned main intention is fulfilled. The snow had a temperature of -1 °C to 0 °C in each experiment at the moment when it was lain on the ice. The mass of the snow and its volume expansion give me the mean density of the snow pack for each experiment (table 5). In order to avoid liquid water run out of the snow, I strained the shredded ice before deploying it. A plastic frame, the so-called snow frame, defines the area where snow covers the ice (picture 10). Starting from experiment 3, the snow frame was sealed with freshwater on the ice before the snow was deployed.

While there were also differences in the absolute temperature values, the main distinguishing feature between the measurements is the amount of snow that lied on the ice (table 5). This differentiation was chosen to investigate the impact of the amount of meltwater that percolates through the ice on its absolute salt content change.

Table 5: Snow and ocean properties

Experiment	1	2	3	4	5
Snow thickness [cm]	3	4	6	6.5	10
Snow density [kg m^{-3}]	618	515	465	490	456
Initial water salinity [g kg^{-1}]	25.3	26.1	26.1	27.0	31.4

Figure 10: New deployed snow in the snow frame on the ice. One T-stick is visible in the upper center and additional insulation of snow harp 3 as a black area in the center.

5 Methods - Numerical model

Numerical models never mirror reality but often help us to understand complex interactions, since small changes and its impacts as well as extreme situations can be studied. I'm using SAMSIM, a 1d thermodynamic model developed by Philipp Griewank, for model studies in this work. As long as the model is capable to simulate the mean state and works in a mass and heat balancing manner, I will assume that process studies can be carried out with the help of the model. A detailed description of SAMSIM is given in Griewank and Notz (2013) and Griewank and Notz (2015). Only the main model principles should be described here.

SAMSIM is a 1d thermodynamic sea ice model with a semi-adaptive grid. That means, the ice gets divided into adaptable vertical layers that always keep a manually configured vertical resolution towards the top and the bottom of the ice. The resolution towards the center of the ice can decrease with increasing ice thickness in order to save computing time. The reason for this distinction is that physical processes increase in complexity towards the boundaries of the ice as well as stronger gradients occur there. Fluxes between the layers and scalar variables are calculated based on energy and mass conserving equations. The structure of the ice which strongly influences desalination processes is parametrized with respect to each single process. Griewank and Notz (2013) and Griewank and Notz (2015) implemented mostly simple and complex parametrizations, but only the latter are used in this work.

5.1 Heat fluxes

Surface fluxes are obtained in SAMSIM as a result of a flux balance. The 2 m air temperature and radiative heat fluxes need to be known among others for this calculation. As described in section 4.4, these boundary conditions do not apply to the conditions in the MPI-M ice chamber. Hence, a simple linear parametrization for surface heat fluxes was developed by P. Griewank in connection with the master thesis of Wiese et al. (2012). The surface heat flux Q_{sens} is determined by the temperature gradient between the ice surface temperature $T_{surface}$ and the air temperature T_{air} and by a stability dependent heat exchange parameter $\alpha_{st,unst}$:

$$Q_{sens} = \alpha_{st,unst} \cdot (T_{surface} - T_{air}). \qquad \text{(15 revisited)}$$

This implemented parametrization was only made for blank ice surfaces and is unable to handle snow covers on the ice, thus a new method needed to be implemented. To keep it simple, I added snow cover to the lab parametrization in almost the same manner as snow is implemented in the standard atmospheric implementation. The difference to the atmospheric implementation is that heat fluxes at the snow surface are here calculated with the lab parametrization of a linear dependency. I assume that the stability parameters α_{st}

and α_{unst} are the same for snow covered and uncovered sea ice. Snow is seen in SAMSIM as one layer, thus it only has one temperature value. By using this temperature to calculate the heat flux in the same way as using the temperature of the uppermost ice layer, I neglect the lower heat conductivity and potentially larger vertical expansion of snow in comparison to sea ice. Model runs in comparison to measurements show that this a valid simplification.

External heat fluxes affect the ice not only at the air–ice interface, but also as ocean heat flux at the ice–sea interface as described in section 4.4. This ocean heat flux is also part of the model forcing and is given in the lab by the heat input of the heating wire $Q_{heat} = k_{heat} \cdot P_{heating}$ and the pumps Q_{pumps}. In order to get a proper model forcing, the mentioned heat flux parameters were determined in a specific experiment, which is also described in section 4.4. Since the outcome of this experiments are necessary as model input, results are given in the following subsection.

5.2 Heat flux parameter determination

As a measurement result parenthesis, I describe in the following the approximation of the introduced heat flux parameters with the help of the heat flux experiment setup described in section 4.4 and the therein specified equation:

$$T_{surface}(t) = \frac{2a_1}{a^2} + \frac{2a_1 t}{a} + \frac{a_2}{a} - \frac{d}{a} + k \cdot e^{at} + a_1 t^2 + ct + a_3. \qquad \text{(20 revisited)}$$

Due to its discontinuity, introduced by altering air temperature regression coefficients a_1 - a_3, the function cannot be used for automatic curve fitting based on least square methods. So I use it to determine the heat flux parameters manually in the following manner. First of all, it is obvious that the impact of the pumps is strongly nonlinear in combination with the other heat sources. To simplify it, 5 W should be assumed as pump heat flux to the ice if the pumps are switched on. Secondly, I start with investigating only the cases where $P_{heat} = 0$. In doing so, I determine the air–ice, respectively air–sea, heat exchange parameters to $\alpha_{st} = 29$ and $\alpha_{unst} = 30$. Having thus obtained the impact of the pumps and the sensible heat fluxes to the air, the impact of the heating wire can be determined to 50% of the real heat input, that means $k_{heat} = 0.5$. The latter differs strongly to measurements especially during warming. I assume that the error is introduced by the non-linear impact of the pumps and thus cannot be defeated in the frame of this work. The so calculated temperature development for the stable and the unstable case is plotted in figure 11. The strong impact of both oceanic heat fluxes is getting obvious. Switching off the pumps negatively affects the calculation and the heating wires influence especially the stable situation remarkably. The atmospheric heat exchange parameters in contrast seem to be well defined for the liquid water situation.

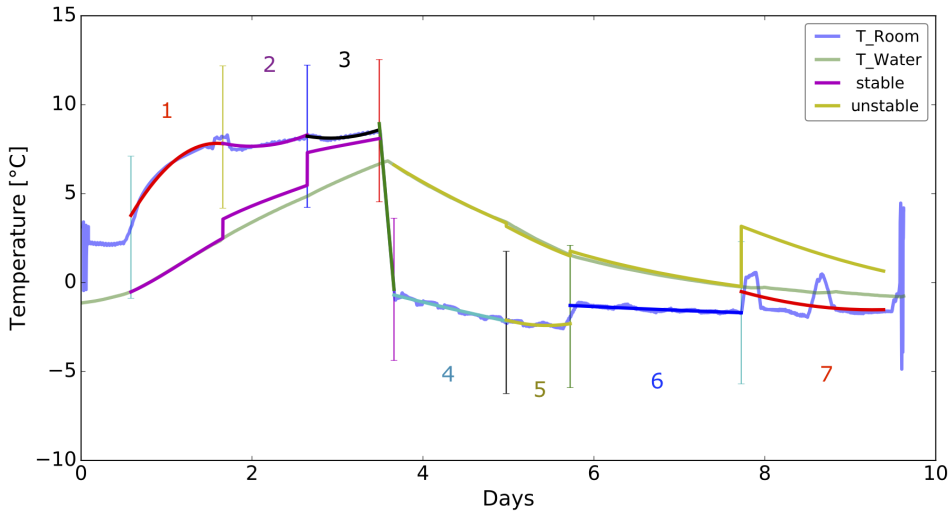

Figure 11: Calculated and measured temperature evolution during the heat flux experiment for stable and unstable situation. The colorful lines represent the particular air temperature fit function for each case. The vertical lines separate the different cases 1-7 given in table 4.

But the here determined α values produce much higher ice thicknesses in SAMSIM than observed in the lab. The initial value for $\alpha_{unst} = 22$ shows a much better behavior while the initial value for $\alpha_{st} = 15$ seems to be to small. Hence as conclusion of the experiments and the experiences I choose $\alpha_{unst} = 22$ and $\alpha_{st} = 21$ as the final parameters. The difference in α_{st} to earlier modeled lab setups can be explained by a strong air ventilation which I installed in the ice chamber. I assume that the discrepancy in the atmospheric heat exchange parameter is introduced by the ice cover in the snow experiments. Nevertheless teaches this experiment a lot about the ratio between the stable and the unstable parameter.

If styrofoam covers the ice in the snow experiments, surface heat fluxes are reduced about 70%. The heat flux parametrization prevents from a more exact calculation based on the heat conductivity of styrofoam. The factor 0.3 is obtained through model and measurement comparison.

5.3 Model freeboard

Another simplification that is used in this work in SAMSIM is located in the freeboard calculation of SAMSIM. The high snow densities and thicknesses in connection with ice thicknesses of about 14 cm would lead to a clear negative freeboard which would lead to intense flooding of the ice surface and the snow cover in the model calculations. However in the lab, only a small fraction ($\sim$0.07) of the floating ice is covered by snow, and thus, the influence on the ice freeboard is marginal. For that reason, I removed the weight of snow from the freeboard calculation in the lab setup.

5.4 Initialization

In order to compare simulated results with measurements, I run SAMSIM with the same forcing as the snow experiments. That means measured timeseries of air temperature, ocean heat flux, snow precipitation, styrofoam cover and liquid water temperature are used as model inputs. I run the model with a temporal resolution of $\Delta t = 1$ s and a vertical resolution of $\Delta z = 1$ cm. The number of possible vertical layers is high enough to keep the resolution constant through the whole timeseries. The relatively rough vertical resolution was chosen since a finer one tends to reduce the harmonic permeability of the layers, and thus impermeable layers appear more likely as a result of the numerical calculations. The coarser resolution prevents the formation of thin impermeable layers by averaging over a larger vertical range. Furthermore is the Courant-Friedrich-Lewy (CFL) stability criterion always by far fulfilled (defined by Griewank and Notz (2013)).

5.5 Snow melt

With the onset of melting, phase changes happen to ice crystals in the snow from solid to liquid water. Snow can be saturated with this melt water up to a certain limit, the maximum liquid water mass fraction $\phi_{l,max}$. That limit is determined in SAMSIM by the solid mass fraction in snow $\phi_{s,snow}$. Griewank and Notz (2015) took the corresponding equation from a laboratory study of Coléou and Lesaffre (1998):

$$\phi_{l,max} = 0.057 \cdot \frac{1 - \phi_{s,snow}}{\phi_{s,snow}} + 0.017. \tag{22}$$

Figure 12 outlines the further evolution of snow melt water in SAMSIM. Excessive melt water from saturated snow gathers at the snow–ice interface, where it forms together with solid parts of the snow a process medium that can be seen as slush-ice layer. The process is thus referred to as „snow-to-slush conversion“ in this work. The slush ice is then added to the uppermost ice layer. The thickness of the slush ice layer is determined in such a way that the gas fraction is 20% (Griewank and Notz (2015) referring to Eicken, Lensu et al. (1995)) and the solid fraction equals the one of the previous time step. By adding the slush, the uppermost ice layer is also growing in thickness. Once the layer has reached one and a half times the initial thickness, the whole ice grid is recalculated. In my setup this is done at 1.5 cm. Griewank and Notz (2015) indicate that their parametrization of snow melt very probably does not apply to the temporal accurate evolution at the onset of flushing. The whole snow cover has to melt before flushing can occur and ice further down gets affected. Apart from that they expect an improvement in realism by their parametrization in comparison to the standard approach that turns snow melt water directly into flushing

melt water. Since later changes in this parametrization will be presented, SAMSIM used with this original setup is called „SAMSIM_original“ to distinguish the results. Furthermore SAMSIM is forced without snow precipitation but with a styrofoam cover, which is referred to as „SAMSIM_styrofoam“. This setup is used to get comparable results to the reference harps.

5.6 Flushing

There are several parametrizations of flushing implemented in SAMSIM. However only the complex one is used in this work since it „represents a physically consistent hydraulic system“ (Griewank and Notz, 2015) and is hence outlined in the following. Flushing in sea ice happens due to a horizontal and vertical percolation of melt water. In doing so, the melt water has to overcome a hydraulic resistance R which differs in the vertical and the horizontal direction. This resistance R is defined in SAMSIM by:

$$R = \frac{\mu}{\Pi(\phi)A}\Delta x, \tag{23}$$

which is dependent on the brine viscosity μ, the permeability $\Pi(\phi)$, the area A and the distance Δx.

Sea ice is traversed by cracks that allows brine and melt water to run off directly into the ocean. These cracks allow melt water that flushes the ice horizontally to escape the ice from each vertical level while melt water that flushes vertically needs to penetrate the ice completely before it reaches the ocean. This process explains the difference in the vertical and horizontal resistance parametrization in SAMSIM, while Δx in the vertical resistance is given by the layer thickness, it is defined as the average distance x to the next crack in the horizontal resistance. The average distance x is given by the ice thickness h_{ice} and the free parameter β through $x = \beta \cdot h_{ice}$, with $\beta = 1$ here. The total flushing resistance of each layer is then based on the sum of parallel and serial resistances. A more detailed

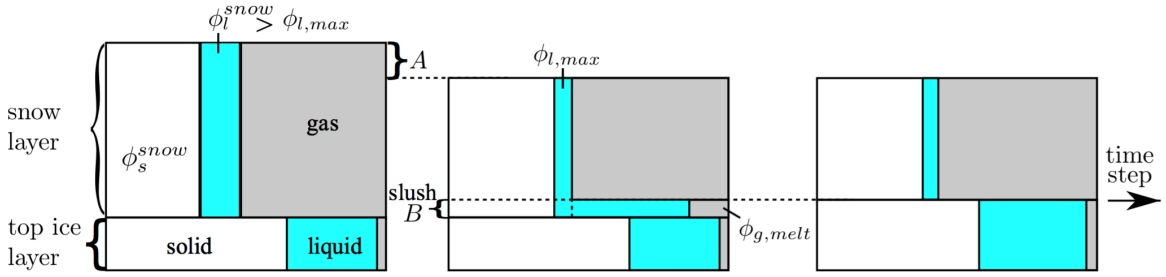

Figure 12: Sketch of the snow-to-slush conversion parametrization in SAMSIM_original. Taken from Griewank and Notz (2015)

description on that method as well as the corresponding equations are given in Griewank and Notz (2015). The flushing resistance is overcome by the hydrostatic head of the melt water which is defined by the height of the melt water column.

SAMSIM is made for multi-annual simulations of mean sea-ice properties as well as first year freezing situations. Melting situations are less evolved in the one dimensional model due to their horizontal heterogeneity (Griewank and Notz, 2015). In this work I will turn these conditions into benefits. Firstly, changes in parametrization cannot only be compared to short term lab measurements but tested on long term simulations too. Secondly, after freezing I can compare model and measurements in an accurate manner to check the forcing, initialization and parametrization used in SAMSIM. And finally, I assume that the SAMSIM simulation after the melting process can be considered as one possible member of a normal distribution facilitates melting simulations. If SAMSIM is not able to simulate one of these cases, I can still use this circumstance to better understand the complex system sea ice.

6 Results - Temperature sensor calibration

Since all physical properties investigated and measured in this work are dependent on temperature, a proper temperature calibration of the DS-Sensors and the T-sticks is crucial. The calibration measurement is described in section 4.5. The recorded reference temperature values $T_{reference,rec}$ need to be corrected by the linear regression equation

$$T_{reference} = 0.99892 \cdot T_{reference,rec} + 0.017612 \tag{24}$$

to equal the values displayed on the sensor $T_{reference}$.

Deviations between measured values and the corrected reference values show a cubic dependency relative to the absolute temperature. I therefore use a least-squares curve fit method to calculate unique calibration coefficients for all 128 temperature sensors (table 14 and 15 in the appendix). The stick labels according to their harps are given in table 6.

Table 6: DS-Sensors according to harps

Harp	snow1	snow2	snow3	ref1	ref2
DS-Sensor	2	3	1 and 7	4	6

The obtained calibration coefficients are tested with the help of a test sample, which equals in its setup the calibration measurement. The standard deviation of a single measurement is calculated for each single sensor by using the reference sensor measurements as the mean value. Calculating the standard deviation of a single measurement means that the result is not additionally scaled by the amount of measurements. Figure 13 shows the improvement in accuracy of about 33% due to the calibration. The T-Stick sensors, which have an own control unit show an even more accurate performance than the DS-Sensors which are connected to the harp control unit. The reason for the better performance must lie either in the control unit or in the sensor element lot. The better performance cannot be caused by the higher measurement frequency of the T-stick controller since the *standard deviation of a single measurement* calculation is independent from the exact number of measurements in large samples. As a result of the calibration I can determine the measurement accuracy of the temperature sensors. Since there are some spikes in the results due to malfunctions of the sensors during this measurement, I use the 65% percentile of the standard deviation values as mean measurement accuracy of the sensors. I thus get:

Table 7: Measurement accuracy of the temperature sensors

Sensors	Accuracy [K]
DS_Sensors	± 0.023
TSticks	± 0.020

These values equal the measurement accuracy of the reference temperature sensor and are smaller than the resolution of the digital sensor elements.

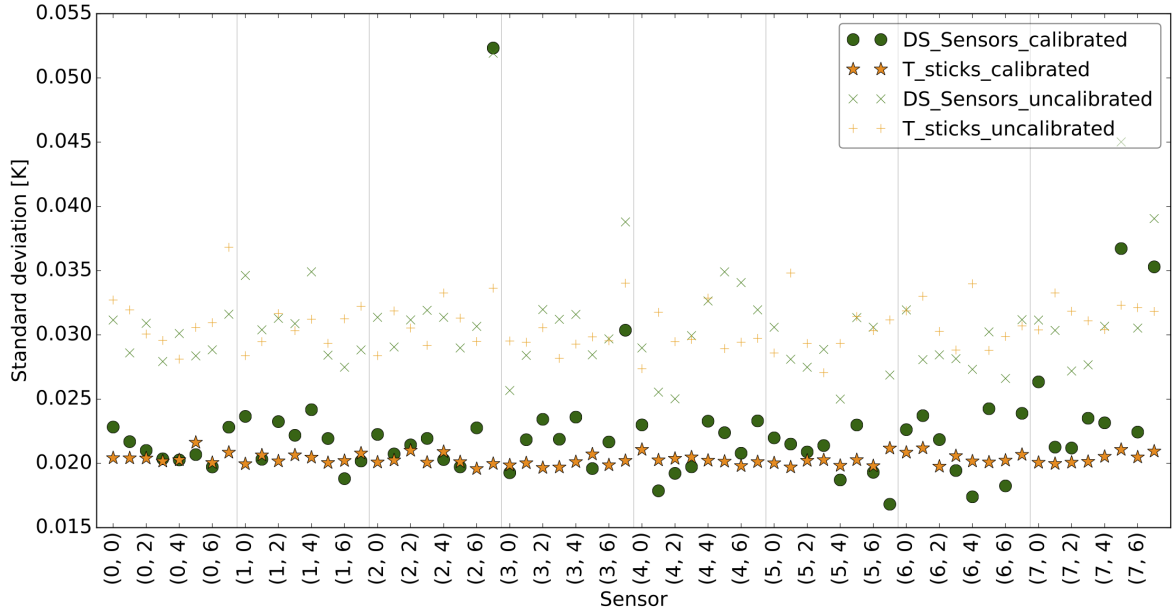

Figure 13: Standard deviations of the temperature sensors DS and Tstick with and without calibration relative to the reference temperature sensor GTH 3700. These deviations are calculated by means of a test sample that was not used for the calibration coefficient calculation. The standard deviations in the calibration sample would be by definition marginal.

7 Results - Salinity-harp validation

In the following, results are presented, which I used to evaluate the measurement accuracy of the harps and to validate their usability in the five snow experiments.

7.1 Reference experiment

7.1.1 Timeseries

All data contains UTC timestamps which get, for the evaluation, transferred into seconds since start of the measurement.

Figure 14 is an exemplary temperature time series from experiment 3. It is clearly visible that the water in the tank was slightly above the liquidus temperature at the beginning of the experiment. Afterwards it cooled down at the surface while ice was already growing at the bottom. Finally the liquid water leveled out at liquidus temperature. That happened in every experiment.

The resistance time series in figure 15 shows different start resistances for each sensor (also dependent on the AC frequency) that are constant until the ice reaches the sensors. From this point the resistance increases up to a certain level in a sigmoidal shape. The continuous curve supports the above mentioned theory of a continuous salinity profile at the ice–ocean interface. The freeze time of the ice surrounding a sensor is hard to distinguish from the curve shape and thus the value of Z_0. Observational ice thickness data and the distance between sensor and cooling plate could be used, but are unusable in the later snow experiment set up. The same counts for manual determination, since the shape differs with the ice growth rate. Hence, I had to find an algorithm that works for every set up. D. Notz (personal communication) used a combination of the temperature and the impedance data earlier:

> Z_0 is the first impedance value that is larger than $\beta = 1.03$ times the impedance when the temperature drops below the liquidus temperature.

Different experiments showed different best matches for β, but 3% has shown to be the best compromise. This algorithm defines Z_0 and thereby the freeze times for each sensor.

7.1.2 Ice growth

Ice grows when enough heat is getting transported away to enable the phase change from liquid to solid water. Heat transport is driven by heat conductivity in the ice which arises through a temperature gradient with lower temperatures in the ice than at the ice-ocean

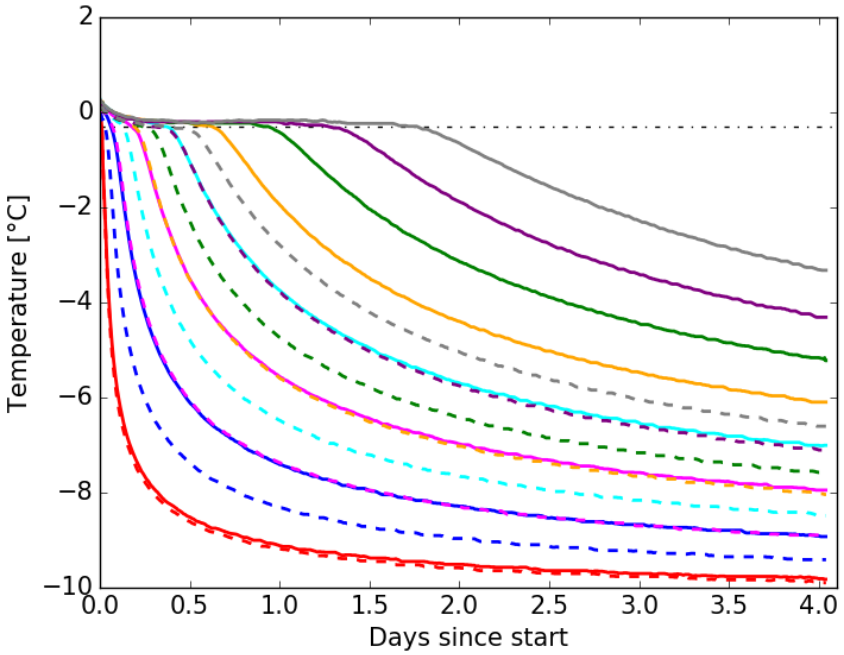

Figure 14: Temperature timeseries from experiment 3, Sensors 0-7. Solid lines: H2cm, dashed lines: H1cm, dash-dot line: liquidus temperature

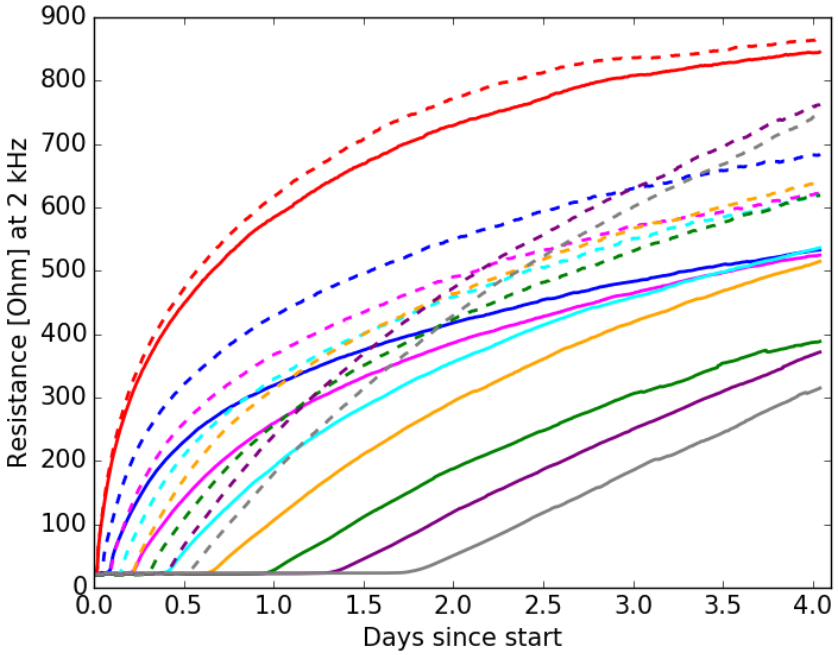

Figure 15: Resistance time series from experiment 3, sensors 0-7. Solid lines: H2cm, dashed lines: H1cm

interface. The standard solution for this process is Stefan's Law which neglects the effects of salt and heat capacity:

$$h_{ice} = 3.5cm \cdot \sqrt{NFDD} \tag{25}$$

with NFDD: Negative freezing degree days, the absolute amount of degrees below freezing temperature times the amount of days.

I find higher growth ranges in my measurements (figure 16). The reason could be either the influence of salt on the heat conductivity and the amount of phase change in the ice or also be caused by the tank. That allows volume expansion only in one direction.

Observational and thickness data obtained from the freeze times of the sensors coincide well. I therefore use a square root shape fit of the freeze times as an ice growth function to calculate the non-dimensional height variable $h_{ice}(t)$:

$$h_{ice}(t) = a \cdot \sqrt{t} + b \; ; \; t \; in \; seconds. \tag{26}$$

The coefficients are given in the plots. The addend b is a compromise for better results and can be explained by extremely large ice growth rates in the beginning when the ice thickness is still small.

7.1.3 Temperature profiles

The vertical temperature profiles in the analytical solution are linear with an anomaly at the ice-water interface, mostly depended on how much the water temperature differs from its liquidus temperature. Measured values equals the analytical solution (figure: 17 and 18), only small deviations in the upper part or small constant offsets can be observed. I assume that both effects are caused by the undefined vertical expansion of the sensors as well as from small deviations of the ice growth function. The transparent part in the figures shows the mean value $\pm$ the standard deviation.

7.1.4 Solid fraction

Larger deviations occur in the obtained volume solid fraction (figure: 19 and 20). Especially the middle and upper part shows differences between measurement and theory as well as between the different sensors. Over the long term all sensors converge to the analytical solution. The two lowest sensors 0 and 1 are skipped for the evaluation, due to above-mentioned growth function difficulties and presumable unsteady conditions at the beginning of the experiments. 6 minutes of sampling time per iteration are probably to long for the first centimeters in the ice. There is a trend that higher sensors show slightly higher solid fractions.

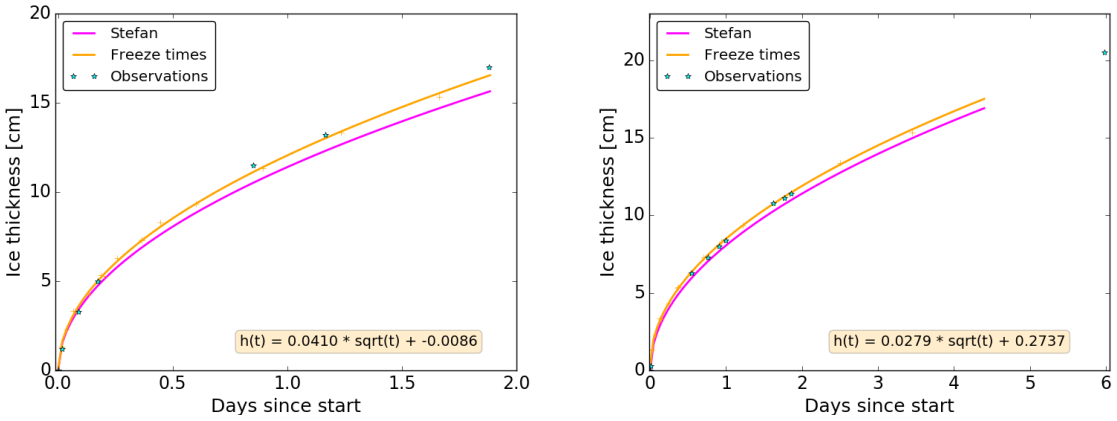

(a) Experiment 2 (b) Experiment 4

Figure 16: Visually observed, measured and calculated ice thickness evolution during reference experiment 2 and 4. The equation coefficients for the freeze time fits are displayed on the bottom of the graphs (with t in seconds).

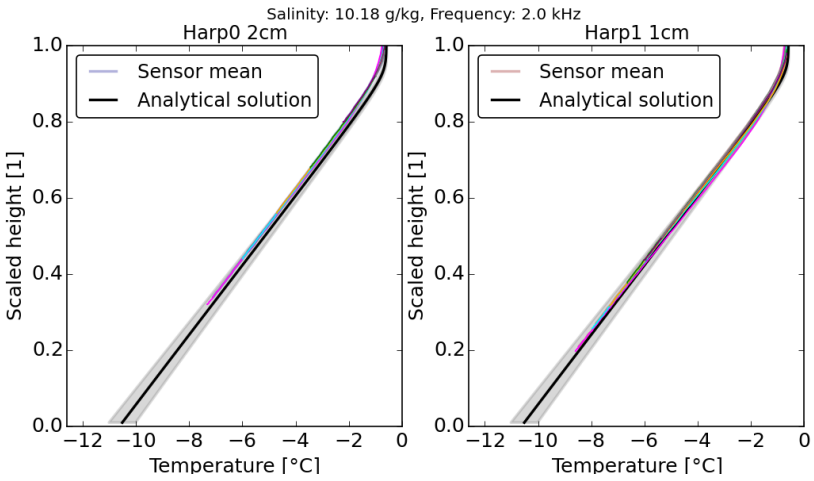

Figure 17: Temperature profiles reference experiment 2, sensors 2-7 from H2cm (left) and H1cm (right) and analytical solution.

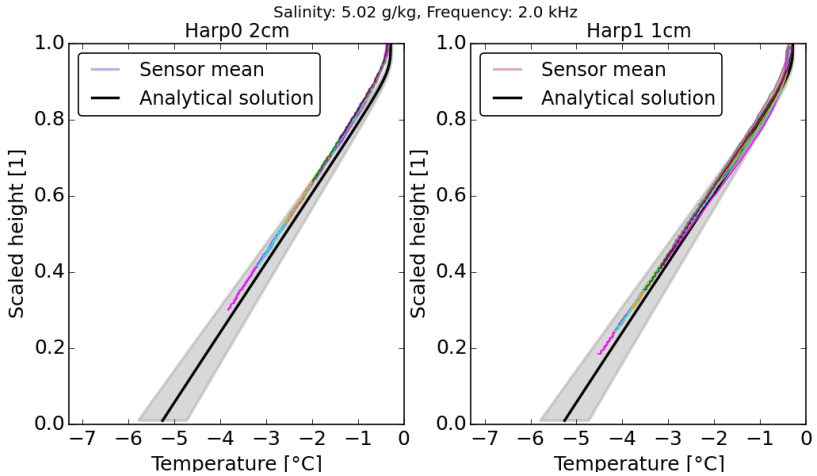

Figure 18: Temperature profiles reference experiment 4, sensors 2-7 from H2cm (left) and H1cm (right) and analytical solution.

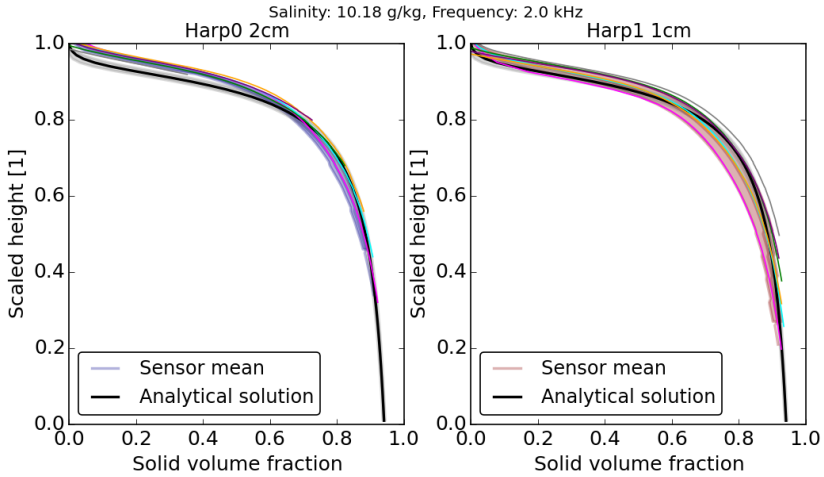

Figure 19: Volume solid fraction profiles experiment 2, sensors 2-7 from H2cm (left) and H1cm (right) and analytical solution, 2 kHz measurement

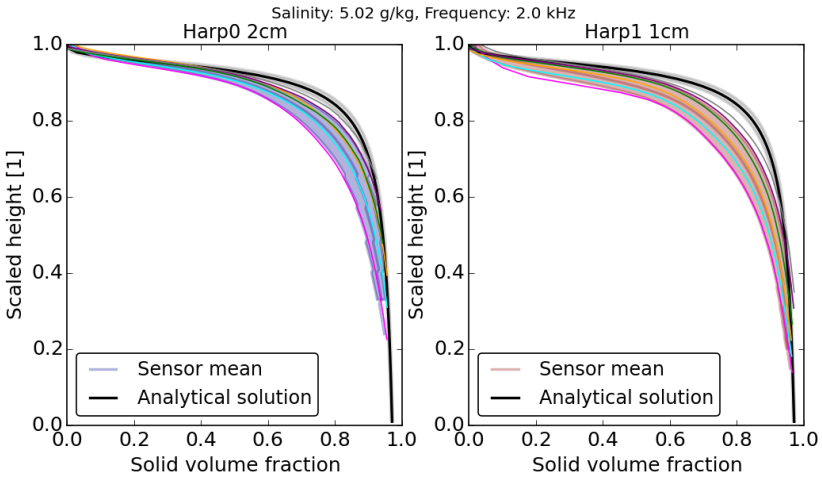

Figure 20: Volume solid mass fraction profiles experiment 3, sensors 2-7 from H2cm (left) and H1cm (right) and analytical solution, 2 kHz measurement

The ice in experiment 1 was strongly heterogeneous with 20 cm deep liquid funnels in 25 cm thick ice. This is also recognizable in the solid fraction data (figure: 21), which shows large deviations. Higher AC frequencies than 2 kHz for the resistance measurements showed a trend to overestimate the solid fraction, especially for higher salt concentrations (figure 22).

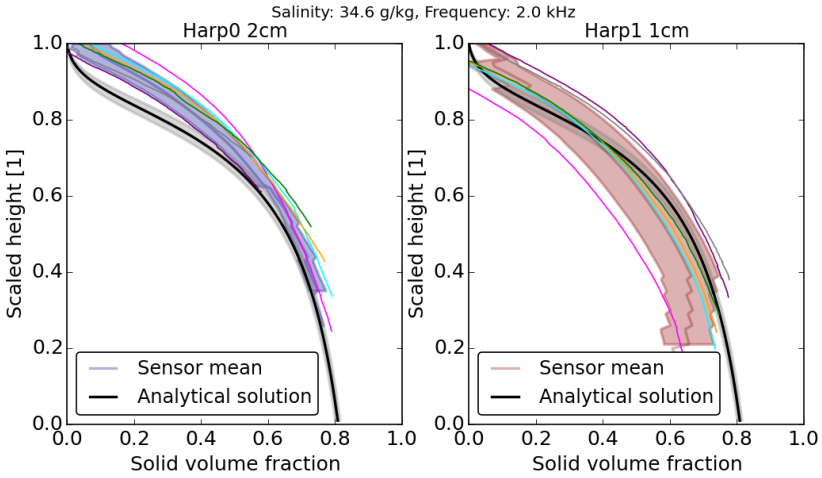

Figure 21: Volume solid mass fraction profiles experiment 1, sensors 2-7 from H2cm (left) and H1cm (right) and analytical solution, 2 kHz measurement

7.1.5 Bulk salinity

Small deviations in temperature or mass solid fraction lead to large differences in bulk salinity. Even so, the bulk salinity values for smaller salinities, as they are observed in sea ice, fluctuate close to reality (figure 23, 24, 25). I checked the salinity of the water above the ice in the end in experiment 3 and 4, it had slightly increased, as well as the conductivity between

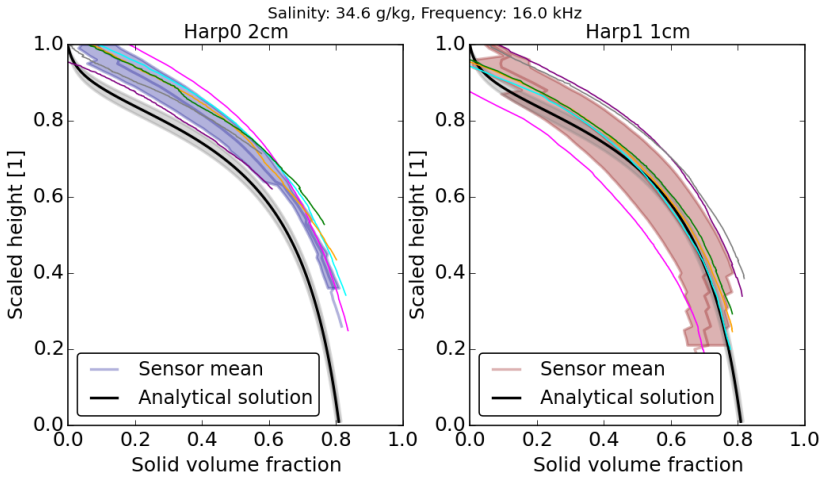

Figure 22: Volume solid mass fraction profiles experiment 1, sensors 2-7 from H2cm (left) and H1cm (right) and analytical solution, 16 kHz resistance measurement

the wires before they have frozen in, but both in a negligible amount. That means, we can assume that the absolute salinity values in the ice are equal to the start salinity.

Experiment 3 shows slightly higher salinity values in the ice center, which are caused by the lower solid fraction values (figure 20). The physical reason for this behavior is not obvious. Since the temperature evolution fits quite well, it must be assumed that either the temperature sensors haven't been measuring in exactly the same level as the wire pair or that the model does not describe the physical properties in the ice properly for that case. In order to transfer the results to sea water instead of NaCl water, one experiment was carried out with the same sea salt as it is used in the snow experiments. The performance of the harps in sea water is almost equal to the performance in NaCl (figure 26). Only the freezing temperature showed small deviations which cause slight errors in the bulk salinity measurements and calculations towards the top.

7.1.6 AC measurement frequencies

I investigate the effect of different AC measurement frequencies for the resistance measurement. Figure 27 shows the mean BIAS of temperature, solid fraction and bulk salinity values from the analytical solution for different frequencies. Standard deviations are also included to evaluate the significance of the mean values. Typical standard deviations from the analytical solution ensemble as described above, are given in table 8. With these, we can better classify the BIAS values. Temperature and solid fraction are thus close to or even within the analytical solution standard deviation.

Considering figure 27 and the bulk salinity plots 23 - 25 in comparison to figure 56 - 59 in the appendix, I decide on using 2 kHz in my master thesis, since liquid fraction and hence bulk

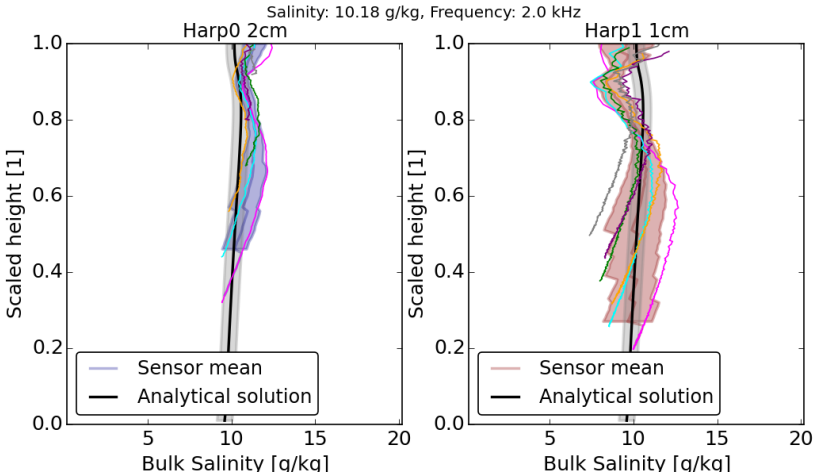

Figure 23: Bulk salinity profiles experiment 2, sensors 2-7 from H2cm (left) and H1cm (right) and analytical solution, 2 kHz measurement

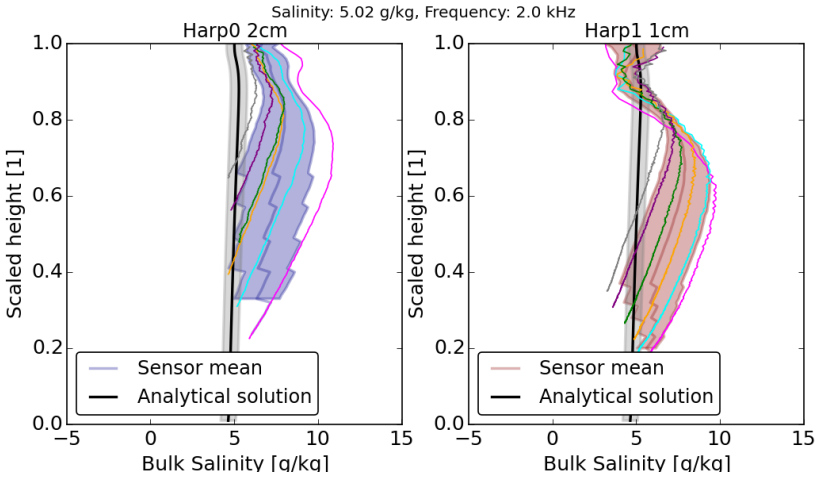

Figure 24: Bulk salinity profiles experiment 3, sensors 2-7 from H2cm (left) and H1cm (right) and analytical solution, 2 kHz measurement

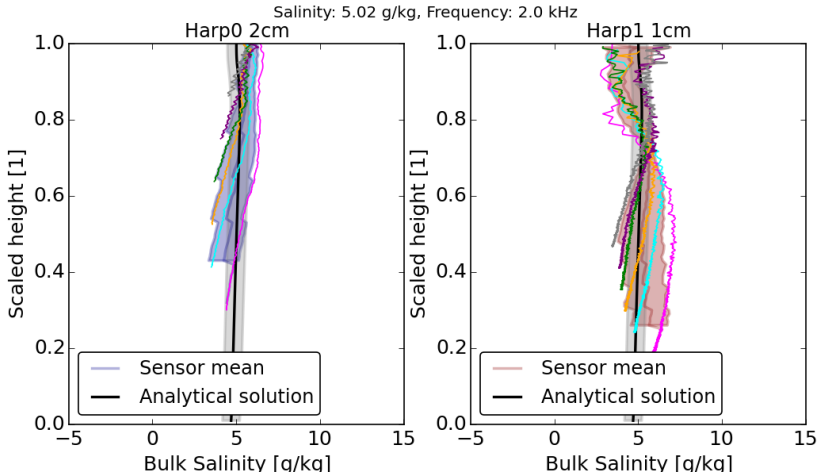

Figure 25: Bulk salinity profiles experiment 4, sensors 2-7 from H2cm (left) and H1cm (right) and analytical solution, 2 kHz measurement

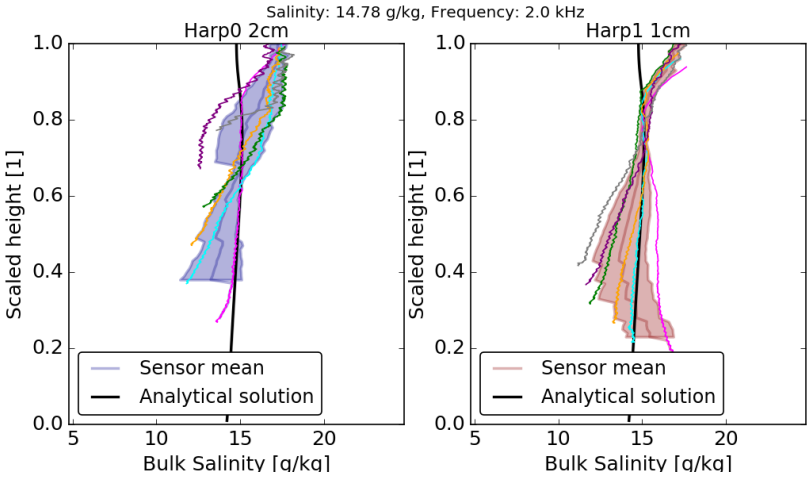

Figure 26: Bulk salinity profiles experiment 5, sensors 2-7 from H2cm (left) and H1cm (right) and analytical solution without standard deviation, 2 kHz measurement

salinity gets underestimated at higher salinities by higher measurement frequencies. However, higher frequencies show better accuracies for the 1cm harp, but that seems to be an effect of averaging the values. Plotting the last measured bulk salinity values of each sensor, which is in this case the trend, relative to the setpoint values, we see a better behavior of the 2 kHz measurement for both harp models (figure:28). The 2 kHz lines are closer to the $1/1$ line than the 16 kHz lines. Another conclusion we can draw from this figure is that the deviations are increasing with salt content and go far above the vertical variability in the analytical solution.

Table 8: Typical standard deviations of the analytical solution ensembles

Variable	Standard deviation
Temperature	0.25
Volume solid fraction	0.025
Bulk Salinity	0.6

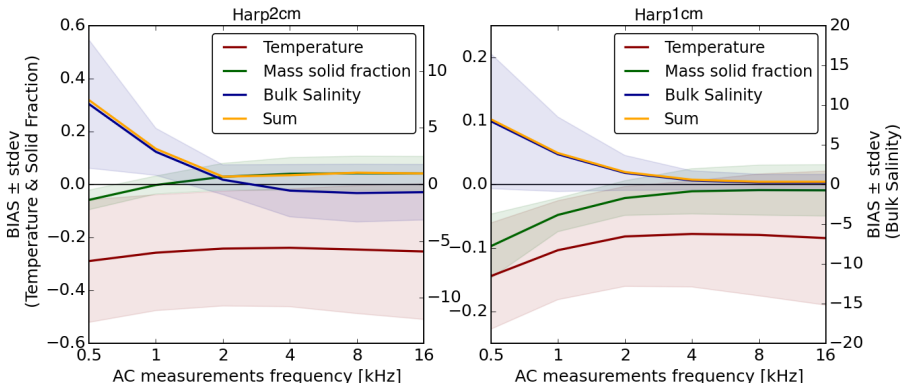

Figure 27: Mean BIAS and its standard deviation calculated for experiments 1-4 dependent on the AC measurement frequency. Left and right y-axis labels are valid for both plots. Line „Sum“ is the sum of the absolute values. The closer the line to zero, the better the measurements.

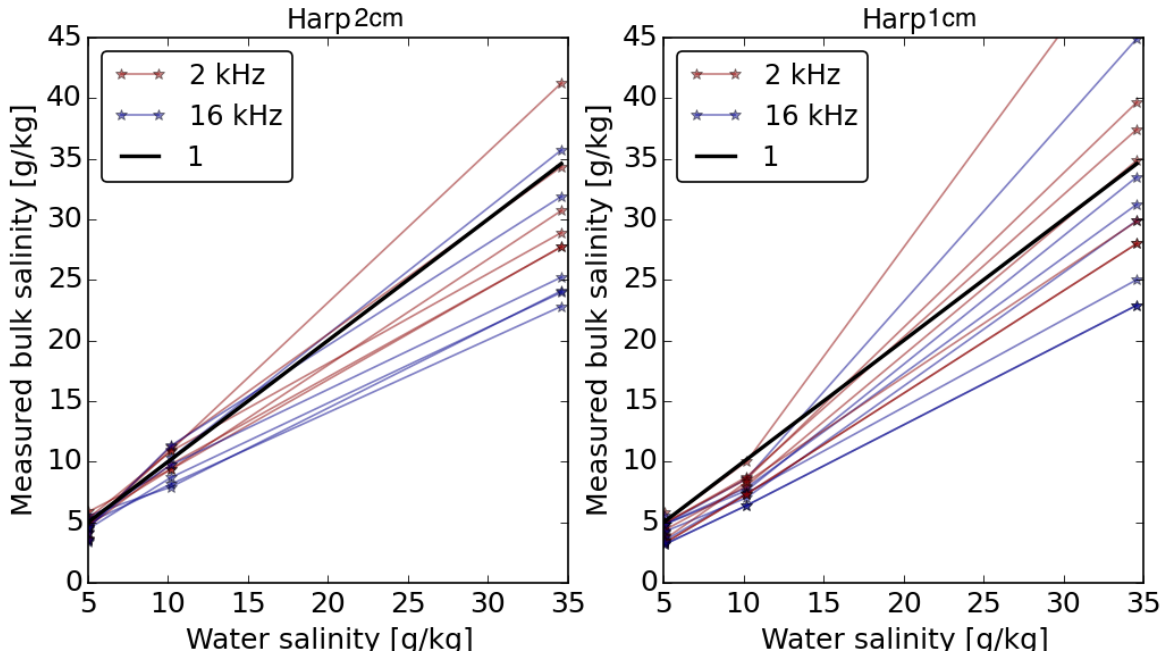

Figure 28: Last measured bulk salinity of each sensor relative to the start salinity in the water for harp 2cm and 1cm. Slight variations in the line colors come from superimposed lines.

7.2 Brine sensitivity

Before giving results to brine sensitivity measurements, I would like to give an understanding of its impact. To do so, I need to state three assumptions concluded from the reference experiment results before:

(I) reference experiment results can be extrapolated on every possible salinity

(II) each initial salinity is connected with one defined Z_0, subsequently the harp is able to measure the same bulk salinity for all possible combinations of temperature and solid fraction.

(III) if deviations occur, solid fraction gets preferably overestimated by the harp, which happens especially at high solid fraction values

Considering brine sensitivity effects in areas of high solid fraction would even more overestimate solid fraction, since the measured impedance $Z(t)$ gets amplified by the brine sensitivity correction. Hence all brine sensitivity effects are neglected as long as harp measurements equal the reference experiments in a way that either the measured bulk salinity equals the start value or that the measured bulk salinity is smaller than the start value and temperatures are below the initial freezing temperature as well. The latter condition is added since smaller salinities at temperatures below the freezing point comes with higher solid fractions, which

again are likely to be already overestimated by the harps. Furthermore do high solid fractions reduce the impact of the brine sensitivity immensely.

Nevertheless, sea ice with a reduced bulk salinity and a temperature close to freezing point is not captured yet but is of particular interest to study the impact of snow-melt situation. In this case, temperatures are above the freezing point of the initial salt solution since freezing point temperatures are rising with decreasing salinities. Considering brine sensitivity in this case is equivalent to correcting Z_0 and thus, fulfilling assumption (I) and (II) again. Therefore it was obvious to calculate the salinity dependency of the brine sensitivity from Z_0 values. To do so, I took the initial $\gamma_0 = Z_0^{-1}$ values from all reference experiments, calculated their equivalent at a temperature of 0.5 °C and finally fitted a function to these values. The temperature corrected conductivity $\gamma_{0.5}$ is calculated through equation (27), which is a result of brine sensitivity investigation made with older harp models. The slope is close to the one in Notz, Wettlaufer et al. (2005) and thus adopted.

$$\gamma = \gamma_{0.5} - 0.00167 \cdot (0.5 - T) \tag{27}$$

The temperature corrected values are displayed in figure 29. It is obvious that the brine sensitivity correction is essential for high temperatures which lead to small brine salinities. Otherwise errors in the solid fraction of up to the factor two are very likely. The quantity of data points is minimal but the shape of a necessary fit-function equals the suggested square root fit in Notz, Wettlaufer et al. (2005): steep slope at low salinity ($<$ 10 g kg^{-1}) and almost flat at high salinity ($>$ 30 g kg^{-1}) (figure 29). However, none square root fit was able to fit the slope in an adequate precision. Hence, an exponential fit was chosen with the appropriate coefficients from table 9:

$$\gamma_{0.5} = a + b \cdot e^{-c \cdot S} \tag{28}$$

Table 9: Coefficients of exponential brine sensitivity fit

Harp	a	b	c
1 cm	0.115	-0.115	0.098
2 cm	0.101	-0.101	0.102

It should be mentioned here that the brine sensitivity correction does not apply to the reference experiments as described above but must be considered in the snow experiments.

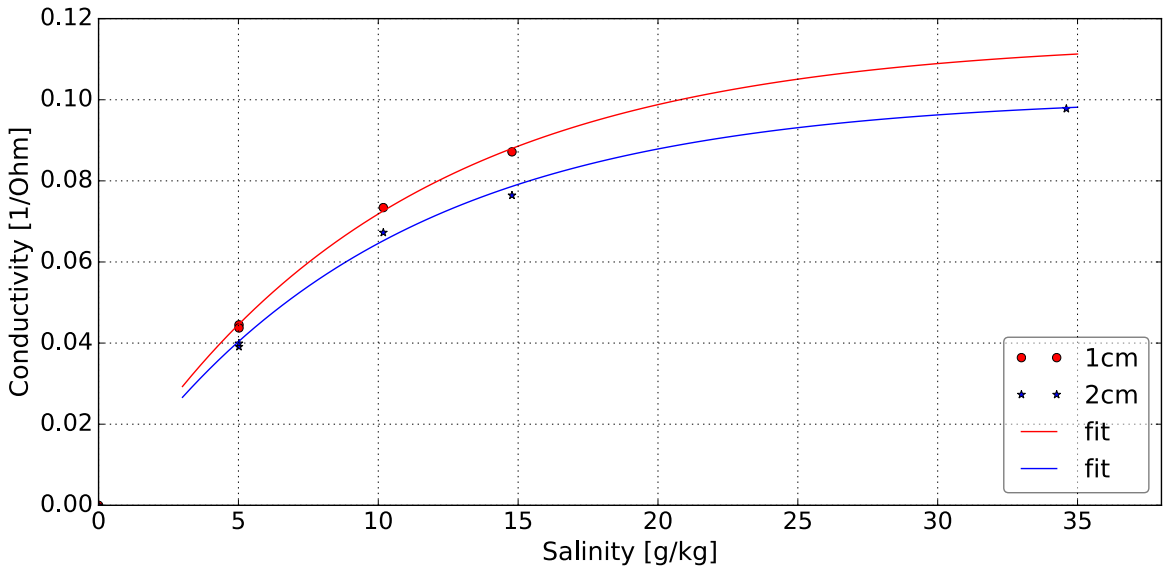

Figure 29: Temperature corrected conductivities $\gamma_{0.5}$ of 1 cm and 2 cm harp from reference experiments. The fits are based on equation (28) and the coefficients from table 9.

7.3 Snow experiment measurement validation

Having made harp measurements plausible by the help of reference experiments, additional reference sensors were deployed in the snow experiments to survey absolute harp measurement values continuously as mentioned in section 3.4. The liquid water column in the large tank was well steered by the pumps during all experiments. The difference between the SBE measurements at the bottom and the RBR measurements close to the ice–water interface was always in the small range of calibration uncertainty of the RBR sensor. In order to obtain the total salt amount in the ice, the ice thickness is needed. In this work, the thickness is seen as the vertically lowest $\phi_s > 0.15$ threshold. If this calculation method fails, e.g. during flushing when similar values occur more then once in the ice, I determine the greatest gradient in solid fraction and the depth of its lowest sensor defines the ice thickness. Since the ice develops a lens shape at the bottom as described in section 4.2, the over-all ice volume is calculated from the area of the large tank times the ice thickness times the fraction of a 5/4 trapeze. In doing so, the trapeze compensates the lens shape.

As an example, the salt balance calculations for experiment 4 is given in figure 30. First of all it must be mentioned that in other experiments, the errors are slightly higher (about 1 g kg^{-1}) . Nevertheless does figure (30) shows how sophisticated the harp measurements are. The calculated liquid water salinity equals the measured one for large parts. Only during melting periods differences occur, which could be explained by a very rough ice bottom as well as a well-marked lens shape of the ice and thus an overestimated ice volume. The start as well as the end values in calculated salinity are close to the measured, which confirms the

temporal stability of harp measurements. Some artifacts are visible at the very start which originates from the ice thickness calculation that fails at very small thicknesses.

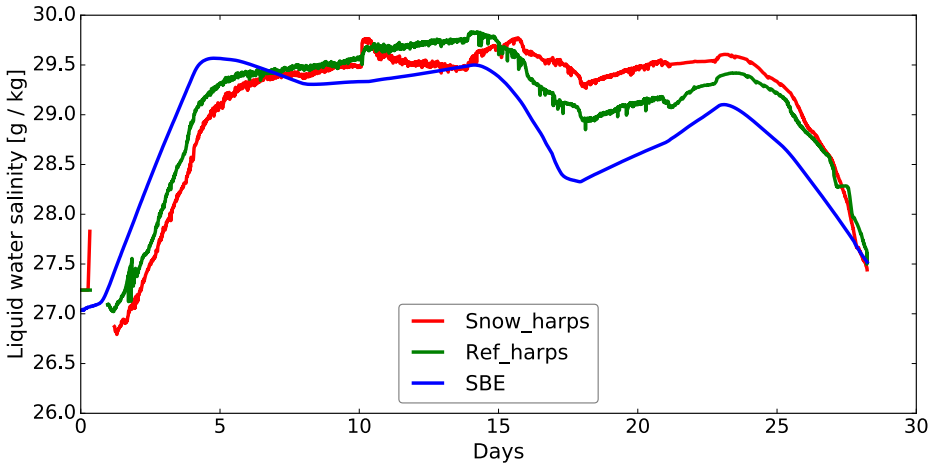

Figure 30: Measured water salinity (SBE) in the large tank during snow experiment 4 and estimated salinity based on mean bulk salinity and ice thickness from snow harps and reference harps.

Only two ice core measurements from experiment 4 are available to validate harp data. The cores of experiment 5 can only be used as stand-alone measurement, this is due to a malfunction of the harps which is described in section 8.

Both profiles of experiment 4 cores and the related harp measurements are given in figure 31. The ice thicknesses at the core locations were smaller since they were taken to the outside of the ice floe. Beside the thickness differences, both measurements, harp and core, coincide quite well in the absolute amount of salt in the ice, as well as the profile shape in core4.ref2. One of the huge advantages of harp measurements over ice cores becomes clear, the steady profile of bulk salinity at the ice bottom gets resolved by the harps.

As a result of this section, I draw the conclusion that the harp measurement system is not only able to enhance the temporal and spatial measurement resolution versus ice cores, but also works reliable with regard to absolute salinity values.

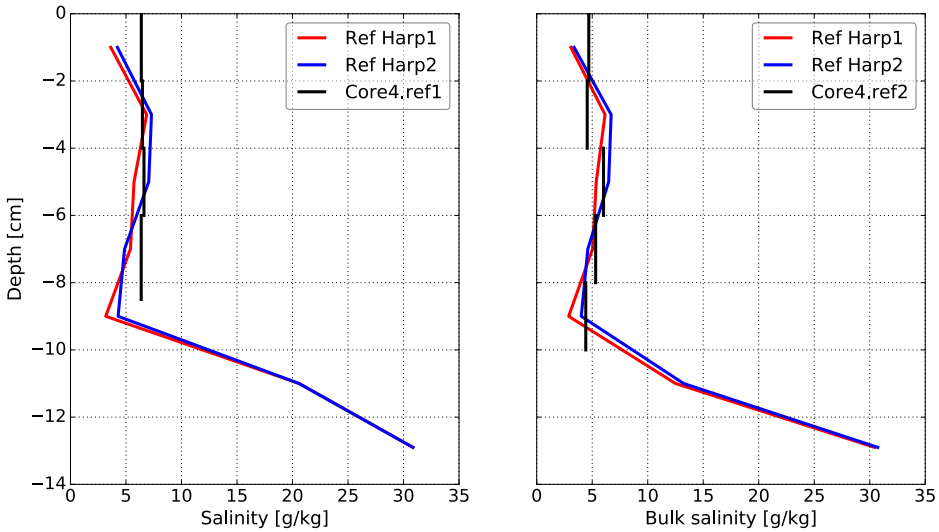

Figure 31: Reference harp 1 and 2 and ice core bulk salinity profiles during refreezing in experiment 4. Specifications are taken from table 3.

7.4 Workhorse conclusions

From the evaluation of the reference experiments as well as the ongoing validation during the snow experiments, I draw the following conclusion for the sea-ice salinity, liquid fraction and temperature measurements in my master thesis:

- From statistic and manual evaluation I figured out that I should use 2 kHz as resistance measurement AC frequency
- The averaged measurement accuracies of the harps relative to the analytical solutions are:

Table 10: Measurement accuracies - 2 kHz

Variable	BIAS	Standard deviation
Temperature	-0.16	$\pm$ 0.15
Volume Solid fraction	0.00	$\pm$ 0.04
Bulk Salinity	0.94	$\pm$ 1.76

- The smaller the salinity values are in conditions well below freezing point, the smaller the standard deviation and the offset of the measurement becomes
- Z_0 is the first impedance value that is larger than $\beta = 1.03$ times the impedance when the temperature drops below the liquidus temperature.

- vertically and temporally highly resolved measurements in the ice in an usable accuracy range are possible with the harp
- a comparison experiment with sea salt showed that the results from the NaCl reference experiments can be transferred to the snow experiments with sea salt
- the brine sensitivity needs to be considered in conditions near the melting temperature of sea ice
- the harp provides plausible absolute values and is temporally stable during the snow experiments
- data logging malfunctions can still occur and must be identified manually (more on this in section 8).

8 Results - Snow experiments

Five snow experiments were conducted in the large tank with an increasing amount of snow cover from experiment 1 to 5. Small problems occurred with the measurement electronics in experiment 1 and 2, which were likely introduced by another measurement system that was deployed in the same tank. While the temperature values are not affected, the impedance measurements show small steps (figure 32). The steps are corrected by absolute values in the evaluation. Stronger problems occurred in experiment 5 in which impedance measurements were affected again but in a not explicable way. Harp measurements from experiment 5 are thus not evaluated.

In experiment 4 all sensors worked properly and the flushing setup was well developed relating to the sealing of the snow frame. It is therefore exemplarily investigated further in section 8.1.1, while vertical profiles of experiments 1-4 are used to get statistical values in section 8.2. Before experiment 4 gets examined closely, the other experiments should be sketched here, so that the statistical investigations can be understood. The main observations are given in table 11.

The melted snow mass is derived from the initial amount of snow reduced by the amount of freshwater ice that remained on the ice after melting, for which I assume the density of freshwater ice.

8.1 Snow experiment 4

8.1.1 Measurements

Experiment 4 lasted 27.3 days, during which the air temperature varied between -14 °C and 3 °C (figure 33). A snow cover with a mass of 2.7 kg and a thickness of 6.5 cm was applied

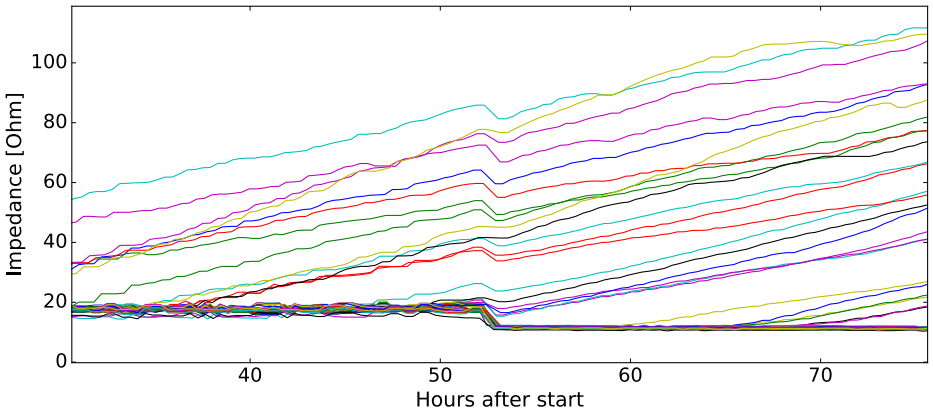

Figure 32: Impedance values over time from all deployed harps in experiment 1. Shown is the time when a jump in the measurements happened.

Table 11: Snow and melt phase properties experiments 1-5

Experiment	**1**	**2**	**3**	**4**	**5**
Ice thickness below snow Lab/SAMSIM [cm]	11/12	14/ 13	15/18	15/13	15/-
Ice thickness below styrofoam Lab/SAMSIM [cm]	16/13	13/13	15/18	13/13	15/-
Mass snowmelt [kg m^{-2}]	15	14	24	25	34
Snow thickness after melt [cm]	0.5	1.2	0.9	1.5	2.5
Time snowmelt [days]	1.5	1.8	3	3	3.1
Time styrofoam [days]	1.5	2	4.8	7	3.1
Snow frame sealing	no	no	partly	tight	tight

after 10 days. At the same time, all relevant bare parts of the ice were covered with 2 cm thick styrofoam plates. The air temperature was then kept constant to get an equilibrium state and afterwards slowly increased up to 2 °C on day 15. Melting started already on day 14 when the air temperature close to the ice surface was slightly above 0 °C. After 2.5 days of melting, the snow cover was reduced down to 1.5 cm. The styrofoam cover was removed then, since the thermal insulating effect of the snow was largely reduced. The ice reached a thickness of 15 cm at the snow harps and the reference harps. At the end of the experiment, all ice was melted away.

In experiment 4, the ice grew during the first 5 days as it can be seen in the timeseries plots figure 34 - 36. If not otherwise mentioned, effects described in this section are measured by all harps that are either part of the snow harps or the reference harps. Within the first 5 days a strong vertical temperature gradient developed in the ice, with temperatures below -5 °C at the top and freezing temperature at the bottom of the ice (figure 34). Air temperature changes affect quickly the internal temperature of the ice. The horizontal differences in temperature between the snow and the reference harps are minimal in the first third of the experiment, before snow and styrofoam are deployed. A more exact error estimation for the horizontal homogeneity at this time is given in section 8.2. The deployment of snow on the ice causes a jump in temperature in the ice, which I explain in section 9. Before melting, the ice below the styrofoam is a few deci-Kelvin warmer then the ice below the snow. During melting, the ice below the snow gets about 1 K warmer than below the styrofoam. After the snow and the styrofoam is gone, temperature profiles are again very similar between the snow and the reference harps.

Shortly after freezing, the ice adopts a bulk liquid fraction between 0.1 and 0.2 (figure 35). This fraction keeps constant until the snow, respectively styrofoam, gets deployed on the ice. Small differences well below $\pm$ 0.1 occur in the horizontal plane, but are all within the

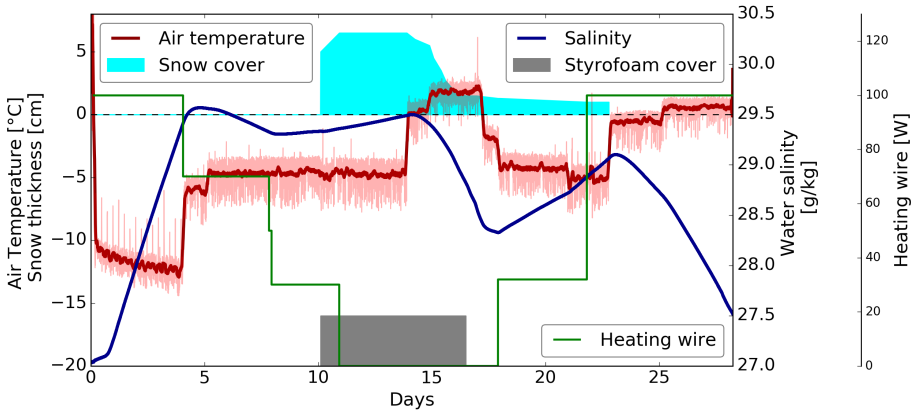

Figure 33: Temporal evolution of air temperature (thick red line is a running mean), liquid water salinity, snow cover and heating wire heat input during experiment 4. The styrofoam cover is only temporal classified, the thickness of the styrofoam is 2 cm in real.

measurement accuracy of the harps. There is no short term influence of the styrofoam on the liquid fraction, but a great one by the snow. With deploying the snow on the ice, liquid fractions in most of the ice are dropping below 0.1 while liquid fractions in the uppermost ice-layers are increasing strongly and are keeping constant at the bottom as expected due to continuity. One day after deploying the styrofoam, the reference harps measure a slight decrease in liquid fraction in the lower fourth of the ice. With the onset of melting, all harps measure a strong increase in liquid fraction in the ice, starting at the top and evolving downwards. Values are reaching up to 0.3 in the upper ice layers. Refreezing of the ice afterwards makes the ice around the snow harps close to be pure solid ice with liquid fractions well below 0.1, while the reference ice levels out between 0.1 and 0.2. The small liquid fraction in the snow harp values reaches down nearly the whole ice column in snow harp 1 and 3 while snow harp 2 shows low values only down to half of the ice thickness. The latter also shows a strong increase in liquid fraction evolving from the bottom of the ice during melting.

Bulk salinity measurements are very sensitive to small errors in temperature and liquid fraction, especially for low liquid fractions or high temperatures. A liquid fraction error of 0.1 to 0.2 doubles the bulk salinity, while a temperature error of $\pm$ 1 K leads to about $\pm$ 16 g kg^{-1} error value in brine salinity. Luckily, impedance measurement errors are small at low liquid fractions and the single point temperature measurement error presumably also small, since horizontal differences are small in temperature (figure 34). Errors in the temperature measurement itself are negligible. We still should have in mind that even though absolute salinity values seem to be right (section 7.4), a qualitative evaluation of bulk salinity

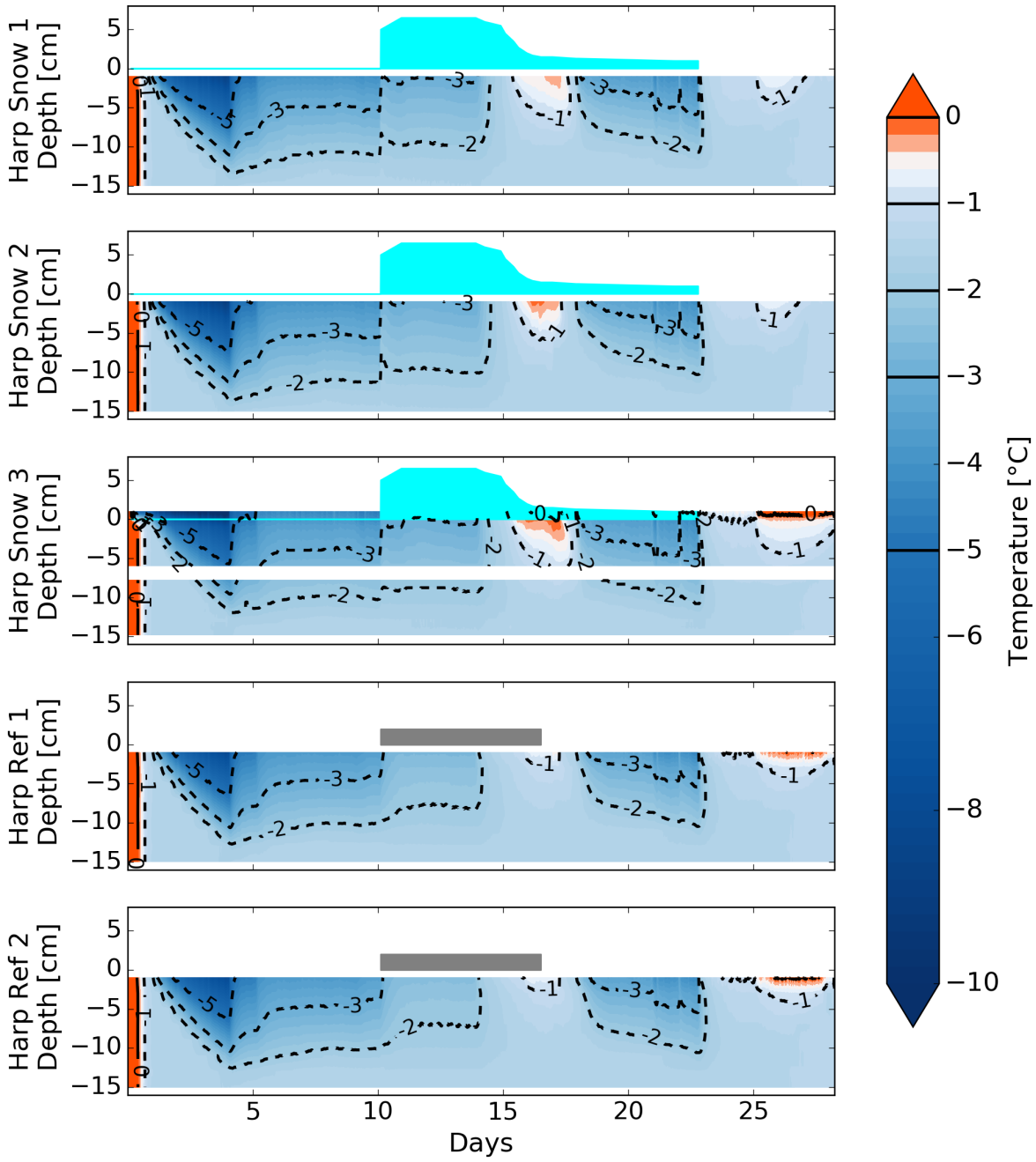

Figure 34: Temporal and vertical evolution of temperature in the ice and the water at five different harps: Snow harp 1-3 and ref harps 1-2 during experiment 4. Furthermore displayed is the snow cover (cyan) and the styrofoam cover (grey). The ice extent around the sensors can be drawn from figure 35. The horizontal data gap in snow harp 3 measurements at a depth of 7 cm comes from the arrangement of two 1 cm harps one above the other. Both 1 cm harps form together snow harp 3.

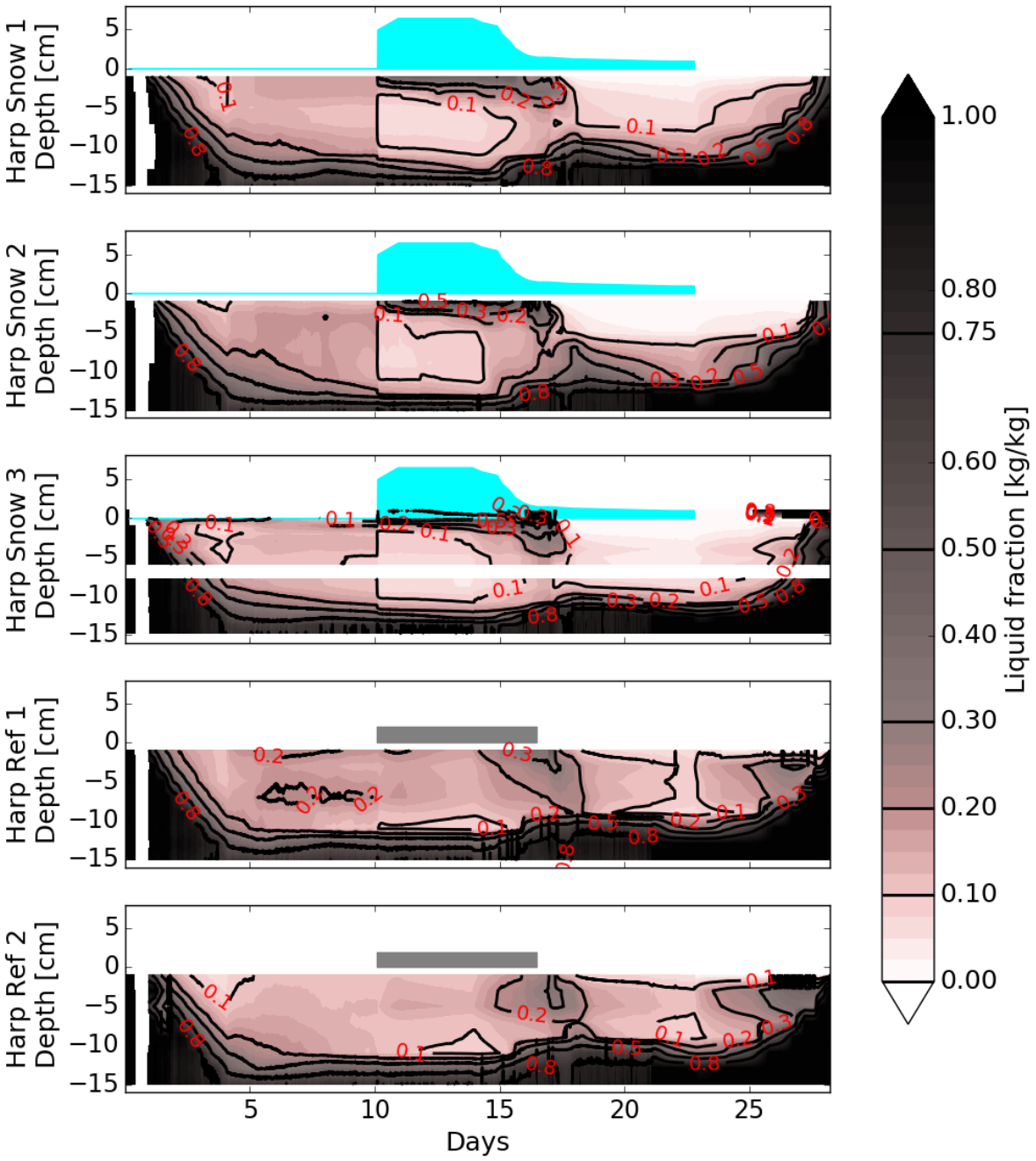

Figure 35: Temporal and vertical evolution of mass liquid fraction in the ice and the water at five different harps: Snow harp 1-3 and ref harps 1-2 during experiment 4. Furthermore displayed is the snow cover (cyan) and the styrofoam cover (grey). Extremely dark areas at the bottom of the ice indicate liquid ocean water.

measurements should have a higher attention than an exact quantitative one. So does the bulk salinity decrease at all harps directly during freezing (figure 36) and a vertical c-shape evolves. Only reference harp 2 does not measure a c-shape profile, probably the harp was frozen into the ice a little bit lower than all other harps. The deployment of snow on the ice leads to an immediate increase of salinity directly below the snow and a much larger decrease of salinity in the vertical center of the ice, this effect is discussed further in section 9.1. A much smaller impact is measured below the styrofoam where a less saline bubble develops in the lower third of the ice. All bulk salinity profiles are temporally steady after the snow and styrofoam deployment, except from snow harp 2 again, whose measured profiles develops within the first two days, after which it gets steady, too. The onset of melting, that means when the snow cover starts to decrease, causes a development in the bulk salinity of the ice below. From the ice surface downwards, the ice gets less and less saline. Bulk salinity values are decreasing by up to 15 g kg^{-1} directly in the upper layers, while they are constant in areas where they are already at very low values of about 3 g kg^{-1}. The penetration depth of the desalination effect is very variable between the harps. While snow harp 1 measures changes only in the upper 4 cm, snow harp 2 measures changes down to 7 cm and snow harp 3 a slight decrease of bulk salinity in the whole column. Especially very high bulk salinities get removed by the snow melt. Snow harp 1 and 2 measure a slight increase of bulk salinity in the lower fourth of the ice column. There is no effect due to melting measured below the styrofoam. The reference ice, respectively saltier ice, melts faster near the end of the experiment than the fresher ice that had been covered by the snow before (as Wiese et al. (2012) observed, too).

Sea ice cannot become warmer than the freezing temperature of its bulk salinity during melting. Hence, the less salty the sea ice is, the warmer it can become during melting. In order to investigate the temperature evolution independent from this limitation, I calculated the temporal evolution of the difference between the measured temperature in the ice and the locally given freezing temperature based on the bulk salinity. The difference is given in figure 37. The ice temperature is well below freezing temperature during freezing times. It never exceeds the freezing temperature apart from the ocean beneath and at the surface at the end of the experiment. During snow melt, the temperature of the upper ice layers underneath the snow reaches almost melting temperature. This is not the case below the styrofoam cover. However the ice below the styrofoam is closer to melting temperature before the onset of melting than the ice below the snow. All profiles are almost equal during refreezing.

As in all other four experiments, the melt rate of the snow cover started slowly, increased afterwards and stopped before the whole snow was melted away. A distinct thick snow layer remained on the ice (picture 38a). This snow layer had changed from white snow to a solid

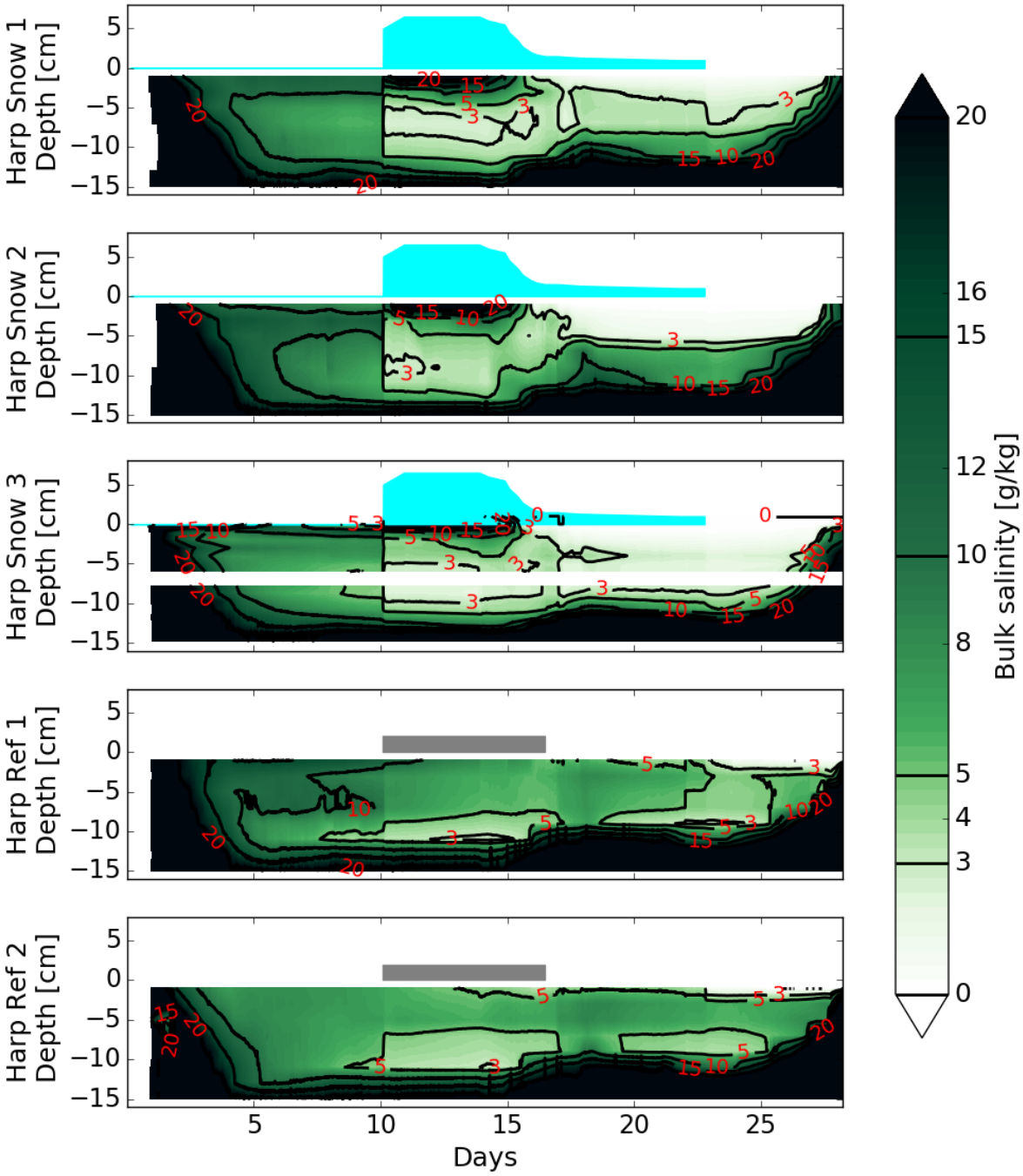

Figure 36: Temporal and vertical evolution of bulk salinity in the ice and the water at five different harps: Snow harp 1-3 and ref harps 1-2 during experiment 4. Furthermore displayed is the snow cover (cyan) and the styrofoam cover (grey). The ice extent around the sensors can be drawn from figure 35

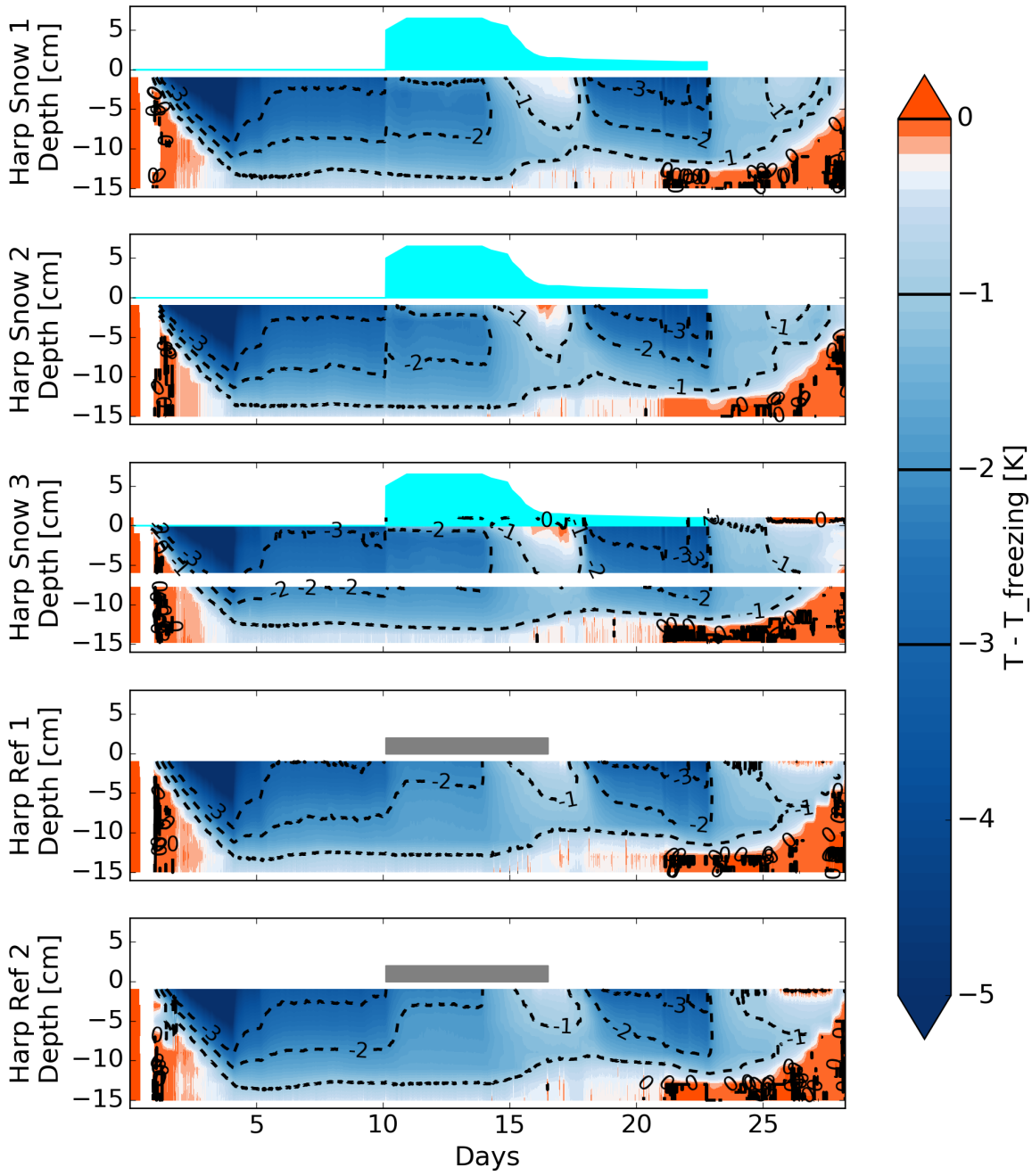

Figure 37: Temporal and vertical evolution of the temperature minus the freezing temperature in the ice and the water at five different harps: Snow harp 1-3 and ref harps 1-2 during experiment 4. Furthermore displayed is the snow cover (cyan) and the styrofoam cover (grey).

fresh ice layer with several gas inclusions and meltponds on top. After each experiment the complete ice floe was melted away. The remainder of the snow cover was the last to melt (picture 38b).

8.1.2 Model run

The simulated sea ice by SAMSIM_original reaches a maximal thickness of about 12 cm after the freezing period (figure 39). Temperatures are going down to less than -5 °C in the ice during freezing and increase with depth. Simultaneously, the ice becomes very solid with liquid fraction values below 0.1 and the salt content decreases. On day 4, the ice warms rapidly after increasing the air temperature, while the salinity keeps constant and the liquid fraction increases slightly. The temperature profile changes in the following slightly due to changing ocean heat fluxes. No flooding occurs when the snow accumulates on the ice since the mass of snow is unconsidered in the freeboard calculation as mentioned in section 5. The snow cools down after accumulation due to the lower air temperature. On day 14, the snow temperature rises up to melting temperature and the snow becomes wetter within one day and in the mid of day 15 the snow thickness starts to decrease. One and a half day later, the snow cover has melted completely away. The temperature in the ice below the melting snow rises above -1 °C and the liquid fraction in the ice increases strongly up to 0.4 with the onset of melting. After the melting period, the temperature falls below -3 °C again in the upper ice layers and increases rapidly again on day 22 when melting starts. The liquid fraction is directly proportional to the temperature where the bulk salinity is constant. A 4 cm thick almost fresh ice layer develops on top of the ice during melting. This layer is a result of the snow-to-slush conversion in SAMSIM_original. The conversion assumes a bulk gas content of 20% in slush ice based on observations made by Eicken, Lensu et al. (1995). That content can be seen in the gas content plot in figure 39, where the only remarkable phenomenon is exactly this slush layer with 20% gas content. SAMSIM is so far not evaluated concerning its gas content calculation (Griewank personal communication), hence the gas fraction is only used to identify the „slush layer“ and a further study of the gas content is not given here.

The SAMSIM_styrofoam simulation results of the reference harps are given in figure 40. The temperature profile equals the one in SAMSIM_original with snow. Only the amplitude of extreme temperatures towards the ice surface during snow melt and refreezing is smaller in the styrofoam simulation. The ice bottom shows the same behavior to change its extent with changes in the oceanic heat flux: Increasing thickness if oceanic heat flux is small and decrease at higher heat fluxes. The liquid fraction profiles equals the SAMSIM_original simulation insofar, as if there was no slush conversion. During melting, the whole ice column gets affected by flushing. Melting of the uppermost ice layer leads to this. Since the temperatures

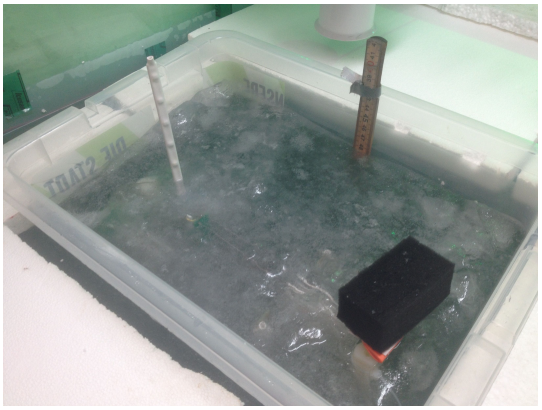

(a) Remaining snow layer after snow melt in experiment 4.

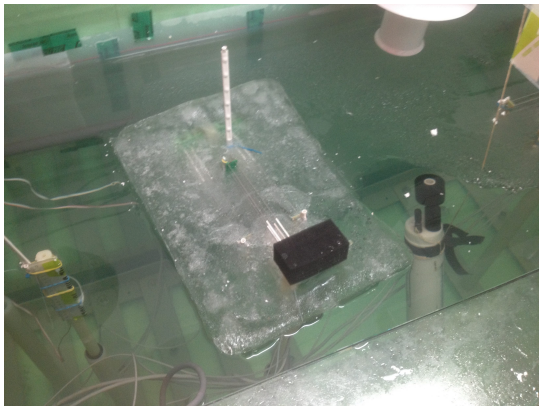

(b) Snow oddment after everything else was melted away in experiment 3.

Figure 38

are higher there, the brine is less salty than below and therefore is able to desalinate the ice below. In order to exclude gravity drainage as desalination process here, it was manually proven that almost all brine displacement is caused by flushing rather than gravity drainage.

8.2 Horizontal homogeneity

In the following, vertical profiles in the ice are investigated in terms of the horizontal homogeneity in the ice. To do so, I choose three characteristic profiles from each experiment evolution:

- **„homogeneity state“** straight before snow gets deployed on the ice, all harps (as mentioned in section 4.6)
- **„before melting state“** when ice reached equilibrium with snow on top, only snow harps
- **„after melting state“** when air temperature was set below freezing point again, only snow harps

Since ice thicknesses differed between the experiments and also between the different harps, all vertical levels are normalized by the ice thickness to make the vertical profiles comparable. In doing so, I assume that the physical properties in the ice are independent from the real ice thickness. At the same time, measured and modeled data was vertically interpolated in order to get it on a default grid with 0.01 resolution from -1 to 0. The first case „homogeneity state“ is used to determine the horizontal homogeneity in the snow experiment ice covers.

Figure 41 shows the mean horizontal standard deviations of temperature, bulk salinity and liquid fraction in all evaluable snow experiments 1-4. Furthermore, the raw standard

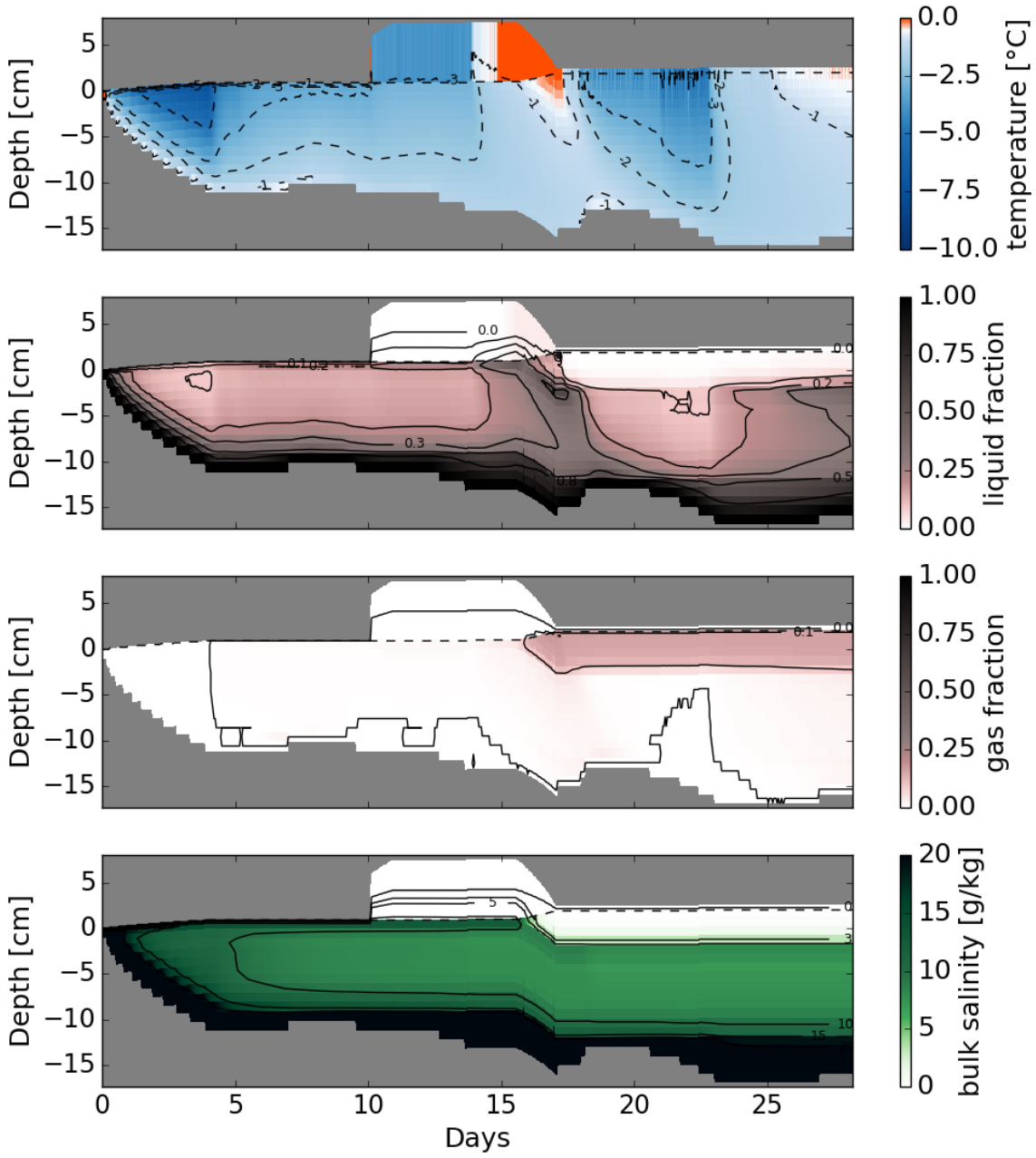

Figure 39: Temporal evolution of temperature, liquid fraction, gas fraction and bulk salinity in the ice during experiment 4 modeled by SAMSIM_original with snow. The contour lines equal the bounds in the measurement results, figure 34 - 36.

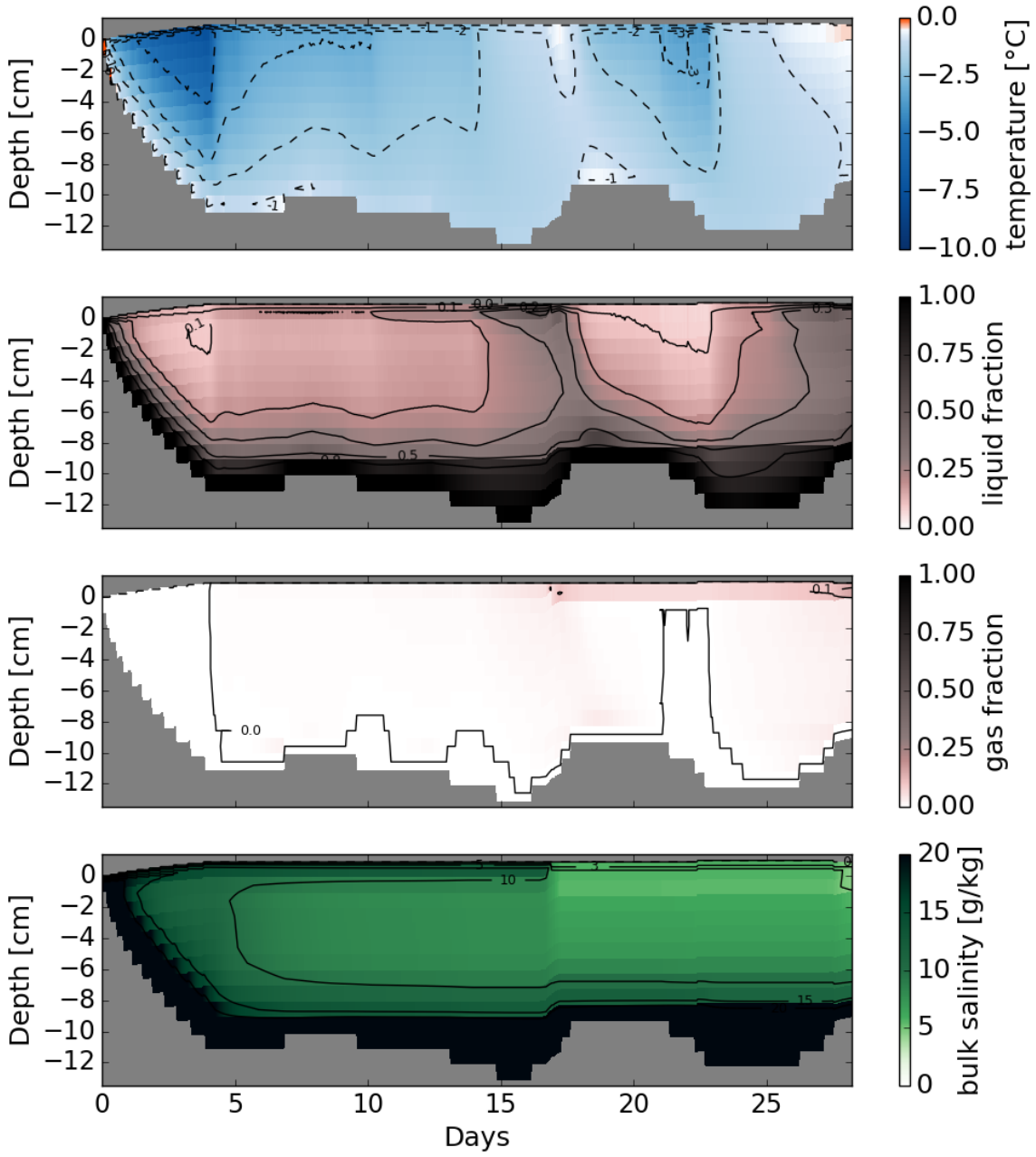

Figure 40: Temporal evolution of temperature, liquid fraction, gas fraction and bulk salinity in the ice during experiment 4 modeled by SAMSIM_styrofoam. The contour lines equal the bounds in the measurement results, figure 34 - 36.

deviations per experiment are given. Averaging standard deviations is an unrepresentative method. The maximum error of the raw standard deviations relative to the mean standard deviations is $\pm$ 0.025 for liquid fraction, $\pm$ 0.11 K for temperature and $\pm$ 2 g kg^{-1} for bulk salinity. All mean standard deviations have its smallest value at the bottom of the ice in -1 normalized depth (table 12). A local maximum in standard deviation is located at -0.9 normalized depth. Above that, the standard deviation of temperature and salinity is increasing to 0.134 K, respectively 2.4 g kg^{-1}, while the liquid fraction deviation is stable at 0.035.

Table 12: Mean horizontal standard deviations of temperature, bulk salinity and liquid fraction in the ice tank after freezing in exemplary depths

normalized depth	**temperature [K]**	**bulk salinity [g kg^{-1}]**	**liquid fraction**
-0.2	0.134	2.387	0.035
-0.6	0.078	1.781	0.037
-1.0	0.037	0.862	0.026

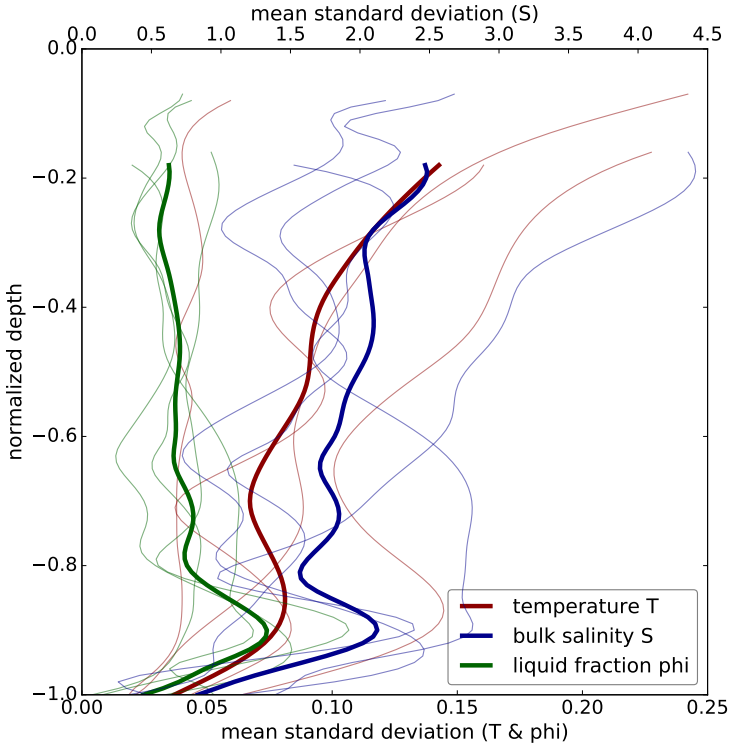

Figure 41: Mean values of the horizontal standard deviations of temperature, bulk salinity and liquid fraction from snow experiments 1-4 (thick lines) and raw the standard deviations from each single experiment (thin lines). The various upper bounds of the lines come from the different immersion depths of the harps.

8.3 Measurement and model comparison

All four evaluable snow experiments are used to investigate the capability of SAMSIM to reproduce the three main properties temperature, bulk salinity and liquid fraction in the SAMSIM lab setup. To do so, the typical temporal states mentioned in section 8.2 are investigated in vertical profiles. SAMSIM is initialized with the air–ice heat exchange parameters I determined in section 5.2. Model runs showed that ice thicknesses still differ between measurements and numerical simulations in the range of centimeters. I assume this is caused by the non-linear impact of ocean heat input. I skirt this mismatch by normalizing the depth coordinates by the ice thickness. Ice is a good insulator and its growth follows a square-root shape, with smaller rates for thicker ice. Ice thickness is therefore very sensitive to small differences in heat fluxes when it is thin, which is the case in the lab. Since the model should help me to understand processes evoked by the snow cover, a qualitative evaluation with a normalized depth coordinate is sufficient enough. Firstly, the above mentioned „homogeneity state“ is used, to check if the model setup is able to reproduce this simple state without snow (figure 42a - 42c).

SAMSIM is able to reproduce the temperature profile of snow experiment 1 and 2 where the modeled profiles lie within the range of $\pm$ two times the standard deviation. Only at the bottom of the ice SAMSIM shows a special behavior with an area of much warmer ice. In experiment 3 modeled temperature values are up to -1 K lower than measured, with larger differences toward the top of the ice. At the same time, the standard deviation of measured values is marginal. However in experiment 4, SAMSIM is up to 0.8 K warmer than the measurements towards the top of the ice. In the lower half of the ice SAMSIM is within the standard deviation of the measurements. Some further insights I can draw from figure 42a are that the temperature profile in ice is mostly linear after freezing, the bottom of the ice is always at freezing temperature and at least in the MPI-M ice lab horizontal homogeneity increases towards the top of the ice (as mentioned in section 8.2).

The mass liquid fraction profiles of SAMSIM fit well into the measurements (figure 42b). In experiment 1, 2 and 4 the profiles are even within the range of standard deviations. Small differences only occur during experiment 3 in the whole column where liquid fractions are underestimated by 0.1 as well as in the lower quarter of the ice during all experiments.

Bulk salinity, forming the link between temperature and liquid fraction, is well presented in SAMSIM (figure 42c). All modeled profiles are within the range of standard deviations of the measured values and close to their mean values. The latter supports the modeled results since the standard deviations of the measured values are relatively large. All profiles show a slight c-shape and a strong increase in salinity towards the bottom of the ice. Related to the local temperature maximum towards the bottom of the ice, numerical results show a peak in

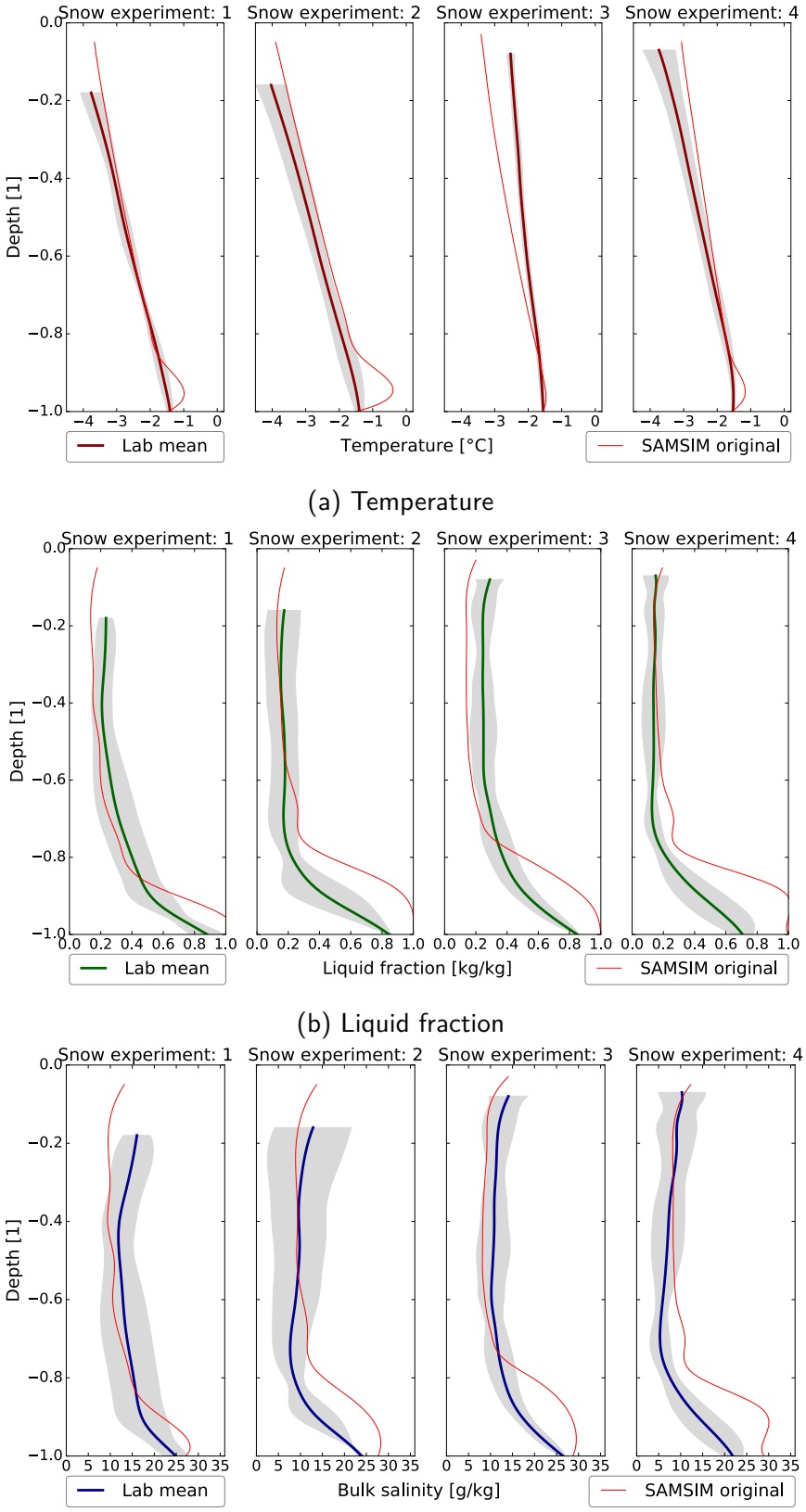

(a) Temperature

(b) Liquid fraction

(c) Bulk salinity

Figure 42: Vertical profiles of temperature, mass liquid fraction and bulk salinity at normalized depth from measurements and corresponding SAMSIM simulations at the „homogeneity state“. Measurement lines show mean values from all 5 harps ± two times the standard deviation

salinity above the bottom too. This local maximum has higher values in bulk salinity than the liquid water below.

I continue with investigating the „before melting state“ (figure 43a - 43c). In doing so, the capability of the snow setup in SAMSIM under lab conditions is investigated. The setup is newly introduced into the model physics as described in section 5. In this state only snow harp measurements are investigated.

Differences in temperature profiles between SAMSIM and measurements are smaller than in the „homogeneity state“, while they are qualitatively the same: Experiment 1 and 2 show the best behavior while in experiment 3 the temperature towards the top gets underestimated by SAMSIM and in experiment 4 overestimated (figure 43a). Experiment 1 and 2 show a slight c-shape while the profiles in experiment 3 and 4 are still linear decreasing upwards. Both trends are captured by SAMSIM. The local maxima in temperature close to the ice bottom are smaller than in the „homogeneity state“. With disregarding the reference harps in this state and therefore strongly decreasing the horizontal expansion of the measurement site, standard deviations become much smaller in comparison to the „homogeneity state“.

The strong decrease in standard deviation leads to a poorer consistency in liquid fraction, too. Modeled liquid fractions are mostly beside the range of standard deviation, apart from experiment 1, where standard deviations are huge. Nevertheless, modeled liquid fractions are close to the measured values and own the same features in their vertical shape. Differences increase in the lower third of the ice.

Bulk salinity is well modeled in the upper two-thirds of the ice for experiment 1-3. In experiment 4 the measured c-shape is much more pronounced than the modeled, this feature is mentioned in section 8.1.1 already and is further discussed in section 9.1. Mean bulk salinity values in the upper two-thirds of the ice are at about 10 g kg^{-1} before melting.

The „after melting state“ is in the issue of this work the most significant one. SAMSIM results are in this case slightly post processed in order to be comparable to harp measurements. The reason and the way in doing so should be explained in the following method parenthesis:

SAMSIM has an implemented snow to slush conversion method as described in section 5. Positive heat fluxes from the atmosphere into the snow cause warming and finally melting in the snow. Excessive snow melt water together with the lowest solid snow layer form slush ice that gets added to the uppermost ice layer. Since SAMSIM has a prescribed maximum vertical extension of the uppermost ice layers, at some point, the grid must be recalculated at the top. SAMSIM uses 1.5 times the prescribed maximum vertical extension as a threshold. Ice that used to be in the uppermost layer migrates therefore numerically downwards into lower ice layers. The same would count for harps that measure theoretically in the numerical simulations. Since they are frozen and therefore fixed in the ice layers, they would migrate

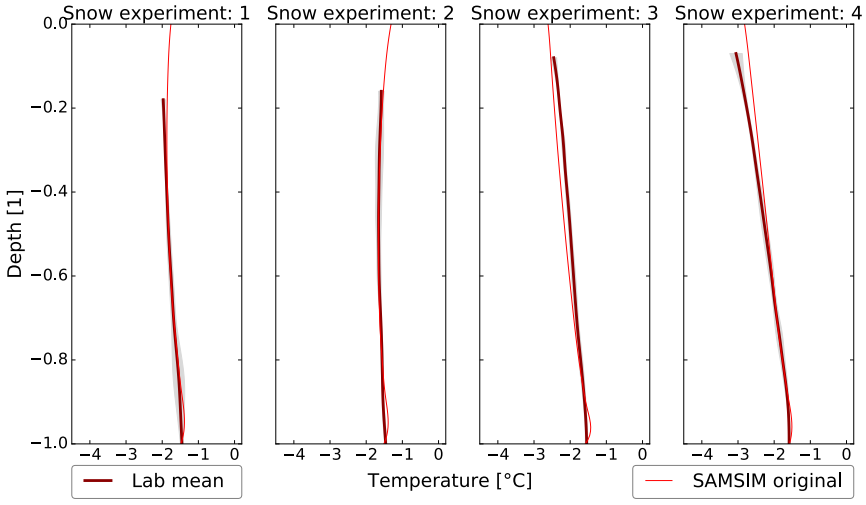

(a) Temperature

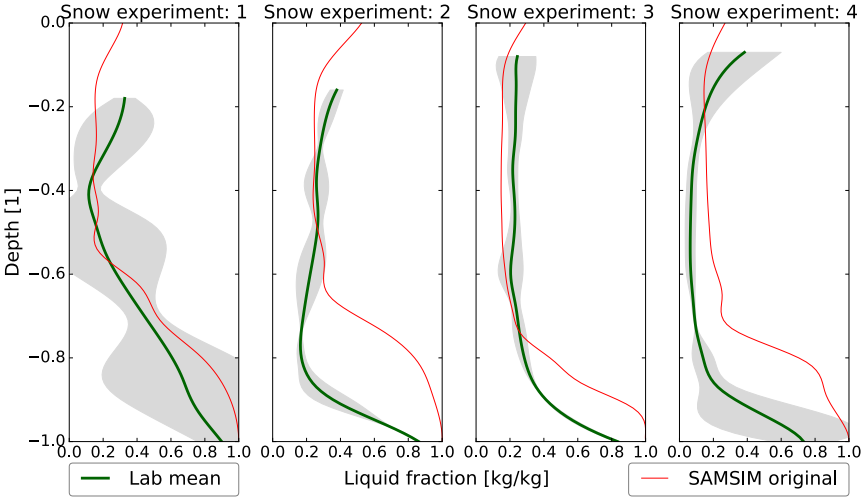

(b) Liquid fraction

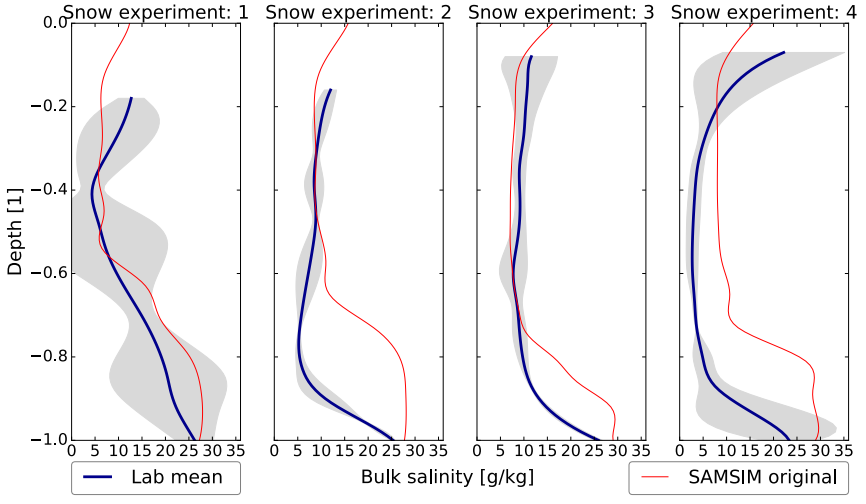

(c) Bulk salinity

Figure 43: Vertical profiles of temperature, mass liquid fraction and bulk salinity at normalized depth from measurements and corresponding SAMSIM simulations at the „before melting state“. Measurement lines show mean values from all 5 harps ± two times the standard deviation

downwards with the ice in the simulations during snow melt. This migration can be of no interest for pre–post comparison of numerical snow melt situations, but is of high interest to investigate and understand the effects behind changes in the physical properties of sea-ice during snow melt. I therefore developed the SAMSIM-HARP simulation, in which the vertical migration of the initial top ice layer gets tracked during the whole SAMSIM run. In doing so, I can post-process the numerical model results and consider solely the vertical fraction of the ice, in which the harps would be able to measure. To give an example: if 3 cm of slush ice is added to the top ice layer during the snow melt and the maximum vertical extension of the layer is $\Delta z = 1$ cm, then the ice grid gets recalculated six times: always when 0.5 cm of slush is added to the top layer, the maximum of $1.5 \cdot 1.0$ cm is reached. The top of the primary uppermost ice layer is therefore at the end of the snow melt period in a depth of 3 cm. If all the snow is gone and the ice starts to melt at the top, the layer would of course migrate upwards again. With having a depth of 3 cm of the initial ice layer, the SAMSIM-HARP simulation cuts away the uppermost 3 cm of the results and provides the remaining ice again with a normalized vertical coordinate between 0 and -1 to make it comparable to the harp measurements. Small errors are introduced by this simulation since numerical results from below the water level can be thus brought into regions above the level which is in the normalized coordinate at about -0.1. In doing so, the so-called hydraulic head in the ice is influenced and thus, brine fluxes too. Nevertheless, the SAMSIM-HARP simulation is a helpful representation of numerical results to compare them with harp measurements.

Profiles calculated in this way are given in figures 44a - 44c. Starting with temperature profiles in figure 44a that shows the state after melting: The modeled profiles match the measured ones very good in experiment 1 and 2, while in this case, in experiment 3 and 4, the temperatures are underestimated by up to -0.6 K in a depth of -0.2.

Liquid fraction profiles show a strong heterogeneity in the ice in experiment 1 and 3, which fits to observed melt ponds on the ice (figure 44b). Especially in experiment 2 and 3 SAMSIM_original is able to approach the mean liquid fraction profile measured by the harps, while SAMSIM_original underestimates the liquid fraction of about 0.3 in experiment 1 and overestimates it by 0.2 in the center in experiment 4.

Even though measured liquid fractions in experiment 3 show a strong heterogeneity, the bulk salinity is well defined in this experiment (figure 44c) in the upper two-thirds. The same small heterogeneity counts for the measurements in experiment 2 and 4. Only experiment 1 retains its heterogeneity. SAMSIM underestimates the mean bulk salinity in the upper two-thirds of the ice in experiment 1, matches it exact in experiment 2 and overestimates it in experiment 3 and 4. The modeled profiles are in this vertical range almost constant. The same counts for measured values in experiment 2 and 4, while experiment 3 shows a decline

towards the top of the ice, where the ice is fresh, like in experiment 4. Experiment 3 shows furthermore a higher heterogeneity in the lower third.

Changes of bulk salinity during melting indicate an impact of the snow cover on the salt content in the ice. I therefore start with comparing differences between the „before melting state“ and the „after melting state“ with and without snow cover. The former investigations are made with the mean of snow harps 1-3 as well as the SAMSIM_originalal setup, corrected with SAMSIM-HARP (figure 45a). The latter, that means the investigations without snow cover, are made with ref harps 1-2 in comparison to the SAMSIM_styrofoam setup (figure 45b). In order to quantify the changes in salt content, I divide the vertical coordinate into 10 bins of size 0.1 and integrate over their salinity (equations 6). A small error originates from such lab to model comparison since their ice thicknesses were unequal, but the method is sufficient enough for this study.

In experiment 1 no change in salt content occurs below the snow cover in the upper third of the ice (figure 45a). In the center the salt content increases in the lab measurements and at the bottom it decreases. The decrease as well as the constant content is captured by modeling and measurements. Constant salt contents are the case in experiment 2 too. However, in experiment 3 a strong decrease is measured in the upper two-thirds while the salt content increases in the lower third. SAMSIMs original setup shows absolutely constant values over the whole column. In experiment 4 the measured shape is the same as in experiment 3 with slightly smaller values. SAMSIM again derives no changes. Only between -0.7 and -0.9 depth some changes are modeled.

Without snow as freshwater source but still similar heat fluxes no sharp trend of desalination in the ice is visible as it is in experiment 3 and 4 below snow. In experiment 1 some salt loss occurs in the upper and the lower third of the ice during the measurements, while SAMSIM calculates even small increases in the center (figure 45b). Experiment 2 displays a constant profile in measurements and a slight s-shaped profile with much larger values in SAMSIM. Model and measurements agree extremely well on the profile in experiment 3: decreasing salt content in the upper and the lower layers, while the center is relatively stable with only small decreases. In experiment 4 finally stronger increases in salt content are measured in the lower third, where SAMSIM on the other hand shows a small trend of decreasing salt contents.

The impact of snow on the salt content is in experiment 1 negative in SAMSIM and positive in the measurements. In experiment 2 the impact is zero in the measurements and in SAMSIM positive in the upper half and negative below. Experiment 3 and 4 however show a clear trend of desalination in the upper two-thirds of the ice due to a snow cover. The former shows a strong positive effect at the bottom while the latter shows even here a strong negative effect of snow on the salt content. SAMSIM shows slight positive effects in both experiments.

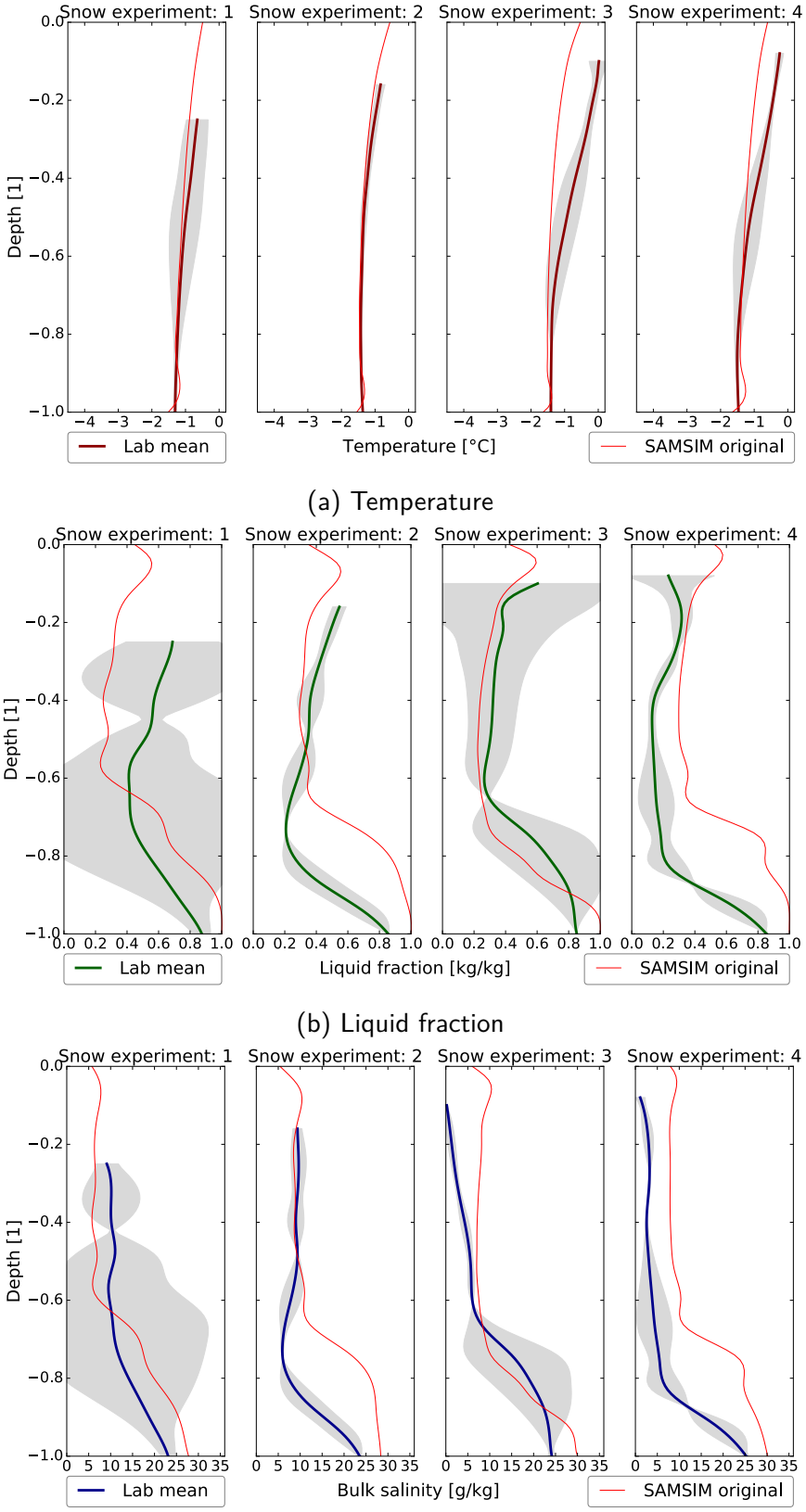

(a) Temperature

(b) Liquid fraction

(c) Bulk salinity

Figure 44: Vertical profiles of temperature, mass liquid fraction and bulk salinity at normalized depth from measurements and corresponding SAMSIM simulations at the „after melting state“. Measurement lines show mean values from all 5 harps ± two times the standard deviation

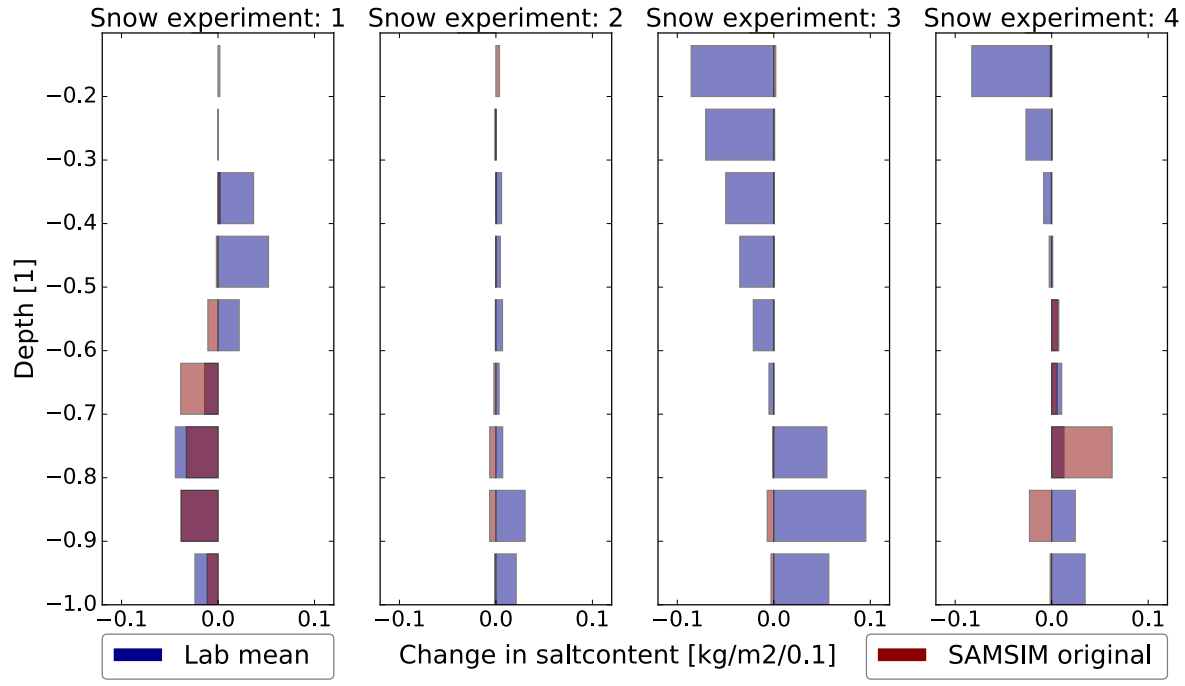

(a) Snow cover

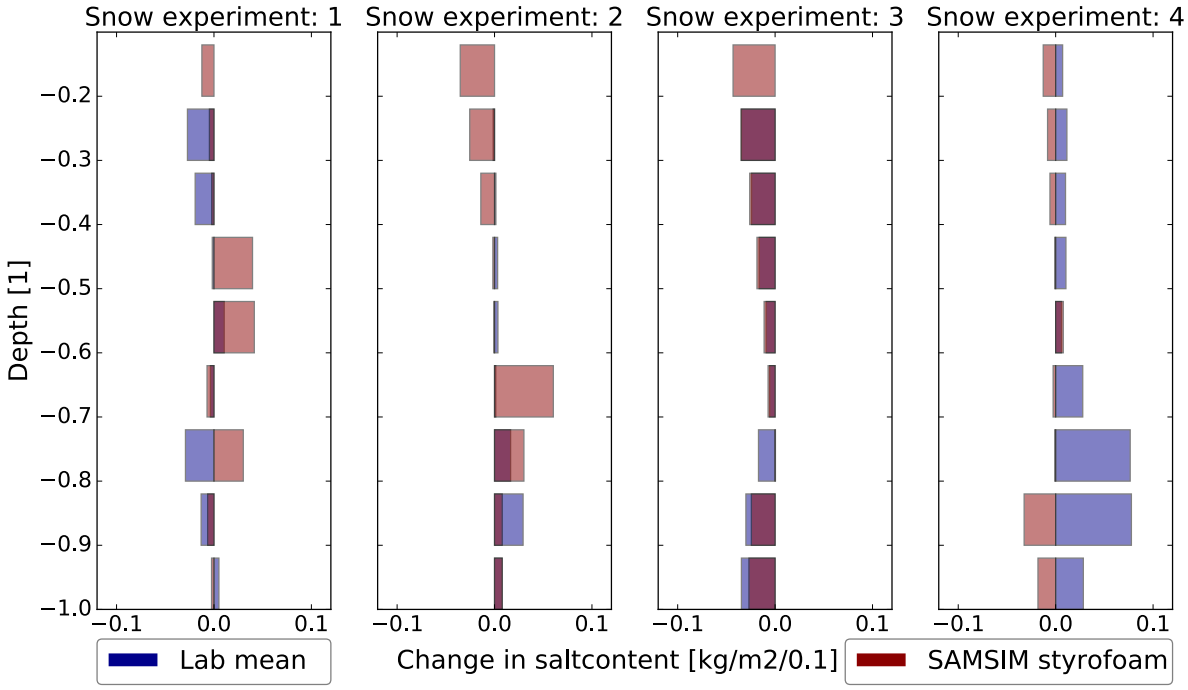

(b) styrofoam, reference

Figure 45: Vertical profiles of salt content change in the ice between „before melting state“ and „after melting state“ beneath the snow cover a) and beneath the styrofoam b). Negative values stand for decreasing salt content during melting.

The temporal evolution of the bulk salinity profiles in experiment 4 during melting is given in figure 46. The onset of snow melt is retarded in the SAMSIM simulation but the melt rate is eventually higher. Measured and modeled bulk salinity vary strong before the onset of melting as displayed by figure 43c above. The vertical salinity profile of the lab ice is much more c-shaped than the modeled one. In the furthermore temporal evolution, melting snow gives rise to a measurable decrease of bulk salinity in the lab. However in SAMSIM_original the snow-to-slush conversion adds salt-free ice layers to the top of the sea ice cover. The red line in the center graph indicates the former ice surface which starts to migrate downwards due to the snow-to-slush conversion. This indicates the reason for the SAMSIM-HARP simulation, which is given in the bottom graph of figure 46. No change in sea-ice salinity is modeled in this simulation. A saw-tooth pattern develops in the ice during melting due to the threshold-driven grid recalculation in SAMSIM.

8.4 Quantitative desalination

The impact of the snow cover on the sea ice salinity is evaluated regarding to the available amount of freshwater on the ice. To do so, I subtract the salt content change during melting beneath the styrofoam from the change beneath the snow. In this way, the isolated influence of the freshwater source on top of the ice can be investigated. Changes are calculated for the upper 60% of the ice only in order to neglect the error-prone lowest part of the ice measurements and simulations (figure 47). The lab measurements show an almost linear trend in which larger amounts of freshwater come along with stronger decreases in salinity in the ice. This linear trend is independent from the initial amount of salt content in the ice. Almost 80% of the trapped salt gets flushed out of the upper 60% of the ice. The ratio between the absolute salt content change to the available freshwater fits well to the typical ratio of dissolved salt in water.

However, experiment 1 with the smallest snow cover shows an increasing salt content. This indicates a negative impact of the snow on the desalination. SAMSIM_original together with SAMSIM_styrofoam acts anticyclically to the lab measurements: The snow cover in the model has only in experiment 1 a positive impact on the desalination. In all other experiments SAMSIM calculates a somewhat stronger desalination of the ice beneath styrofoam than below snow. I assume this deviation is caused by an improper surface heat flux setup below the styrofoam in SAMSIM and an overestimation of surface melt water flushing.

The salt content change due to melting snow is zero at a mass ratio $m_{meltwater}/m_{ice}$ of 17%. That means, blank ice desalinates more than snow covered ice when the mass of the snow cover is less than 17% of the ice mass. Heavier snow covers desalinate the ice more than a melting blank ice surface, the grade of desalination is in doing so 11% salt loss per

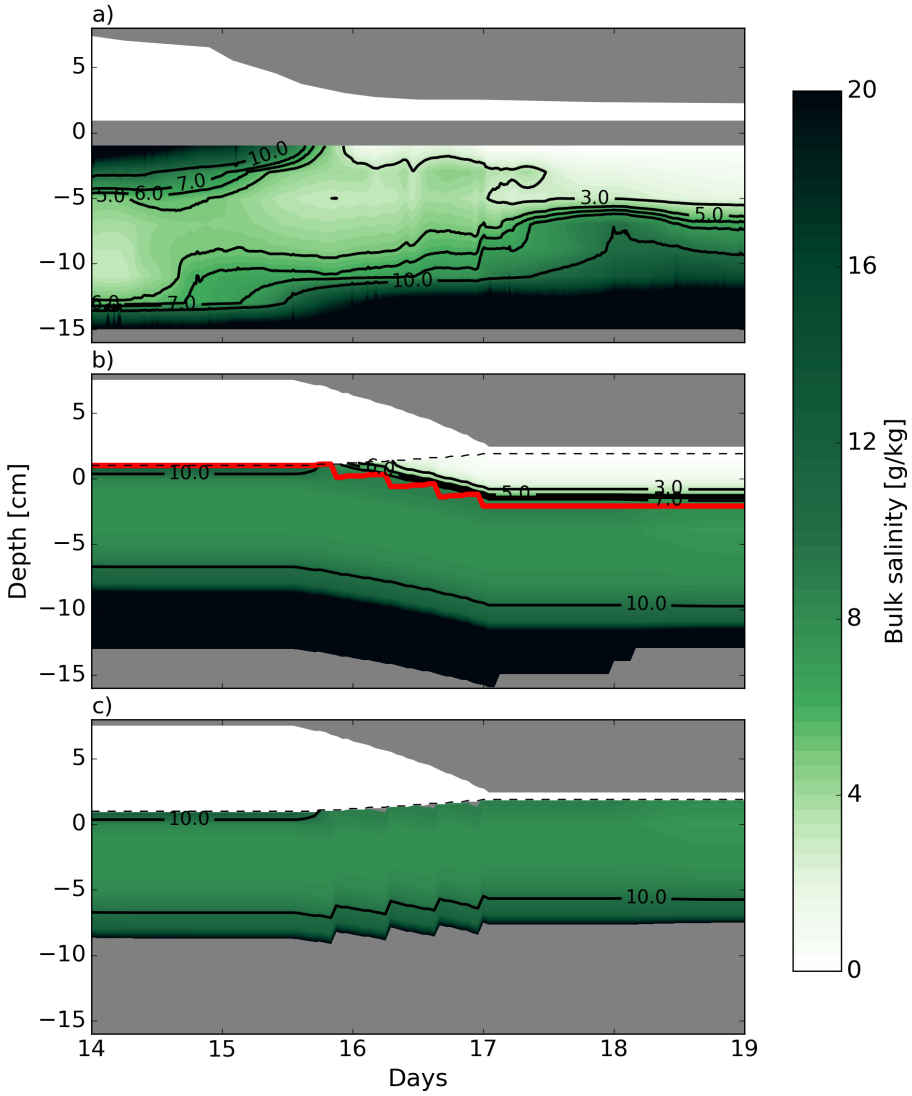

Figure 46: Temporal evolution of bulk salinity profiles in the ice. **a)**: Snow harp 2 measurements. **b)**: Raw SAMSIM_original results, the red lines indicates the former ice surface that migrates downwards due to the snow-to-slush conversion. **c)**: SAMSIM_original results post processed with the SAMSIM-HARP simulator. The ice profiles is thus directly comparable to the lab measurements.

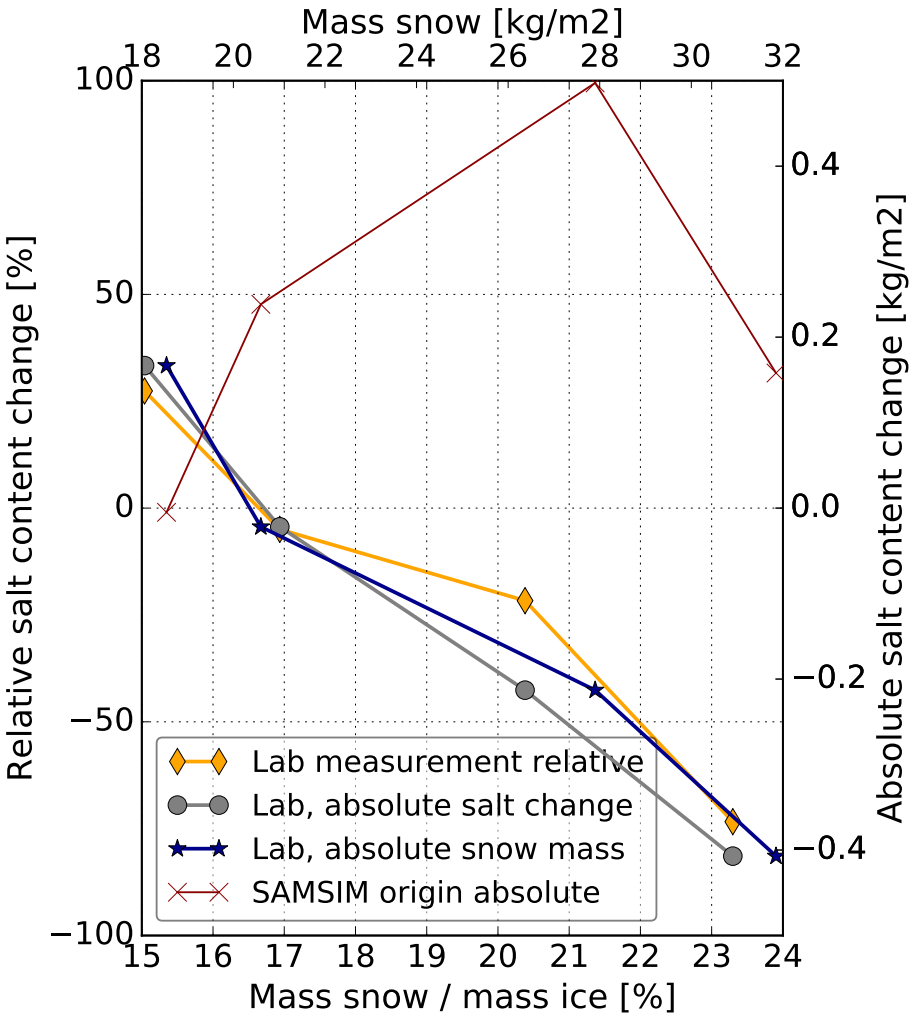

Figure 47: Salt content change due to the snow cover in the upper 60% of the ice during snow melt subtracted by the amount of salt change below the styrofoam. Displayed is the relative change of salt content, which is the absolute change divided by the amount of salt before melting dependent on the relative amount of snow, which is the absolute amount of snow divided by the ice mass (orange). Furthermore, the grey line is the absolute desalination dependent on the relative amount of snow and the blue line is only dependent on absolute values. The dark red line shows absolute values of SAMSIM.

percent snow weight above 17% ice weight. This linear regression is greatly simplified because the curve must converge to -100% salt change or higher values in reality. Negative salinity values are impossible. However, the suggested maximum snow mass of 25% which is needed in the linear relation to make the ice completely salt free fits well to the typical bulk liquid fraction of about 0.25 in the ice below during melting, which I also measured. The amount of snow would be theoretically able to replace almost all salty brine in the ice with freshwater. Furthermore, the somewhat linear shape of the measurements confirms, that the amount of salt change is also dependent on the bulk salinity of the ice before melting. Very saline sea ice has a higher permeability than less saline sea ice close to the melting point temperature. Melt water can thus penetrate easier into the ice skeleton and replace salty brine. The similar shape of all lines confirm that the described behavior is independent of the scaling method.

Owing to a malfunction of the measurement electronics harps measurements from experiment 5 are not evaluable. Nevertheless, experiment 5 is the only experiment with ice core data from before and after melting from the snow and the reference area of the ice floe. This ice core data is presented here in order to complete the presented desalination series.

Experiment 5 had the thickest snow cover with a snow mass of 45.6 kg m^{-2}. The grade of desalination below this snow cover is distinctive as can be seen in figure 48. The impact of flushing on the salinity profiles fits the behavior of experiment 3 and 4. The lengths of the cores vary strong, which is probably caused by the different locations where they were taken and the lens shape of the ice floe or due to broken off pieces from the ice core that remained in the water. However, the important upper parts of the ice cores are affected neither from that nor from remarkable brine outflow. Core5.snow1 and Core5.snow2 disagree only in the vertical expansion. Their salinity profile shapes resemble each other quite well. The same counts for Core5.before and Core5.ref, it seems like that the lower part of Core5.ref is missing. Bulk salinities in the upper half of the ice decrease during melting from about 7 g kg^{-1} to 1-5 g kg^{-1} below the snow. The surface height of the ice increases slightly due to remaining freshwater ice on the sea ice floe. The freeboard of the entire floe remains constant since the snow area is comparable small to the overall floe area. The change in salt content of the upper 60% of the ice is calculated by normalizing the depth coordinate. Results are given in table 13. The salt mass is normalized by the factor 0.1 which equals salt expelled from ice with a total ice thickness of 10 cm. This slightly smaller ice thickness reduces the amount of salt content change in experiment 5 in comparison to the other experiments. A small amount of salt decrease of about 1 g kg^{-1} is also measured on the reference side.

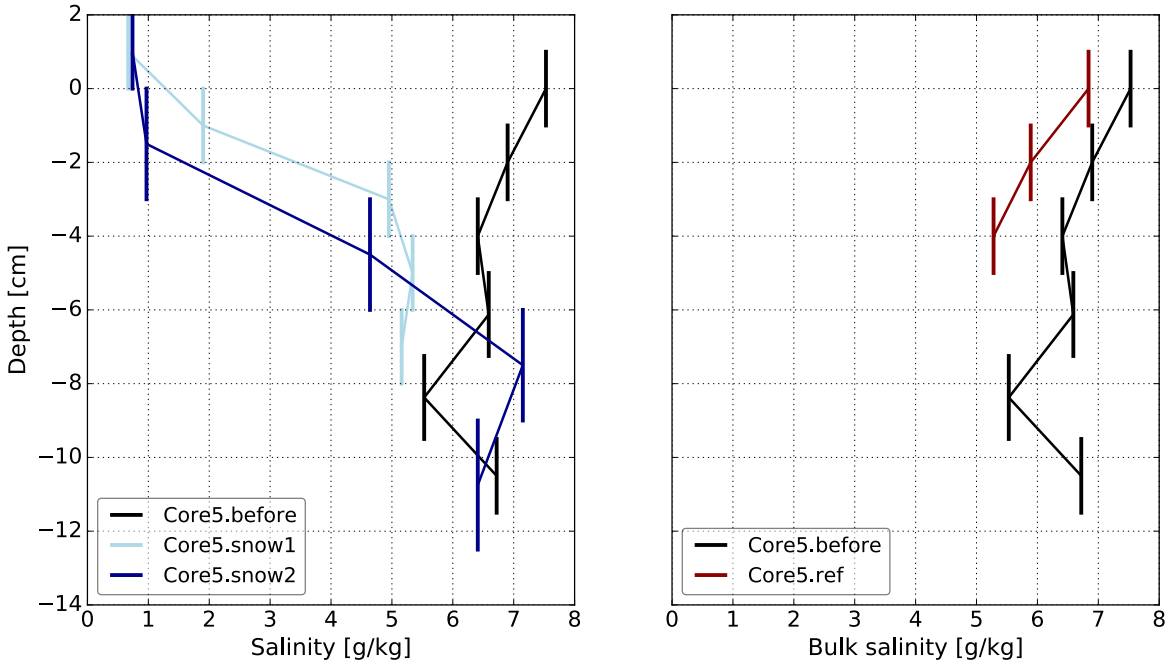

Figure 48: Ice core salinity profiles from experiment 5. Profiles from below the snow cover are displayed on the left hand side and reference cores on the right hand side. The labels are introduced in table 3.

Table 13: Salt content change in experiment 5 ice cores during melting.

ΔCore	**Salt content change [kg m^{-2} 0.1^{-1}]**
Core5.snow1 - Core5.before	-0.174
Core5.snow2 - Core5.before	-0.176
Core5.ref - Core5.before	-0.033

9 Discussion - Snow experiment

The measurements and simulations match the physical understanding of sea-ice thermodynamics and air-ice-sea interaction. Both methods equal each other well after freezing. The temperature at the ice bottom is at freezing temperature of the underlying seawater, the temperature in the ice follows the trends in air temperature, there is a steady salinity profile at the ice bottom and the overall bulk salinity decreases during ice growth. The liquid fraction decreases down to about 0.1 and a c-shape salinity profile develops. Since that counts for all recorded time series, I recorded thus a notably data set for further model evaluations.

9.1 Snow experiment 4

Things change and become more particular with the accumulation of snow on the ice: The deployment of snow on the ice causes a jump in temperature and salinity in the measured ice in experiment 4, which I assume is an effect that has its origin during ice growth:
In experiment 5, a small layer of liquid brine turned up during ice growth on the ice surface. The difference in density between solid ice and liquid brine leads to a pressure increase in the brine pockets while they are getting colder as described by brine expulsion. At the ice surface, this pressure can lead to a sudden release of brine, which then flushes on top of the ice. In experiment 5, this release must have happen within one night, while we did not observe the ice. The fact that the brine on top of the ice was liquid even though the air temperature was at about -13 °C and that salinity measurements of this brine showed values of about 120 g kg^{-1} confirm the assumption that the brine is expelled from the uppermost ice layers. I did not noticed the liquid in the experiments before, but I assume the same effect happened, since the experiment execution was the same. Similar observations were made before by Perovich and Richter-Menge (1994) and Notz (2005). The temperature of the ice surface in experiment 4 is well below -3 °C while I deployed the snow with a temperature slightly below 0 °C (section 4.6). Hence, a change of the temperature profile in the ice can be expected due to the warmer snow on top of the ice as well as due to the insulation properties of snow that reduces the air–ice heat exchange. A scale analysis suggest a timescale of about 1.5 hours for this change (based on the heat conduction equation 7, with $q = 0$), but the measured jump happened within one measurement cycle of about 10 minutes. That means, another, even stronger, effect must have acted that is based on mass exchanges rather than diffusive heat fluxes. The permeability of ice is strongly dependent on its liquid fraction (equation 8) and thus, at a locally given bulk salinity on its temperature. A small increase in temperature due to the warmer snow can therefore have a strong small-scale effect on the ice surface permeability. The permeability would rise due to warming, which then gives liquid water on

top of the ice the possibility to percolate into the sea ice. Temperature measurements show an increase of temperature in the ice, with the fastest increase not at the top of the ice, but in the center (figure 49).

The only reason for this increase can be penetrating liquid water with a lower salinity than the surrounding brine salinity. In the following, heat energy needs to be transported away and therefore enables freshwater to solidify. Hence an increase of temperature comes in this case with a decrease in liquid fraction, which I measured indeed (figure 35). However the measured magnitude of phase change of about 0.05 is too high for the small increase of temperature of less than 1 K in the ice. I assume a small measurement error due to brine sensitivity (section 7.2) is the reason for this inconsistency. It is further unclear which imbalance causes the heat flux. The fresher water that penetrates into the ice has its origin in the snow and from top of the ice. Since the temperature profiles always keep their slope with lower value towards the top of the ice, the fresh brine cannot be from upper ice layers. I assume instead that the water is on the one hand liquid water content of the snow that remained despite straining the snow and on the other hand meltwater from the snow: Salty water can easily move into snow as flooding experiments have shown in the past (Aukan, 2016). So that one can assume that the extreme salty brine on top of the ice immediately moved into the snow, and due to its lower freezing temperature, melted away a specific amount of freshwater ice (as salt on icy roads does). The energy that is needed for this melting could be the reason that in figure 49 the upper layers warm slower than the center of the ice. The super salty brine layer on top of the ice is very probably also the origin for the increase in salinity in the upper ice layers. The higher liquid fraction in the uppermost ice layers allows the salty brine to penetrate into the ice. Why the freshwater and the salty brine kept clear from each other is unknown and thus only the observed results and their presumable origins are discussed here. Nevertheless, the salt mass balance measurements given in section 7.3 show that the harp measurements are reliable in experiment 4.

The differences in temperature between the snow and reference harps before and during melting confirm a little lower heat conductivity of the styrofoam in comparison to the snow cover. The ice below the styrofoam warms stronger relative to its freezing temperature while the air temperature is still well below freezing point (figure 37). During melting the ice below the styrofoam remains colder relative to its freezing temperature. The ice beneath the snow however almost reaches its freezing temperature. SAMSIM_original and SAMSIM_styrofoam both capture the temporal temperature evolution. Peaks in the surface temperature during melting and refreezing are damped in the styrofoam simulation due to the higher bulk salinity which has a lower freezing point during melting and a higher heat capacity during freezing. The typical c-shaped bulk salinity profile after freezing is captured by both simulations as well as an increase in liquid fraction during melting. Two untypical behaviors occur at the bottom

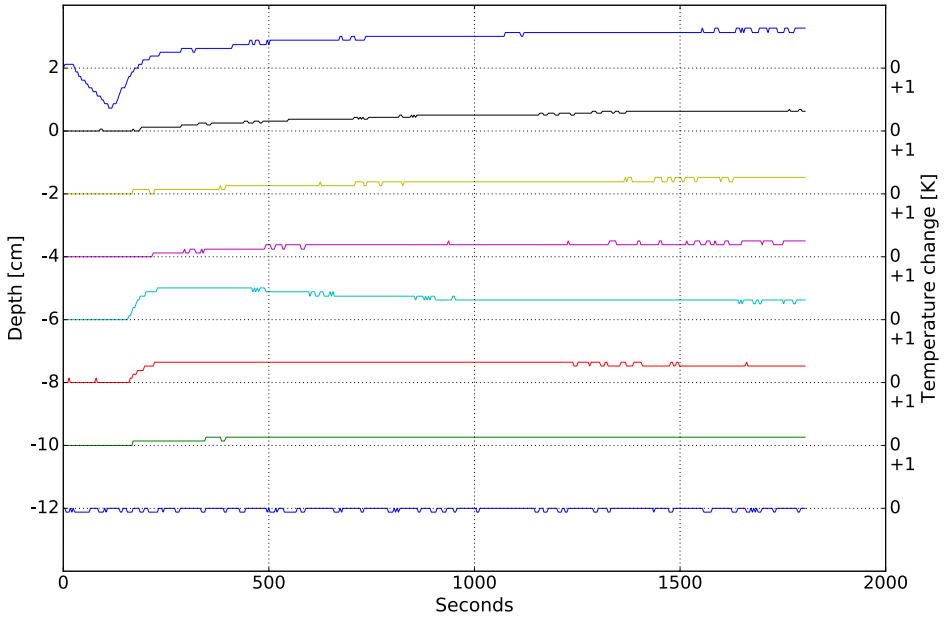

Figure 49: Temporal changes of temperature in the ice and directly above during snow deployment measured by T-Sticks which were fixed on snow harp 2. The space between two horizontal grid lines equals a temperature change of 1 K.

of the ice, changes in the oceanic heat flux influence the ice thickness much stronger than observed in the lab and local temperatures maximums form near the bottom. I assume that both of these effects are numerical artifacts that evolve due to forced boundary conditions on the ice bottom. The styrofoam furthermore overestimate the observed desalination during melting. Either this is due to the simplified atmospheric heat flux setup and a concurrent underestimation of heat conductivity through snow or SAMSIM overestimates flushing that is caused by melting of the upper ice layers. At the end of the experiment the ice was completely melted away, as lab measurements and observations confirm, but this melt is neither simulated by SAMSIM_original nor by SAMSIM_styrofoam. The reason for that is most likely an incomplete implementation of the oceanic heat flux since the ice in the lab was mainly melted away by heating the water.

In conclusion, I obtain three effects of the snow cover on sea ice salinity throughout analyzing experiment 4. Firstly, deploying styrofoam on the ice and thus simulating the insulation properties of a snow cover, leads to a small decrease of bulk salinity in the ice below. The reason for that is a slight increase of temperature in the ice which could lead to gravity drainage if the critical Rayleigh number is reached. If the same occurred below the snow cover in experiment 4 remains unclear, since two even stronger effects happened there. They are discussed within this section before. Secondly, super salty brine that was expelled onto the ice surface before, was flushed back into the ice by the snow and freshwater

from the snow penetrated into the ice and led to flushing. All these effects on salinity before melting occurs were much more pronounced in experiment 4 than in any other experiment. But due to the well-developed snow setup one can trust this results to a high degree and they were partly observed in the other experiments too. So happened the flushing in experiment 1 and a slight decrease in salinity below the styrofoam in experiment 3. While gravity drainage through warming is likely to occur also in nature, it remains unclear whether the observations below the snow cover meet natural circumstances or are only an artifact of lab measurements. The third effect of the snow cover occurs during melting. Changes in the bulk salinity as well as rapidly warming of the ice beneath the snow cover indicate that warm and less saline water penetrates into the ice from the surface. The affected ice warms rapidly up to its freezing point during flushing. An imbalance in the temperature–brine salinity linkage develops, but the dominance of latent heat needed for phase changes compared to the heat capacity of ice prevents large changes in the liquid fraction. The ice compensates instead the change in brine salinity predominantly by warming rather than by freezing. Quantitative values of the desalination process are given in section 8.3.

9.2 Horizontal homogeneity

The range of liquid fraction values is limited by definition to 0 to 1, horizontal standard deviations are thus expected to be the smallest in comparison to temperature and bulk salinity deviations. This assumption applies to the statistical results in section 8.2. The liquid water below the ice is robust to local perturbations, hence standard deviations are the smallest close to this interface. Above the interface, all mean horizontal standard deviations show a local maximum, which is caused by the normalizing process of the vertical axis. Gradients in the ice are mostly largest close to the ice–sea interface. Hence, small errors in the ice thickness affects the standard deviations at a depth level of about -0.9. Temperature deviations increase towards the ice surface. The ice is cooled or heated from the atmosphere. Small local deviations in the air temperature field above the tank can therefore lead to temperature differences in the ice, especially to horizontal differences close to the air–ice interface. Measured bulk salinity deviations follow this trend since the calculated brine salinity depends on the single point temperature measurements.

9.3 Measurement and model comparison

The capability of SAMSIM to model the measured mean state in the ice after freezing is encouraging. Even though the temperature profiles are slightly different towards the top of the ice after freezing due to complex heat fluxes in the lab, salt fluxes seem to be well

parametrized since modeled liquid fraction and bulk salinity profiles are always within the area of the mean measured value ± twice the standard deviation. That means the numerical result is within the range of 95.45% of all expected measurements as long as the horizontal heterogeneity in the ice is normally distributed, which I assume for that reason. Only towards the bottom of the ice a presumable numerical artifact develops with too high temperatures due to forced boundary conditions there. This area is affected by the depth normalizing too and should be thus not further investigated here. The depth normalization is presumably the reason for differences in the liquid fraction and bulk salinity towards the bottom too.

In experiment 4, SAMSIM's temperature calculation differs about 1 K from the measured temperature in the upper ice layers while the horizontal differences in the ice tank are marginal. It must be therefore assumed that the atmospheric heat flux parametrization in SAMSIM is not able to represent measured reality here and works slower than measurements indicates. The marginal standard deviation in comparison to colder profiles suggest that bare ice in the lab has a higher horizontal heterogeneity at lower temperatures. The heterogeneity decreases as soon as the ice starts to warm. The insufficient heat flux parametrization is also the reason for ice thickness differences between measurements and simulations given in table 11. Nevertheless, the results are close and definable enough to use SAMSIM in order to analyze processes.

All measurements and simulations suggest the typical c-shaped vertical bulk salinity profile in the ice, which I explained in section 1.2. The development of the profile is therefore a sign for the accuracy of the physical understanding of gravity drainage and its parametrization in SAMSIM.

The impact of snow on the ice salinity during melting is getting obvious in the before and after melting states results finally. In both experiments 3 and 4 presented here, in which the frame around the snow was sealed to the ice surface and in doing so meltwater was forced to percolate into the ice around the snow harps, strong decreases in the sea-ice salt content are measured below the snow. Both experiments simulate best natural circumstance where an area-wide snow cover has the same effect as the sealed frame around the snow in the lab, except for the possibility of large cracks in the ice where meltwater can easily run-off. Figure 45a displays unambiguously the consequences of freshwater flushing in sea-ice as described in section 1.2. A strong decrease of salt content in the upper layers goes along with a slight increase further downwards. Due to lower temperatures towards the top of the ice at the onset of flushing, brine salinities are higher at the top than further downwards. As soon as this saltier brine starts to percolate downwards it enhances the bulk salinity right there. The overall amount of freshwater flushing in both experiments was not sufficient enough to flush away the salty brine in the whole ice column or the ice permeable enough so that gravitational overturning develops. In order to compare the measured values with SAMSIM results, the

presented SAMSIM-HARP simulation is used. SAMSIM shows in figure 39 and figure 46a & b the capability to reproduce roughly the impact of snow melt on the ice beneath, but not the process of flushing itself (figure 45a). The implemented snow-to-slush conversion works well to calculate multi-annual conditions where it is no matter how and when exactly the melting snow affects the salinity. But for this work, where SAMSIM is used to understand the process itself, the implementation is not sufficient enough (figure 46c). For this reason, SAMSIM_original gave rise to a change in the understanding of snow melt and flushing in comparison to existing implementations in models which I present in the following section 10.

Two further impacts of snow on sea ice salinity during melting can be drawn as conclusions in addition to section 9.1. Firstly, the downwards displacement of brine during flushing can lead to an increase of bulk salinity in the lower part of the ice if the ice is still colder towards the top. And secondly, the increase in bulk salinity as a result of the snow cover in experiment 1 relative to the styrofoam cover suggests that a thin snow cover that insulates the ice on the one hand, but does not supply enough meltwater for flushing on the other hand, counteracts desalination. The same happened in SAMSIM simulations of experiment 2-4. This effect becomes clearly visible by evaluating the quantitative desalination figure 47, from this I obtain the mass ratio $m_{meltwater}/m_{ice} = 17\%$ as a threshold at which the amount of desalination is equal. Furthermore, the measured salt changes confirm the expected relation: the larger the amount of snow that melts above the ice, the larger the decrease in salt content in the ice beneath. The relative change in salt content dependent on the initial amount of salt follows this behavior. The evaluation of salt content change in experiment 5 based on ice cores fits in almost seamlessly with the harp measurements in the other experiments.

10 New snow melt implementation in SAMSIM

The temporal evolution of bulk salinity in the ice beneath melting snow (figure 36) supports the idea of immediate flushing since effects in the ice are measurable immediately after the onset of melting. The observation at the end of melting mentioned in section 8.1.1 that - relatively independent from the temperature evolution during melting - distinct freshwater ice remained on top of the sea-ice, supports the idea of melting applied in SAMSIM. Hence, a combination of both ways seem to be closer to reality than the so-far used methods. In the following I explain this combination with the implementation in SAMSIM. I assume the incomplete melting of the snow cover originates from the resistance of the formed solid fresh ice layer against warm temperatures. As soon as all insulating „white“ snow is melted,heat fluxes warm up the ice beneath and lead to phase changes in the sea-ice skeleton rather than melting the remaining solid freshwater on the ice first. This assumption is supported by the strong increase in liquid fraction in the ice after the snow melt decreased in experiment 4.

10.1 Melt water segmentation

The snow-meltwater formation keeps equal to SAMSIM_original, but before the meltwater is used to form slush, a defined fraction of the meltwater gets subtracted (scetch 50). The remaining freshwater forms slush as before, but less. The subtracted meltwater gets passed to the complex flushing routine presented in Griewank and Notz (2015), which determines the amount of possible run-off through flushing dependent on the hydraulic head and the permeability of the ice below. The residual meltwater from that remains in the uppermost ice layer, without forming slush on the way getting there.

In order to define the fraction of meltwater that remains for snow-to-slush conversion, a mass specific segmentation parameter is introduced: $k_{snowflush}$. In order to obtain a value, I took the remaining solid slush-ice masses m_{remain} on the ice from all experiments and calculated their mass fractions relative to the initial snow masses $m_{initial}$. As a mean value I obtain m_{remain}:$m_{initial}$ = 1:3 and thus $k_{snowflush}$ = 0.75, which means 3/4 of the meltwater is used for flushing and $1/4$ remains for snow-to-slush conversion.

As a result of the new parametrization in SAMSIM (sketch 50), the added slush layer B_{new} is thinner, the solid fraction of the snow $\phi_{s,new}$ is higher and the liquid fraction of the uppermost ice layer $\phi_{l,new}(z = 1)$ is smaller in comparison to the old parametrization in SAMSIM after each timestep during melting. The latter has the effect that in cases where melting continues after the snow has gone, the onset of flushing through melting of the upper ice layers is likely to occur a bit later. In the following, this SAMSIM setup will be referred to as „SAMSIM_2017“.

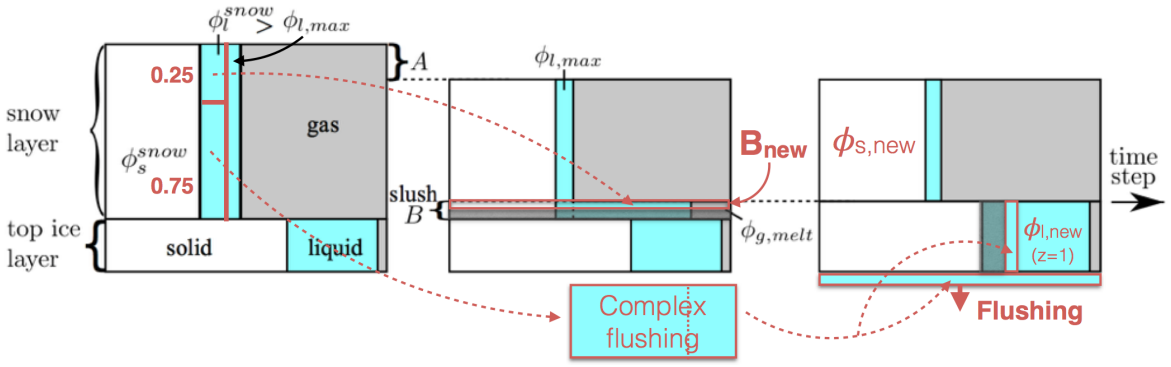

Figure 50: Illustrated changes in the snow meltwater run-off parametrization of SAMSIM. 1/4 of the meltwater is used for snow-to-slush conversion, while 3/4 run-off into the uppermost ice layer (z=1). Dependent on the permeability and the hydraulic head, a portion of that flushes the ice below. The residual remains in the ice layer. Original sketch taken from Griewank and Notz (2015) and modified afterwards.

Beside the implementation of the change in the parametrization, check functions were built into the code to check mass and energy conservation in the changed routines. Lab and field observations (Gourdon, 2016) showed a larger gas fraction of the upper ice layers than the model assumes before melting. The permeability calculation in SAMSIM given by equation (8) considers only the liquid fraction ϕ_l. The ice is thus almost impermeable in the model, once ϕ_l gets marginal due to extremely fresh ice. Since observations showed furthermore that liquid water can easily run-off through the gas inclusions, I added the gas fraction to the permeability calculation in SAMSIM_2017:

$$\Pi(\phi_l) = 10^{-17}(10^3(\phi_l + 2\phi_g)^{3.1}. \tag{29}$$

The factor 2 amplifies the impact consciously. Gas inclusions as they were observed in the lab are likely to occur in quickly grown ice (Tsurikov, 1979). The gas fraction is indeed not a verified variable in SAMSIM, but in the upper ice layers, where it strongly affects flushing, gas inclusions are mainly a result of the snow-to-slush conversion. In this conversion, gas inclusions are based on observations by Eicken, Lensu et al. (1995).

Additionally, the horizontal run-off of melt water was decreased by setting the average distance x to a crack in the ice to $x = 10 \cdot h_{ice}$ and the height of the melt water column h_{mw} on the ice was added to the hydraulic head calculation $\Delta p = \rho g(freeboard + h_{mw})$ in the complex flushing routine (compare section 2.4.2 in Griewank and Notz (2015)). The calculation of the impact of flushing meltwater on the bulk salinity by the complex flushing remained the same as presented in Griewank and Notz (2015).

The stability of the new SAMSIM_2017 model code is tested based on a 4.5 years long

data set from the SHEBA campaign site which was also used in Griewank and Notz (2015) (figure 8 therein). The resulting temporal evolution of the bulk salinity is given in figure 51. The model runs stable without any novel restriction. SAMSIM_original and SAMSIM_2017 (figure 51) simulate almost the same salinity profile over several years. Small changes are only visible during melting after the third year. It is unclear whether this difference is a numerical artifact or due to the change in parametrization.

10.2 Flushing occurs earlier

With the atmospheric and oceanic forcing of experiment 4, SAMSIM_2017 shows on short timescales a changed flushing behavior in comparison to SAMSIM_original (figure 52). Meltwater penetrates into the sea ice in contrast to only forming a solid ice layer on top of the sea ice. The lack of the 20% gas fraction in the uppermost layer shows distinctly in comparison to figure 39 the smaller amount of slush formation. The ice gets slightly warmer during melting in the 2017 setup and the impact of flushing in the ice below is visible immediately after the onset of melting. More snow remains on the ice after melting in the 2017 setup and the ice stays warmer in the further evolution of the experiment. And finally, there is no impact of the 2017 parametrization on the model before the onset of melting.

Zooming especially into the time of snow melt, figure 46 c) from section 8.3 changes to figure 53. The strength of desalination remains still below the measured one, but changes in the ice are measurable despite SAMSIM-HARP simulation in SAMSIM_2017. That means freshwater percolates into the ice in contrast to forming only fresh layers on top of the ice.

The same behavior can be observed in the vertical salinity profiles of the „after melting state“. A smaller bulk salinity of the 2017 parametrization in comparison to the original setup shows there, that more flushing occurs due to snow melt (figure 54). The influence of the parametrization change is higher in the upper half of the ice column.

The quantitative amount of salt change in different ice depths becomes clear in figure 55.

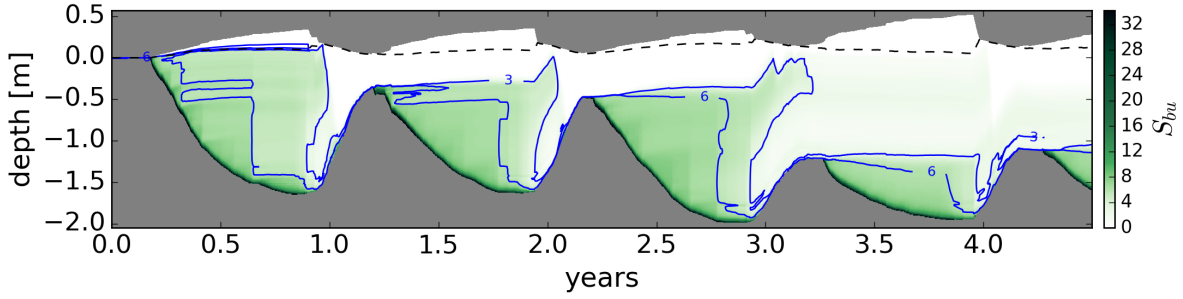

Figure 51: Temporal evolution of bulk salinity in SAMSIM_2017, forced by SHEBA campaign data similar to Griewank and Notz (2015)

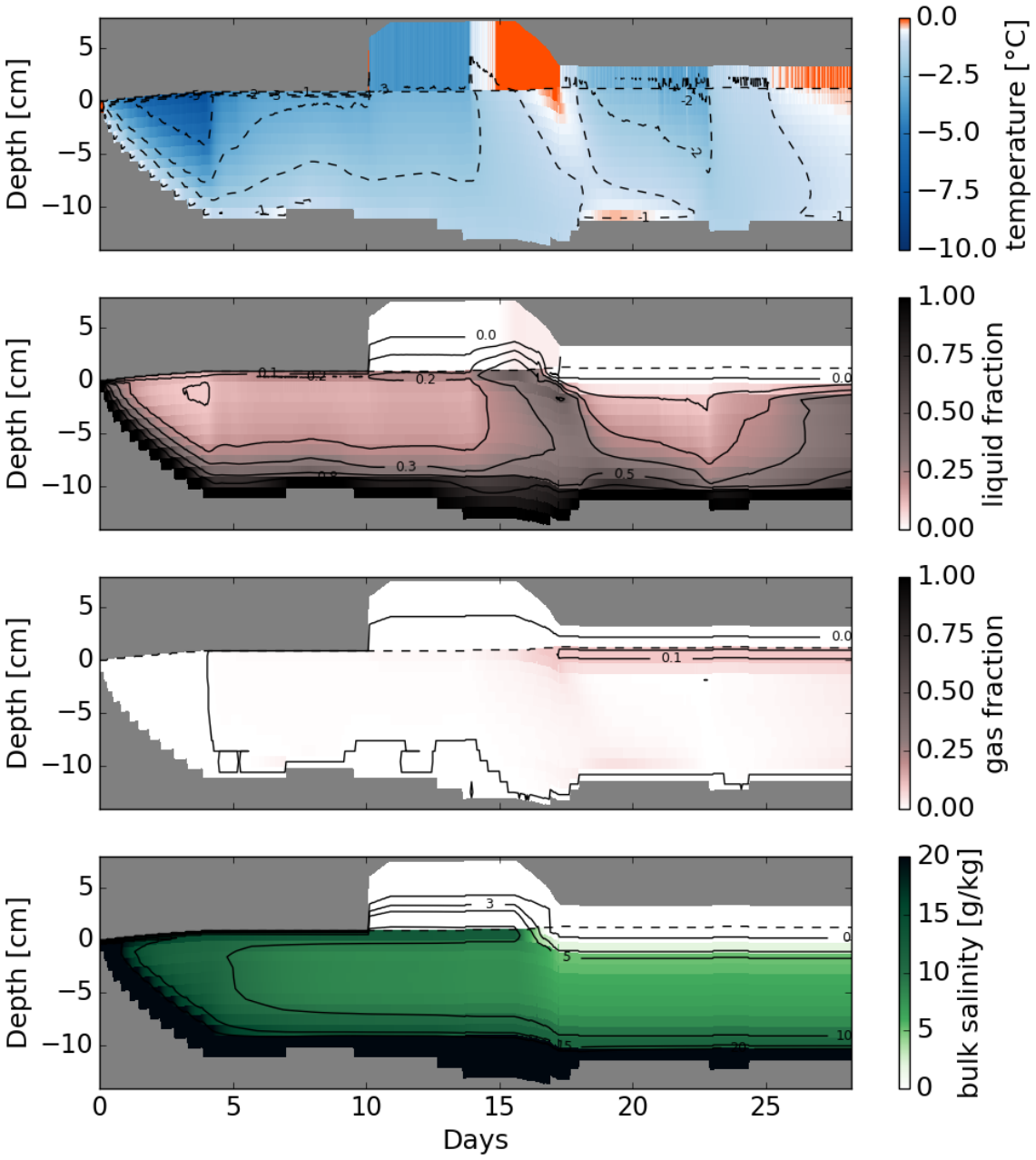

Figure 52: Temporal evolution of temperature, liquid fraction, gas fraction and bulk salinity in SAMSIM_2017, forced by snow experiment 4

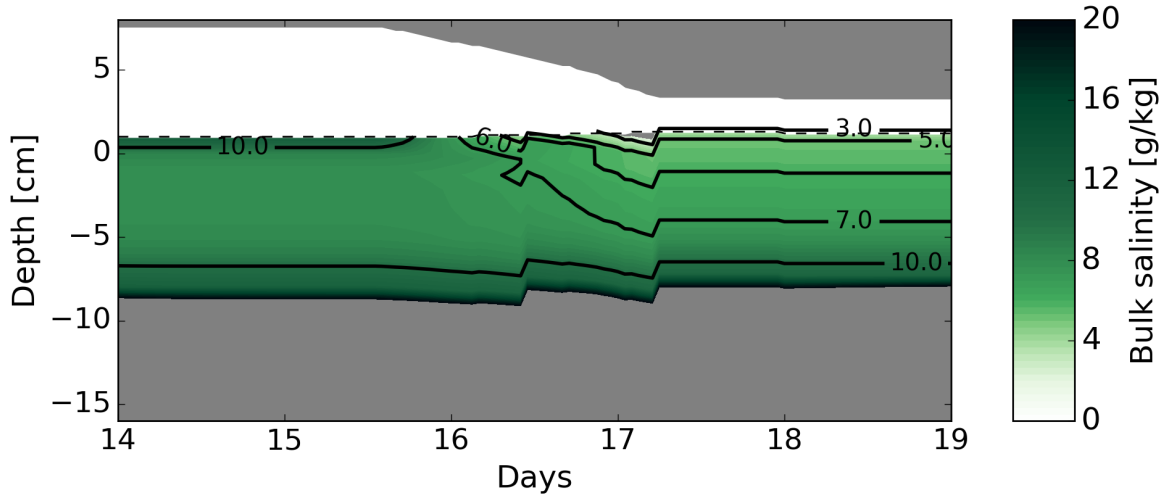

Figure 53: Temporal evolution of bulk salinity in SAMSIM_2017 in experiment 4 during melting. The vertical coordinate is corrected by the SAMSIM-HARP simulation so that it can be compared to the snow harp measurements.

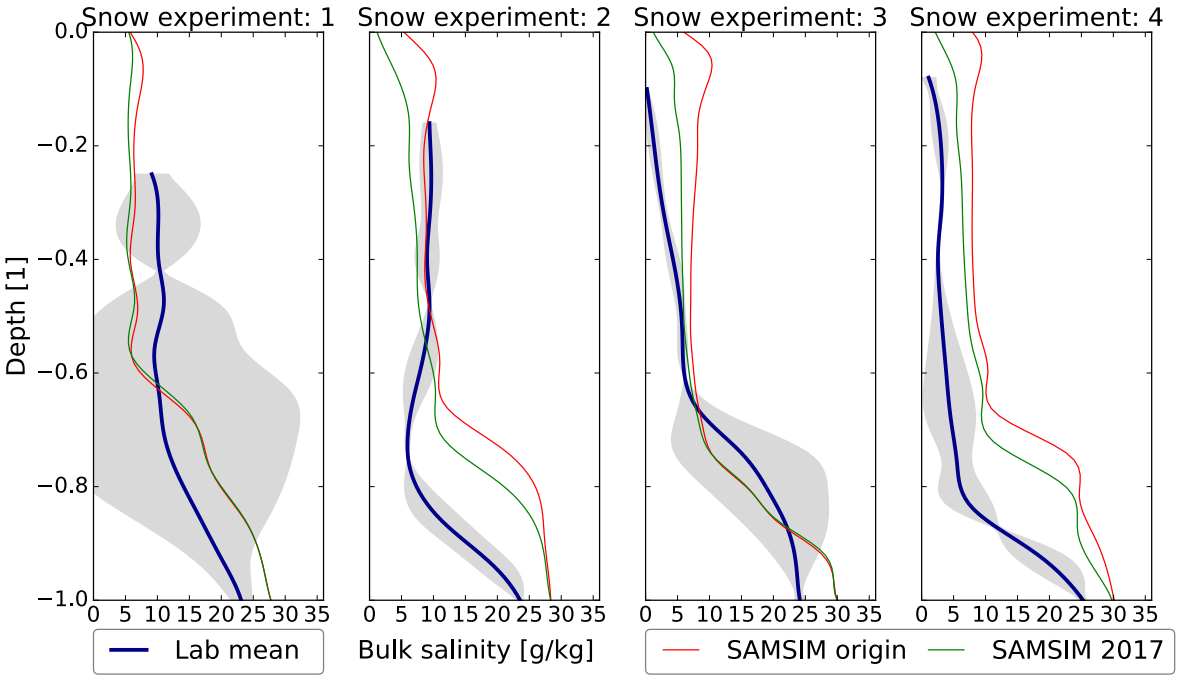

Figure 54: Vertical profiles of bulk salinity at normalized depth from measurements and concerning SAMSIM simulations at the „after melting state“. Measurement lines show mean values from all 5 harps ± two times the standard deviation

In experiment 3 and 4 where no desalination was calculated by the original setup there is a clear trend in the 2017 setup which follows the lab measurements in the upper two-thirds of the ice. Experiment 2 is in this setup overestimated in the amount of desalination and experiment 1 shows fairly the same results as in the SAMSIM_original setup. While the lower third of the ice remains unchanged in experiment 3, SAMSIM calculates in all other simulations a decrease of salt content there. While measurements from experiments 1-3 show a clear trend of increasing salt contents in the lower third.

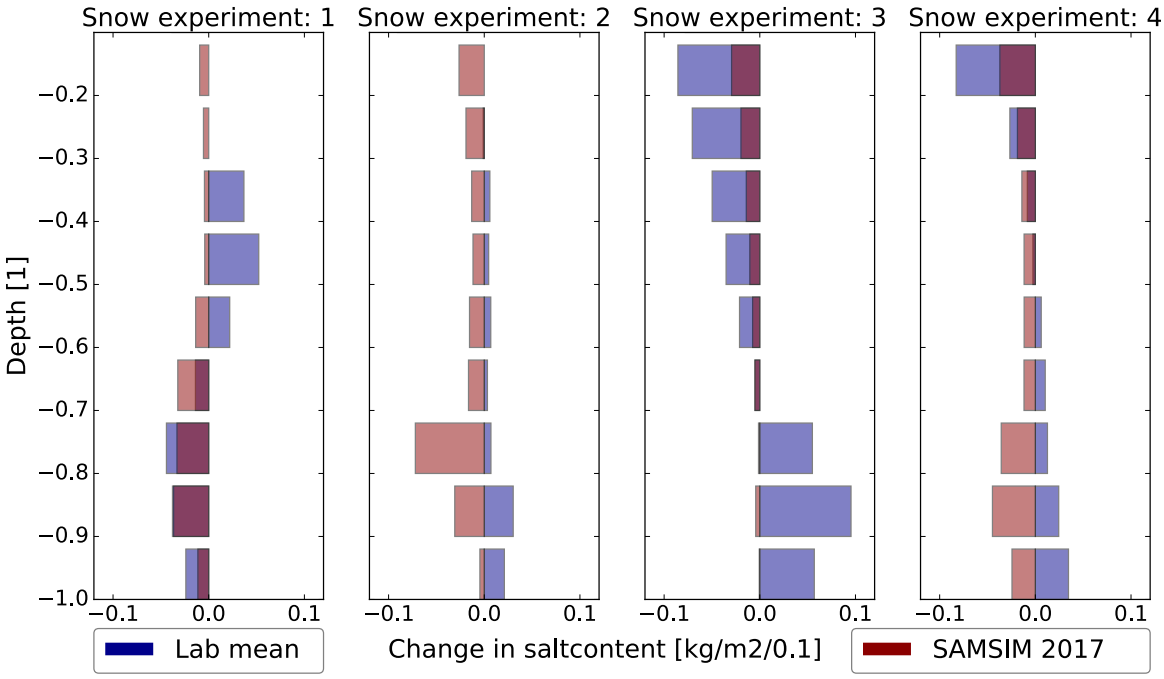

Figure 55: Vertical profiles of salt content changes in the ice between „before melting state“ and „after melting state“. Negative values stand for decreasing salt content during melting. Calculated with modified SAMSIM parametrization: SAMSIM_2017

10.3 The parametrization is qualitatively improved

The segmentation of snow melt water in SAMSIM improves the near-term results in the numerical model in the upper ice layers. Flushing of the ice underneath the snow cover occurs as measurements in the snow experiments indicate. However, the impact of freshwater flushing remains far below measured values in experiment 3 and 4., which suggest that flushing still gets underestimated by the model, which could be caused by the smaller amount of snow melt. The introduction of segmentation leads to flushing while the change in the permeability calculation as well as the change of the horizontal flushing parameter changed the amount of desalination. It must be considered anyway that the amplitude of changes is

dependent on the real ice thickness and not, as treated here, on a normalized vector. This was chosen to evaluate the data in a qualitative way, its influence is much smaller than the obtained differences between measurement and model results. Less snow melt happens presumably due to the lower amount of slush production in the 2017 setup. In doing so, more solid ice crystals remain in the snow cover after each timestep than in the original setup. Hence, a larger amount of snow must be melted. Furthermore, SAMSIM shows the tendency to overestimate flushing during blank ice melt periods. I checked manually at this point that the modeled desalination is almost complete due to flushing rather then due to gravity drainage. Snow has therefore a negative impact on the grade of desalination in SAMSIM while in the lab the impact was negative only for thin snow layers.

11 The impacts of snow on sea ice salinity

The deployed sensor setup allowed for internal sea ice data from lab experiments in an unprecedented resolution. Many small-scale effects were measured in the whole freeze and thaw cycle that are unlikely to be captured by the measurement precision and resolution of ice cores. Beside investigations of lab ice features as the horizontal homogeneity, which are given in 8.2, only effects that are directly associated with the snow cover are of particular interest within the interpretation frame of this work.

From the obtained unique data set, I figured out four impacts of snow on sea ice salinity. Only one of these impacts was able to enhance the bulk salinity of the ice below. The deployment of snow flushed super salty brine (about $S = 120$ g kg^{-1}) that was expelled from the uppermost ice layers onto the ice surface during freezing back into the ice. All other processes led to desalination of the ice below. Firstly, the deployment of snow on the ice floe led to a measured and modeled warming in the lab sea-ice, which enhanced its permeability. This allowed brine to be gravitational circulated. Small amounts of salt escaped the ice at the bottom and therefore reduced the bulk salinity of the lower ice layers. The warming effect of the snow cover on the ice beneath due to insulation is probably smaller in nature since the snow also shadows the ice. This effect does not occur in the dark lab as well as during polar night. Secondly, flushing led to a measurable desalination of the ice center directly after the snow deployment in experiment 4, caused by liquid water that ran off from the snow into the ice. Since natural snow precipitation contains assumably less liquid water this effect is unlikely to occur in nature. However, due to meteorological extreme situations in the Arctic atmosphere rain could cause such flushing events independently of snow melt. Thirdly, I proved that snow acts as a fresh water source on the ice that leads to flushing during snow melt. The measured impact was stronger than the modeled. But a change in the SAMSIM parametrization of melting snow improved the modeled results qualitatively. In contrast to earlier model parametrizations, it was observed in this work and implemented in SAMSIM that one quarter of snow melt water remains at the ice–snow interface and three quarter flush immediately into the ice as soon as the solid ice skeleton is permeable enough. While the bulk salinity towards the top of the ice decreased during flushing, increasing bulk salinity was measured further down in the ice. This emerges from the downward displacement of colder and thus saltier brine within the ice. Only large flushing events can desalinate the ice in the whole vertical expansion. The more snow melted on the ice, the greater the salt decrease was in the ice beneath. I measured a maximum salt content change in the upper 60% of 15 cm thick ice during melting of about -0.37 kg m^2, respectively -70% of the salt content, caused by the snow cover. And finally, the impact of a thin snow layer can be even negative on desalination in comparison to the impact of a blank ice surface because the snow

cover insulates the ice, which becomes thus not permeable enough for the small possible hydraulic head of the melt water column. I found a threshold in the mass relation between snow and ice below at 17%. If the snow cover weight is above 17% of the ice mass, melting snow was able to desalinate the ice. Linearly extrapolated, a melting snow cover with the mass of 25% of the ice below would make the ice completely salt free. This result fits to the observed liquid fraction of the ice during snow melt which was close to 0.25. That means, in this case all salty brine would be replaced by fresh melt water.

I therefore conclude that snow has an influence on sea ice salinity, especially during melting. In this measurements, only small snow layers and the back flow of salty brine from the ice surface were able to increase the overall bulk salinity of snow covered sea ice in comparison to blank sea ice. I found out that thick snow layers during melting and the increment of permeability due to warming beneath the insulating snow cover lead to immediate desalination of the ice in the experiments and in the modified SAMSIM simulation. The modified implementation in the model that one quarter of the snow-melt water remains at the ice surface during melting and forms a numerical average over the horizontal heterogeneous surface conditions was most adequate in comparison to the horizontal resolved measurements and observations. Three quarters of the snow-melt water showed to percolate directly into the sea-ice matrix. And finally, I figured out that brine expulsion onto the ice surface had a strong impact on the sea-ice salinity measurements afterwards and is important for the salt balance in the ice. It should be thus included into highly resolved sea-ice models.

12 Outlook

This work gives an overview about the different impacts of snow on sea-ice salinity in the lab and in SAMSIM and furthermore describes a functional measurement method and lab setup. Many more investigations need to be done to be able to improve the understanding of each single impact and correct the quantitative representation of flushing in SAMSIM for short-term studies. However, it should be mentioned that global climate models are unlikely to benefit largely from a numerical improvement as Griewank and Notz (2013) stated already for an improved gravity drainage parametrization.

Further studies need to improve firstly the understanding of the heat flux balance in the lab to allow for a proper representation in SAMSIM. Secondly, a study could check if bubbles of increasing bulk salinity in the ice during melting, as they were observed in some experiments, come from an intake of ocean water into warm ice due to the density change during internal melting: A melting solid ice skeleton possibly leads to reduced pressure areas in the ice that need to be filled with underlying ocean water. Another point that could only be touched in this work due to a lack of detailed observations are the exact mechanisms that triggered gravity drainage after snow deployment and their interaction. On the one hand, the saltier the ice is, the less it would warm due to its lower heat conductivity. But on the other hand the less it would need to be warmed up to reach the critical threshold for gravity drainage, since its liquid fraction would be higher at the same bulk salinity. SAMSIM and its proper gravity drainage parametrization would be a helpful tool for this study as soon as heat fluxes are sufficiently represented. I completely prevented snow ice creation in the lab and model setup. This contradicts the natural impact of such thick snow layers as they are used in this work on thin ice and hence the linearly derived mass ratio thresholds of 17% and 25% for a positive flushing impact of snow and the complete desalination of the ice below. I expect a great impact of the salt in snow ice on the snow melt behavior as well as on flushing. The ice lab in connection with the salinity harp setup gives a great opportunity for further snow ice studies. Finally, we need to get a much deeper understanding of the immediate impact of snow deployment in experiment 4.

13 Appendix

Table 14: DS-Sensor calibration values

DS_Stick:Sensor:	a1	a2	a3
0:0:	-0.000296264943436	1.00859133603	-0.0413048985517
0:1:	-0.000207980362736	1.00940284516	-0.0765282424943
0:2:	-0.000240102713313	1.0102334919	-0.104314982074
0:3:	-0.000287787994858	1.00970410257	-0.0875706637352
0:4:	-0.000243080288204	1.01152592858	-0.105175913606
0:5:	-0.000205533072822	1.01101122437	-0.0994899521005
0:6:	-0.000227681247185	1.01003410453	-0.0695213959308
0:7:	-0.000220204571471	1.01042476821	-0.144019347911
1:0:	-0.000306235952581	1.01062390598	-0.0211039223951
1:1:	-0.00021170007443	1.01109250192	-0.096607001792
1:2:	-0.000237426840762	1.00894894538	-0.0876580269763
1:3:	-0.000231442583609	1.00982991104	-0.0055440392337
1:4:	-0.000253832057146	1.00992532266	-0.00281265550085
1:5:	-0.000224258489362	1.00993089463	0.0223623519925
1:6:	-0.000256929612477	1.00995295473	-0.0461335267525
1:7:	-0.0001876768455	1.01121929096	-0.0184005690372
2:0:	-0.000232335566649	1.01029150229	-0.0237834709481
2:1:	-0.000227380926711	1.01071173488	-0.0595925247806
2:2:	-0.000248464713532	1.01156300359	-0.0456737325679
2:3:	-0.000246684220019	1.01005224869	-0.0724480293024
2:4:	-0.000224749996539	1.01098559984	0.00664810168172
2:5:	-0.000182398439303	1.01155934322	-0.0687196549073
2:6:	-0.000243982549043	1.00837454296	-0.0481049377129
2:7:	-0.000484202880343	1.00809399264	-0.274624978044
3:0:	-0.000276669259054	1.0078314763	-0.0664591380449
3:1:	-0.000235848021346	1.01067098266	-0.0490553294115
3:2:	-0.000225661053044	1.01073701195	-0.0894961782394
3:3:	-0.000211984865045	1.01005801865	-0.00632585375081
3:4:	-0.000181772741795	1.01201158652	-0.0358744093973
3:5:	-0.00024202725183	1.00968783114	0.0374792867684
3:6:	-9.20204692643e-05	1.00976138107	0.00581911552848
3:7:	-0.000126092536596	1.0133283463	-0.0770416646565
4:0:	-0.000189559359088	1.00834091289	0.00948155214511
4:1:	-0.000209376409792	1.01058071798	-0.0688229865423
4:2:	-0.000214656605783	1.00806160751	0.0114821403752
4:3:	-0.00017441941559	1.00977098473	-0.117015041296
4:4:	-0.000171229194599	1.01152098569	-0.0717227326181
4:5:	-0.000273857636509	1.01292291806	-0.0833637080491
4:6:	-0.000270336277926	1.01171208937	-0.118803630009
4:7:	-0.000258488832211	1.01150441362	-0.0720741560535
5:0:	-0.000222311724594	1.01165987001	-0.150963676055
5:1:	-0.000199986059799	1.00926954183	-0.0892426229654
5:2:	-0.000237039005474	1.01069562782	0.000159026613169
5:3:	-0.000297050055123	1.0082614185	-0.0348308439448
5:4:	-0.000215010521662	1.00967233335	-0.0978237291773
5:5:	-0.000246874561806	1.00864706282	-0.0663683773401
5:6:	-0.000255412640977	1.01012997226	-0.10747374501
5:7:	-0.000172407359155	1.01092153366	-0.104474200369
6:0:	-0.000224831955447	1.01110494569	0.00240327206328
6:1:	-0.000240169291795	1.00969472232	-0.00300919712855
6:2:	-0.000263243811254	1.01110579211	-0.0112241631912
6:3:	-0.000208650009575	1.01207563121	-0.106956515791
6:4:	-0.000153010898633	1.01088112257	-0.0236976762357
6:5:	-0.000192499581888	1.00898144592	0.013601060946
6:6:	-0.000266821515137	1.00940763996	0.0440462714431
6:7:	-0.000286077620588	1.00963954723	-0.0606192688629
7:0:	-0.000263846677421	1.00934889493	-0.117942628677
7:1:	-0.000260489388984	1.01006822492	-0.0915841278536
7:2:	-2.95900106624e-05	1.01481816694	-0.0135235015967
7:3:	-0.0002803567919	1.00971631963	-0.0869643686438
7:4:	-0.000262588578761	1.00892105041	-0.0417398297637
7:5:	-0.000233781365011	1.01030593277	-0.0428171164646
7:6:	-0.000292616480788	1.00915376406	-0.0387172572797
7:7:	-0.000233071711602	1.00713297756	0.00955008768171

Table 15: TStick calibration values

TStick:Sensor:	a1	a2	a3
0:0:	-0.000251762923151	1.01075073018	-0.0332326863896
0:1:	-0.000190826141915	1.01069456202	-0.0653177700327
0:2:	-0.000181486606949	1.00927572628	-0.0536709587689
0:3:	-0.00018842716775	1.00944446159	-0.158146893478
0:4:	-0.000190690269315	1.00830945284	-0.078770700833
0:5:	-0.000263606977903	1.00800823324	-0.109896840556
0:6:	-0.00020487289786	1.00911333309	-0.0735114817822
0:7:	-0.000250665672311	1.01303290089	-0.152499328362
1:0:	-0.000202635527543	1.00837805084	0.0244939343377
1:1:	-0.000189480993687	1.00881905735	-0.0104413854283
1:2:	-0.000203575232362	1.01070732187	-0.131712983025
1:3:	-0.000170287755932	1.00961651462	-0.0598194513961
1:4:	-0.000186745813712	1.00992288903	0.0310655881619
1:5:	-0.000216229782737	1.0085316545	-0.00514261320947
1:6:	-0.00022804588035	1.00970632062	-0.0374723965832
1:7:	-0.000221096546511	1.00980379216	-0.0453900384513
2:0:	-0.000204412142388	1.0084847146	-0.213026177753
2:1:	-0.000202442706201	1.01087606873	-0.0588718353346
2:2:	-0.000215630799299	1.00969089382	-0.100490459078
2:3:	-0.000222038055365	1.00955187302	-0.0877531565071
2:4:	-0.000200689728265	1.0108718684	-0.114074539411
2:5:	-0.000237873286895	1.00981432291	-0.00116738338027
2:6:	-0.000197772163504	1.0093129334	-0.0823509947391
2:7:	-0.0002549645231	1.01109102177	-0.0573867686109
3:0:	-0.000227503656067	1.00881303816	-0.205553992033
3:1:	-0.000187265858427	1.00907516217	-0.200597774896
3:2:	-0.000220240229709	1.01058889872	-0.165081436699
3:3:	-0.000208308797193	1.00891681661	-0.0497220686136
3:4:	-0.000204967153211	1.00852427803	-0.131317480511
3:5:	-0.000219263904412	1.00879098985	-0.1083125481
3:6:	-0.000218794410826	1.00905294968	-0.758611145274
3:7:	-0.000259731510897	1.01120634097	-0.100535367175
4:0:	-0.000206733166195	1.0071492672	0.0300458778957
4:1:	-0.000223894203737	1.01070132679	-0.0885238422554
4:2:	-0.000228180854906	1.00934490431	-0.111677141967
4:3:	-0.000238217427538	1.00875647697	-0.0519088634171
4:4:	-0.00020526724555	1.01136876454	-0.035368275041
4:5:	-0.000206811429777	1.00878840001	-0.144133975614
4:6:	-0.000212978516185	1.00888472861	-0.00684151569679
4:7:	-0.000216721284954	1.00875965734	-0.0669530146975
5:0:	-0.000235352475125	1.00833613646	-0.0982227558105
5:1:	-0.000229983052907	1.01277788602	-0.120448866145
5:2:	-0.000210105490717	1.00860674779	-0.0235011502998
5:3:	-0.000192096072156	1.00718513607	-0.0869483048843
5:4:	-0.000223356236699	1.00976660505	-0.155932746426
5:5:	-0.000226300833401	1.00987835504	-0.112834825509
5:6:	-0.000213293155235	1.00929971471	-0.0571237984231
5:7:	-0.000211109268487	1.00975456637	-0.0288177043461
6:0:	-0.00019686645449	1.0097472222	-0.0478399637863
6:1:	-0.000233102495545	1.01030885937	-0.0983526044931
6:2:	-0.000209355326651	1.0094983031	-0.0122032725697
6:3:	-0.000212846767761	1.00871689566	-0.0485896792513
6:4:	-0.000210200999589	1.01181518245	-0.139638107318
6:5:	-0.000222526412737	1.00811932141	0.0520348760067
6:6:	-0.000221286231114	1.0090093501	-0.0345094116741
6:7:	-0.000190822755635	1.00953632912	0.0271326906956
7:0:	-0.000217102242274	1.00978139124	-0.157667698461
7:1:	-0.000219080664009	1.01149442732	-0.0872089020407
7:2:	-0.000211919872559	1.01012320122	0.00965325513186
7:3:	-0.000218565612263	1.00963326812	-0.0638316293677
7:4:	-0.000188328900461	1.0096355003	-0.0575731516459
7:5:	-0.00021778439311	1.00993123989	-0.10161032896
7:6:	-0.000217345478637	1.01017829042	-0.079936960063
7:7:	-0.000206219188237	1.00967736932	-0.0491657559627

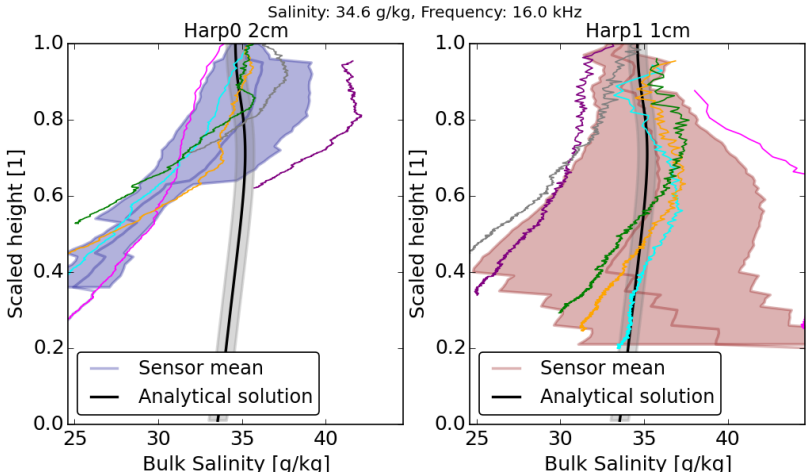

Figure 56: Bulk salinity profiles experiment 1, all sensors of H2cm (left) and H1cm (right) and analytical solution, 16kHz

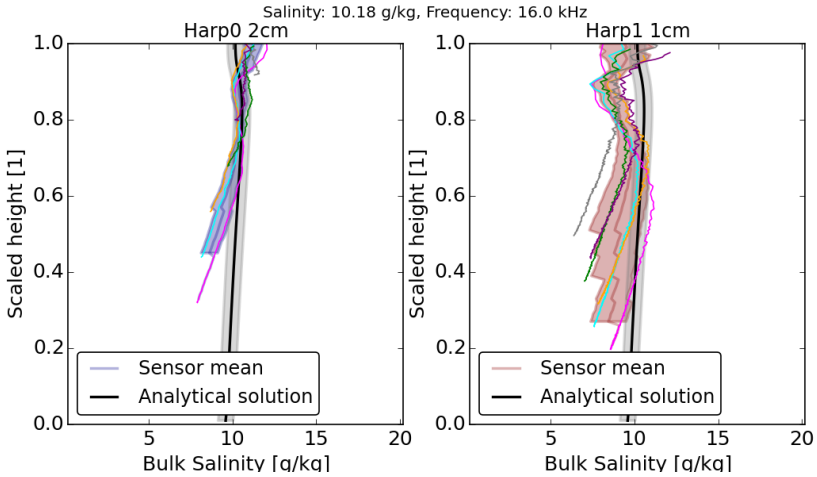

Figure 57: Bulk salinity profiles experiment 2, all sensors of H2cm (left) and H1cm (right) and analytical solution, 16kHz

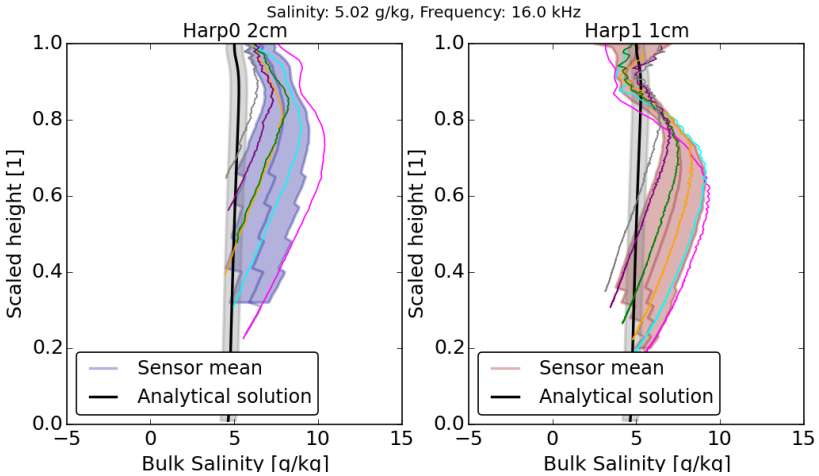

Figure 58: Bulk salinity profiles experiment 3, all sensors of H2cm (left) and H1cm (right) and analytical solution, 16kHz

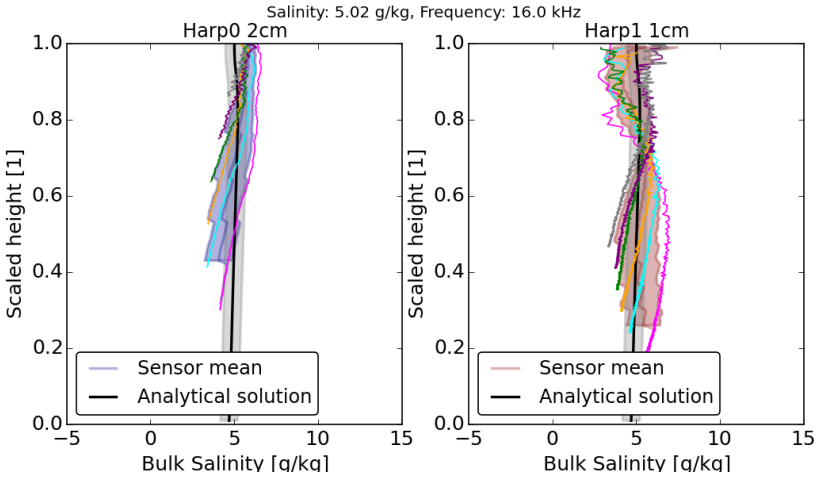

Figure 59: Bulk salinity profiles experiment 4, all sensors of H2cm (left) and H1cm (right) and analytical solution, 16kHz

References

Aukan, I. (2016). "Snow ice formation - capillary rise of brine and sea water through snow in relation to snow density". In: *UNIS AGF-211 Field Report 2016*.

Chiareli, A. et al. (1994). "Segregation and flow during the solidification of alloys". In: *Journal of Crystal Growth* 139.1-2, pp. 134–146.

Coléou, C. and B. Lesaffre (1998). "Irreducible water saturation in snow: experimental results in a cold laboratory". In: *Annals of glaciology* 26.1, pp. 64–68.

Eicken, H., H. Krouse et al. (2002). "Tracer studies of pathways and rates of meltwater transport through Arctic summer sea ice". In: *Journal of Geophysical Research: Oceans* 107.C10.

Eicken, H., M. Lensu et al. (1995). "Thickness, structure, and properties of level summer multiyear ice in the Eurasian sector of the Arctic Ocean". In: *Journal of Geophysical Research: Oceans* 100.C11, pp. 22697–22710.

Eicken, H. and M. Salganek (2010). *Field techniques for sea-ice research*. University of Alaska Press.

Fofonoff, N. P. and R. C. Millard Jr (1983). "Algorithms for the computation of fundamental properties of seawater." In:

Golden, K. M. et al. (1998). "The percolation phase transition in sea ice". In: *Science* 282.5397, pp. 2238–2241.

Gourdon, A. (2016). "Sea-ice density". In: *UNIS AGF-211 Field Report 2016*.

Grenfell, T. C. and G. A. Maykut (1977). "The optical properties of ice and snow in the Arctic Basin". In: *Journal of Glaciology* 18.80, pp. 445–463.

Griewank, P. J. and D. Notz (2013). "Insights into brine dynamics and sea ice desalination from a 1-D model study of gravity drainage". In: *Journal of Geophysical Research: Oceans* 118.7, pp. 3370–3386.

Griewank, P. J. and D. Notz (2015). "A 1-D modelling study of Arctic sea-ice salinity". In: *The Cryosphere* 9.1, pp. 305–329.

Hibler, W. D. (1979). "A dynamic thermodynamic sea ice model". In: *Journal of Physical Oceanography* 9.4, pp. 815–846.

Notz, D. (2005). "Thermodynamic and fluid-dynamical processes in sea ice". PhD thesis. University of Cambridge.

Notz, D., J. S. Wettlaufer et al. (2005). "A non-destructive method for measuring the salinity and solid fraction of growing sea ice in situ". In: *Journal of Glaciology* 51.172, pp. 159–166.

Notz, D. and M. G. Worster (2009). "Desalination processes of sea ice revisited". In: *Journal of Geophysical Research: Oceans* 114.C5.

Pawlowicz, R. (2013). *What every oceanographer needs to know about TEOS-10*. Dept. of Earth and Ocean Sciences, University of British Columbia, Vancouver, Canada. URL: `http://www.teos-10.org/pubs/TEOS-10_Primer.pdf`.

Perovich, D. K. and J. A. Richter-Menge (1994). "Surface characteristics of lead ice". In: *Journal of Geophysical Research: Oceans* 99.C8, pp. 16341–16350.

Shirtcliffe, T. G. L. et al. (1991). "Measurement of the solid fraction in the crystallization of a binary melt". In: *Journal of crystal growth* 113.3-4, pp. 566–574.

Sturm, M. et al. (2002). "Thermal conductivity and heat transfer through the snow on the ice of the Beaufort Sea". In: *Journal of Geophysical Research: Oceans* 107.C10.

Tsurikov, V. (1979). "The formation and composition of the gas content of sea ice". In: *Journal of Glaciology* 22.86, pp. 67–81.

Untersteiner, N. (1961). "On the mass and heat budget of Arctic sea ice". In: *Archiv für Meteorologie, Geophysik und Bioklimatologie, Serie A* 12.2, pp. 151–182.

Untersteiner, N. (1968). "Natural desalination and equilibrium salinity profile of perennial sea ice". In: *Journal of Geophysical Research* 73.4, pp. 1251–1257.

Vancoppenolle, M., C. M. Bitz et al. (2007). "Summer landfast sea ice desalination at Point Barrow, Alaska: Modeling and observations". In: *Journal of Geophysical Research: Oceans* 112.C4.

Vancoppenolle, M., T. Fichefet et al. (2006). "Modeling the salinity profile of undeformed Arctic sea ice". In: *Geophysical Research Letters* 33.21.

Wiese, M. et al. (2012). "Laboratory experiments on the thermodynamics of melting sea ice". MA thesis. University of Hamburg, Hamburg.

Worster, M. G. (1992). "The dynamics of mushy layers". In: *Interactive dynamics of convection and solidification*. Springer, pp. 113–138.

Zeichnung. *http://www.kika.de/der-kleine-eisbaer/sendungen/sendung12674.html; March 19, 2017*.


from: Kika.de

Acknowledges

Ich möchte mich an dieser Stelle ganz herzlichst bei meinen beiden Betreuern Dr. Dirk Notz und Prof. Dr. Felix Ament für die sehr hilfreiche Betreuung meiner Arbeit, die konstruktive Kritik und die zielführenden Ratschläge bedanken. Außerdem vielen Dank an die gesamte Meereisforschungsgruppe am MPI-M für die immerwährende Hilfsbereitschaft und das gute Miteinander. Dabei seien besonders genannt Leif Riemenschneider als Elektronikgenie und Messsytem-Entwickler sowie Philipp Griewank als ehemaliges Gruppenmitglied und Entwickler von SAMSIM, der mir bei jeglichen Fragen zum Model stets äußerst spontan sehr hilfreiche Antworten gegeben hat. Korrekturgelesen haben liebenswerterweise Fritjof Basan, Morten Harms, Karolin Müller, Theresa Mieslinger und meine Familie - vielen Dank dafür!
Und natürlich Danke Karoline für das Durchhaltevermögen.

Selbstständigkeitserklärung

Hiermit versichere ich, Niels Fuchs, an Eides statt, dass ich die vorliegende Arbeit im Studiengang M.Sc. Meteorologie selbstständig verfasst und keine anderen als die angegebenen Hilfsmittel – insbesondere keine im Quellenverzeichnis nicht benannten Internet-Quellen – benutzt habe. Alle Stellen, die wörtlich oder sinngemäß aus Veröffentlichungen entnommen wurden, sind als solche kenntlich gemacht. Ich versichere weiterhin, dass ich die Arbeit vorher nicht in einem anderen Prüfungsverfahren eingereicht habe und die eingereichte schriftliche Fassung der auf dem elektronischen Speichermedium entspricht.

Hamburg, den 20. März 2017